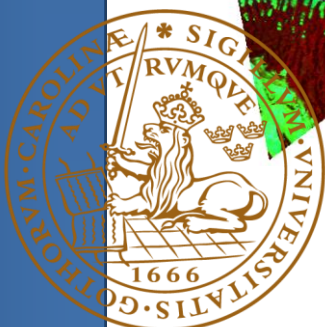
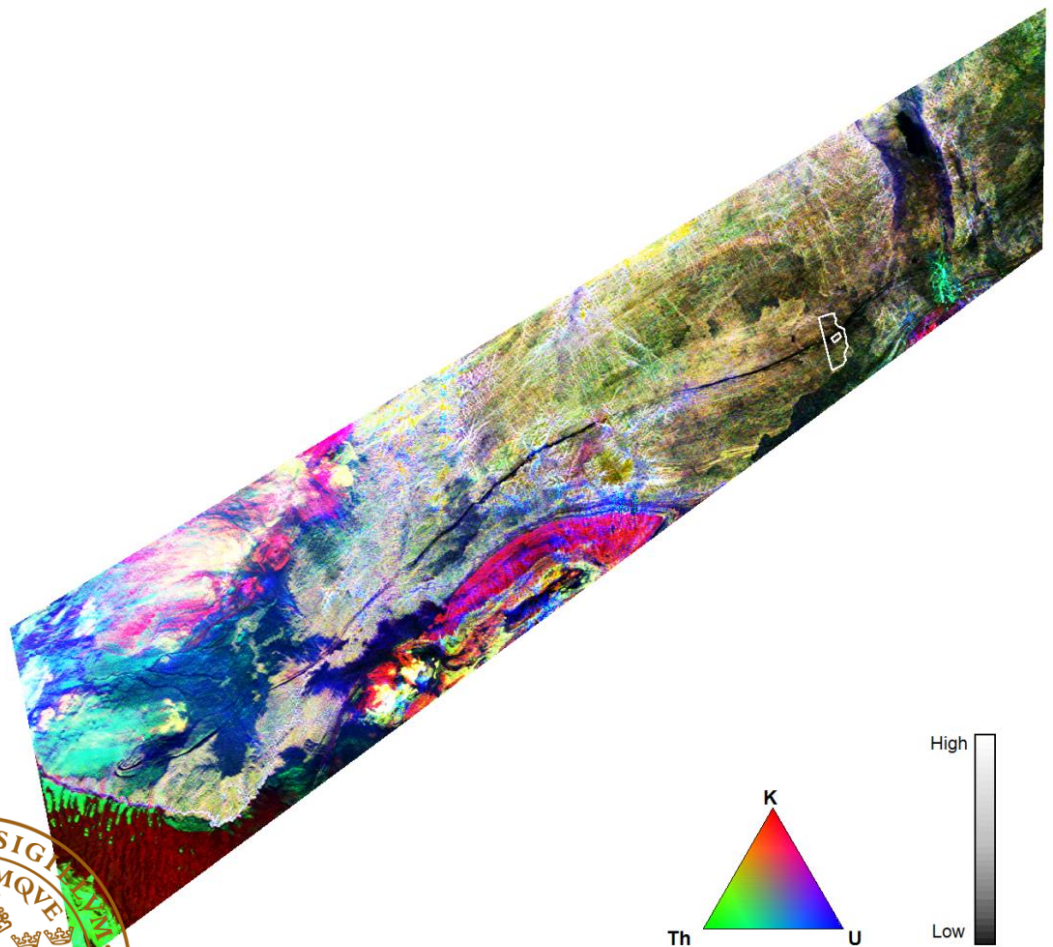


Geophysical ground surveys of the Matchless Amphibolite Belt in Namibia

Cecilia A. M. Jönsson

Dissertation in Geology at Lund University
Master of Science thesis no. 377
(45hp/ECTS credits)



Department of Geology
Lund University
2014

Geophysical ground surveys of the Matchless Amphibolite Belt in Namibia

Master's thesis
Cecilia A. M. Jönsson

Department of Geology
Lund University
2014

Foreword

This thesis is the result of my participation in a collaboration project between the Geological Survey of Sweden (SGU) and the Geological Survey of Namibia (GSN). The project is under the partner driven MeetingPoints Mining organization with main funding from the Swedish International Development cooperation Agency, SIDA. I am sincerely grateful for the opportunity to participate in the project, and would like to express my gratitude to all who have made this possible.

Cecilia Jönsson

Geophysical ground surveys of the Matchless Amphibolite Belt in Namibia

CECILIA A. M. JÖNSSON

Jönsson, C. A. M., 2014: Geophysical ground surveys of the Matchless Amphibolite Belt in Namibia. *Dissertations in Geology at Lund University*, No. 377, 56 pp. 45 hp (45 ECTS credits).

Abstract: Geophysical data provide information of subsurface geological that is not observable by conventional geological mapping. For the Matchless Amphibolite Belt (MAB), extending over more than 340 km, in Namibia, high resolution airborne geophysical data exist but published ground geophysical data is scarce. The belt consists of a 0.5-3 km wide unit of mafic metamorphosed rocks within a metasedimentary unit dominating by schist. The MAB sequence strikes along a NE-SW direction and dips about 40° to NW. The MAB is an important part in the understanding of the evolution of the Damara Belt within the amalgamation of Gondwana in southern Africa at 530 Ma. The belt is also of economical interest with several associated mineralizations. This work shows that gravimetric, electrical and magnetic methods are successful in the identification of different lithological units and properties of these units. The work also show that the electromagnetic Very Low Frequency method (VLF) is not applicable in the area due to lack of adequate transmitters. We also present a structural and lithological three-dimensional model based on geological and geophysical data for the area of study. The electrical self potential (SP) measurements show a distinct negative anomaly over a known sulfide mineralization and the method is proved to be applicable in the area for further prospecting. The gravity measurements identified amphibolite bodies and gave new information of a bulk mass excess to the NW compared to the SE of the belt. The observed gradient in the gravity field cannot fully be explained by the structure and the higher density of the mafic rocks in the MAB and a slight difference (1%) in the bulk density of the surrounding metasedimentary rocks is proposed as an additional source. The ground magnetic measurements confirmed existing airborne magnetic data but resolve the anomalies in more detail. The mafic rocks of the MAB succession do not in general have a large magnetic susceptibility contrast to the surrounding rocks but magnetic field anomalies reveal magnetized lenses within the belt. In the metasedimentary units several thin and distinctly separated magnetic horizons are present. These units represent laterally extensive thin sheets that strike in a NE-SW direction and dip approximately 40 degrees to the NW, concordant with the MAB. This project shows that ground geophysical methods can, individually or in combination, be used to gain new information of the geology of the MAB and that modeling based on geophysical data can successfully be used to test different probable models of the belt.

Keywords: Matchless Amphibolite Belt, geophysics, gravity, magnetic, self potential, 3D-model

Supervisors: Lutz Kübler (SGU), Anders Scherstén (Lund University)

Cecilia Astrid Marie Jönsson, Department of Geology, Lund University, Sölvegatan 12, SE-223 62 Lund, Sweden. Email: Cecilia.Jonsson86@gmail.com

Geofysiska markmätningar över amfibolitbältet the Matchless Amphibolite Belt i Namibia

CECILIA A. M. JÖNSSON

Jönsson, C. A. M., 2014: Geofysiska markmätningar över amfibolitbältet: the Matchless Amphibolite Belt, i Namibia. *Examensarbeten i geologi vid Lunds universitet*, Nr. 377, 56 sid. 45 hp.

Abstrakt: Geofysiska undersökningar kan ge information om geologin under markytan som annars är oåtkomlig för konventionell geologisk kartering. Över det cirka 340 kilometer långsträckt amfibolitbältet, Matchless Amphibolite Belt (MAB) i Namibia, finns det högupplöst geofysisk data från flygmätningar medan publicerad data från markmätningar är sällsynt. MAB består av ett 0,5-3 kilometer brett bälte av metamorft omvandlade mafiska bergarter omgiven av metamorfa sedimentbergarter främst, skiffrar. Bältet stryker i en nordöstlig-sydvästlig riktning och stupar ungefär 40° åt nordväst. Amfibolitbältet utgör en viktig geologisk enhet i förståelsen kring utvecklingen av Damara-sekvensen som är en del i sammanslagningen av Gondwana för ca 530 miljoner år sedan. Ur en ekonomisk synvinkel är bältet också viktigt då flertalet mineraliseringar är kända längs dess utsträckning. Tyngdacceleration- och elektrisk själv-potential- (SP) undersökningar samt markburen mätning av jordens magnetfält, visas i denna studie ge information om litologiska enheter i och i anslutning till MAB. Den elektromagnetiska Very Low Frequency metoden (VLF) visas olämplig i undersökningsområdet då inga lämpliga sändare finns för området. Vi presenterar också en litologisk och strukturell tredimensionell modell baserad på geologisk och geofysisk data från av undersökningsområdet, Friedenau Farm 40 km sydväst om Windhoek. SP mätningar visade på en tydlig negativ anomali över områden där sulfidmineraliseringar är kända sedan tidigare och visar att metoden är lämplig för fortsatta studier av mineraliseringar i området. Tyngdaccelerationsmätningarna detekterade amfibolitkroppar och visade dessutom en gradient i tyngdkraftsfältet som inte enbart kunde förklaras av amfibolitbältets densitetskontrast gentemot omgivningen. En ringa densitetsskillnad mellan sedimentbergarterna i nordväst och sydost om bältet föreslås som ytterligare en källa till gradienten. Mätningar av jordens magnetfält från marken visar en bra överensstämmelse av positionen för anomalier jämfört med flygmätningar. Data insamlad från marken ger en mer detaljerad geometrisk information om källorna till anomalierna. De mafiska bergarterna som utgör MAB visar i allmänhet inte en stark magnetisk kontrast jämfört med omgivande bergarter men det förekommer hög-magnetiska linser i bältet. I de omgivande metamorfa sedimentärbergarterna med låg magnetisk susceptibilitet förekommer flera tunna magnetiska horisonter. De geologiska enheterna kan representeras av på ytan långsträckta tunna horisonter som stryker i en nordöstlig-sydvästlig riktning och stupar cirka 40° åt nordväst. Detta projekt visar att olika geofysiska metoder kan, individuellt eller i kombination, användas för att ta fram ny information om MAB samt att geofysisk data kan användas som utgångspunkt för att testa olika litologiska och strukturella modeller av bältet.

Nyckelord: Matchless Amphibolite Belt, geofysik, tyngdkraft, magnetometri, själv-potential, 3D-modell

Ämne: Berggrundsgeologi

*Cecilia Astrid Marie Jönsson, Geologiska institutionen, Lunds universitet, Sölvegatan 12, 223 62 Lund, Sverige.
E-post: Cecilia.Jonsson86@gmail.com*

List of abbreviations

CFB – Continental Floor Basalt

CZ – Central Zone

DEM – Digital Elevation Model

GSN – Geological Survey of Namibia

IGRF – International Geomagnetic Reference Field

Ma – Megaannum = one million years

MAB – Matchless Amphibolite Belt

MORB – Mid-Ocean Ridge Basalt

NZ – Northern Zone

OkSZ – Okahandja Shear Zone

OLZ – Okahandja Lineament Zone

SF – Southern Foreland

SGU – Geological Survey of Sweden (Sveriges geologiska undersökning)

SMZ – Southern Margin Zone

SP – Self Potential (or Spontaneous Potential)

SZ – Southern Zone

TDR – Tilted Derivative

VLF – Very Low Frequency

CONTENT

1. INTRODUCTION	10
1.1. RESEARCH BACKGROUND	10
1.2. RESEARCH PROBLEM DEFINITION	11
1.3. PROJECT OUTLINE	11
1.4. LOCATION	11
2. GEOLOGICAL BACKGROUND	13
2.1. PAN-AFRICAN OROGENY	13
2.2. REGIONAL SETTING; THE SOUTH ZONE OF THE DAMARA BELT	14
2.3. MATCHLESS AMPHIBOLITE BELT (MAB)	17
2.4. THE MATCHLESS DEPOSIT (MINE)	19
3. GEOPHYSICAL THEORY	20
3.1. MAGNETICS	20
3.2. THE EARTH MAGNETIC FIELD	23
3.3. GRAVIMETRICS	24
3.4. THE SELF POTENTIAL (SP) ELECTRICAL METHOD	27
4. DESCRIPTION OF INSTRUMENTS AND FIELD APPLICATIONS	28
4.1. MAGNETOMETER	28
4.2. GRAVITY METER	29
4.3. FIELD PROCEDURE FOR SELF POTENTIAL MEASUREMENTS	30
4.4. LABORATORY EQUIPMENT FOR PETROPHYSICAL ANALYSES	31
5. METHOD	32
5.1. DATA PROCESSING	32
5.2. BACKGROUND GEOPHYSICAL DATA	36
5.3. FIELDWORK DESCRIPTION	38
6. RESULT	40
6.1. ROCK CLASSIFICATION AND PETROPHYSICAL RESULTS	40
6.2. GRAVITY	41
6.3. MAGNETIC HORIZONS	41
6.4. SULFIDE MINERALIZATION	44

<u>7.</u>	<u>STRUCTURAL AND LITHOLOGICAL MODEL</u>	<u>45</u>
7.1.	DESCRIPTION	45
7.2.	MODEL RESULT	45
7.3.	DISCUSSION OF LIMITATIONS AND VALIDNESS OF THE MODEL	48
<u>8.</u>	<u>DISCUSSION</u>	<u>49</u>
8.1.	MASS EXCESS; GRADIENT AND FOLD HINGE	49
8.2.	MAGNETIC SIGNATURES	50
8.3.	IDENTIFICATION OF SULFIDE MINERALIZATION	51
8.4.	ELECTROMAGNETIC METHODS	51
<u>9.</u>	<u>FURTHER STUDIES</u>	<u>52</u>
<u>10.</u>	<u>CONCLUSIONS</u>	<u>52</u>
<u>11.</u>	<u>ACKNOWLEDGEMENTS</u>	<u>53</u>
<u>12.</u>	<u>REFERENCES</u>	<u>54</u>

1. INTRODUCTION

1.1. RESEARCH BACKGROUND

The Matchless Amphibolite Belt (MAB) is a prominent geological unit: a 350 km long and 0.5-3 km wide belt with mafic metamorphosed rocks (Miller *et al.* 1983), extending in a NE-SW direction across Namibia. The distinct linearity of the belt raises questions upon its formation and subsequent deformation and metamorphism (Miller *et al.* 2009). The belt is also of economical interest with several known metal deposits (Killick 2000). In Namibia the mining has long been the cornerstone in the economy.

What today constitutes Namibia is an important part in the understanding of the development of Gondwana. The MAB is believed to be a remnant of oceanic crust that formed under an extensional phase during the Damara Orogen that is a part in the development of Gondwana (Miller *et al.* 2008). The MAB is an important piece in the understanding of the geodynamical evolution on a large and small tectonic scale of the area.

From a research perspective, new information to support or test present generic and dynamic models is required. The use of previous not tested geophysical methods in an area may present new features of the present geological units which may answer or raise new questions.

1.1.1. PREVIOUS WORK

The Damara orogen, and the geological units within, has been subject to several geological studies resulting in different conceptual theories upon its formation and development. Martin and Porada (1977) identified two branches within the Damara Orogen, one sub-parallel to present day west-coast of Namibia and one intracratonic ENE-trending branch. The inland branch is referred to as the Damara Belt, the north branch of the coastal belt is called Kaoko Belt and the south Gariep Belt. Martin and Porada (1977) also discuss the occurrence and origin of the MAB. They conclude that MAB might compromise a collision boundary and that a gap between two plates must have existed.

Miller *et al.* (1983) give an extensive description of the geology of whole Namibia and describe the three belts' formation, stratigraphy, structure and metamorphism in detail. The formation of the three belts is suggested to have been initiated between 900 and 100 Ma with widespread fluvial deposition into three rifts trending away from a triple-junction. Continental rupture and formation of a buried mid-ocean ridge is proposed for the formation of the MAB, about 700 Ma.

Gray *et al.* (2006) summarized previous studies and presented new thermochronologic and geochronologic data for the Damara Orogen for improved interpretation of the deformational, metamorphic and cooling histories. The orogenesis in the Damara area is suggested to be confined between 580 and 500 Ma. Data support that the sedimentary rocks that formed during the Damara orogen were created in different deformation and metamorphic eras but consist of similar materials.

The review article by Gray *et al.* (2008) summarizes the Damara Orogen perspective in southwestern Gondwana, its geodynamic evolution, metamorphism and tectonic evolution and conclude that several uncertainties still prevails. Examples of such are the nature and size of ocean basins, their tectonic setting of ocean closure and the presence (or lack) of subduction system and subducting direction.

Description of the Matchless sulfide deposit formation and geochemistry is described by Klemd *et al.* (1987), Klemd *et al.* (1989) while studies of the sulfide mineralogy were performed by Cook *et al.* (1994).

In 1994 the High Resolution Airborne Geophysical Survey Programme was initiated to generate and distribute high-quality geoscientific data to assist mineral exploration in the country. The parameters for the high resolution magnetic and radiometric surveys are 200 m flight line spacing with 2500 m between tie-lines and a ground clearance of 80 m. The sampling distance was approximately 7 m (Hutchins and Wackerle 2007).

1.2. RESEARCH PROBLEM DEFINITION

Many geological studies have been made on the MAB, however published ground measured geophysical data is scarce (during the literature study, none was found within the area of survey). Geophysical measurement can identify geological features which are hidden under the overburden and thus not easily observable. In general geophysical data give information of large subsurface volumes (3D) of rocks while traditional geological mapping only studies the surface (2D). By the combination of the two, surface features can be connects to geophysical properties and thereby more information of the rock units can be obtained.

The MAB is an interesting and suitable candidate to test whether geophysical measurements can give new input to present day models and interpretations of the belt. Interesting in the sense that many uncertainties still prevail of the belt and the processes in relation to its formation. The belt is also interesting from an economical point of view since several mineralizations are associated with it. A lot of structural and geological data exist from the belt making it a suitable candidate to test the output of ground geophysical data.

1.3. PROJECT OUTLINE

1.3.1. AIM

The aim with this project is to test the potential of different ground geophysical measurements in obtaining new or confirm existing information of the belt and its surroundings. A three-dimensional model is aimed to be created of a limited area of the MAB.

1.3.2. RESEARCH OBJECTIVES

- i) To evaluate which geophysical methods are the most suitable in the area around MAB to collect new information of the belt
- ii) Evaluate if there are compositional differences regarding the geophysical properties in the rocks not observable by traditional geological mapping.
- iii) To compile a three-dimensional structural and lithological model based on previous and recently collected geophysical data.

1.4. LOCATION

The Republic of Namibia is a large (approximately 826 000 km²) and sparsely populated (2.3 million inhabitants in 2012) country. The climate is arid and approximately 46% of the surface consists of bedrock exposure. The MAB is a linear geological unit cutting through central Namibia (figure 1 and 2).

The area of study is located within the Friedenau farm, which is located about 40 km southwest of the capital Windhoek (figure 2). The MAB extends through the farm area and is easily accessible by road since the Matchless Mine is located here. The topography is undulating and the vegetation consists of dense shrub land with thorn bushes (figure 3). The whole region (Khomas) is located on a high plateau of approximately 2000 m elevation.



Figure 1 (left). The location of Namibia in southwest Africa. Windhoek is the capital of Namibia.

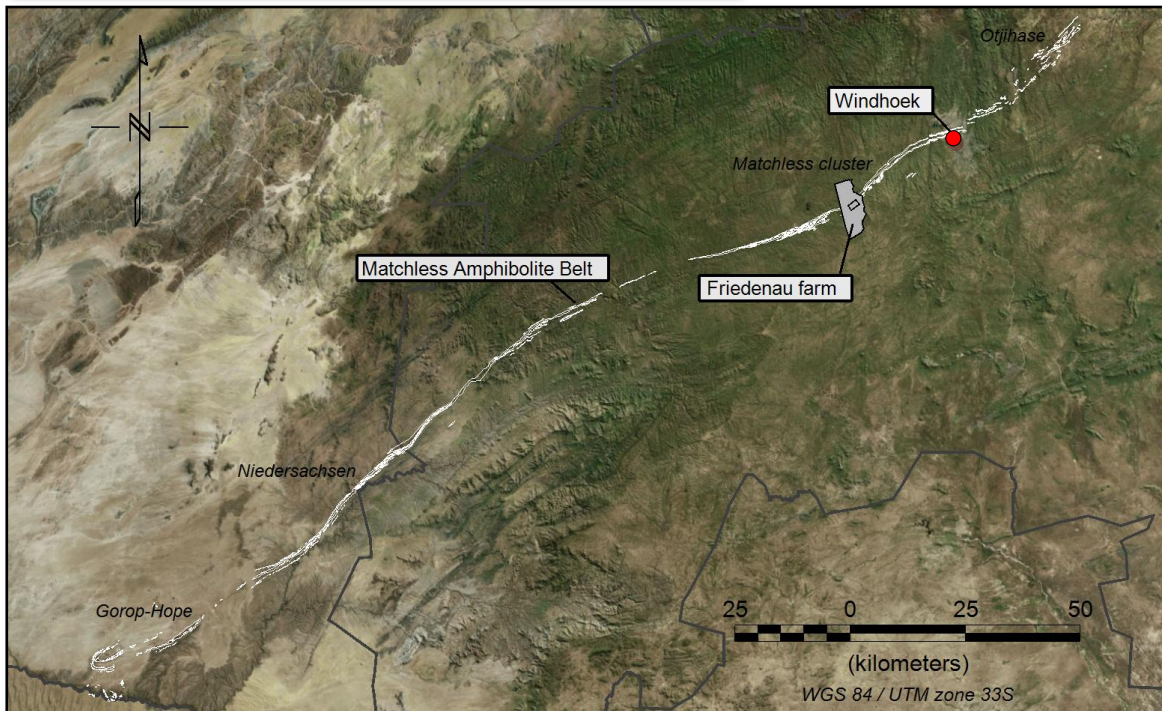


Figure 2 (below). The outline of the Matchless Amphibolite Belt and the location of the study area the Friedenau Farm together with the names of mineralization clusters.



Figure 3 (left). Undulating topography and thornbushes in the arid environment within the area of study. (Photo: Cecilia Jönsson, 2013)

2. GEOLOGICAL BACKGROUND

The Damara orogen is a part of the Pan-African orogen that occurred during the amalgamation of the Gondwana supercontinent.

2.1. PAN-AFRICAN OROGENY

The Pan-African orogenesis is considered to be an extended orogenic cycle with opening and closing of two large oceans during the Neoproterozoic to the earliest Palaeozoic (Kröner and Stern 2005). Three distinctive belts developed between the Congo and Kalahari cratons that became fused together.

Figure 4 shows the main cratons and belts that made up Gondwana at about 530 Ma, the box outlines the Damara area which today roughly corresponds to Namibia and in which the three belts are incorporated: the coastal belts of Kaoko and Gariep and the intracontinental Damara Belt.

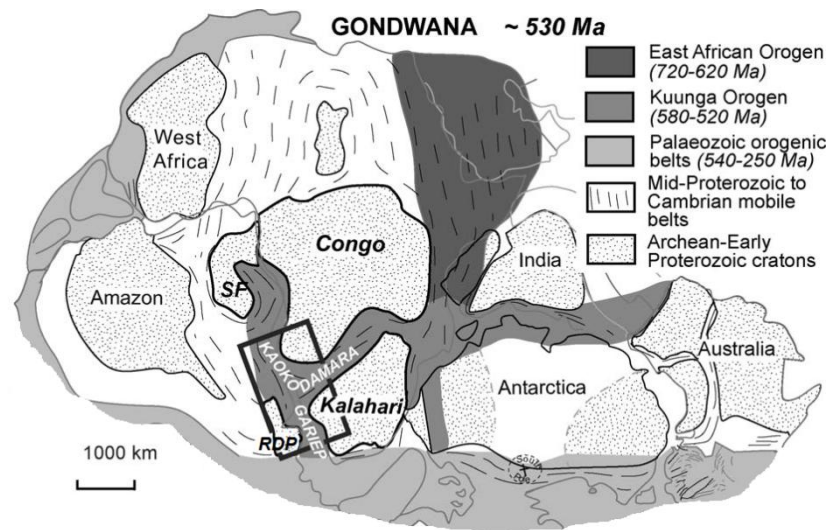


Figure 4. Map of the Gondwana supercontinent at about 530 Ma. The box indicates the location of the Damara orogen. RDP = Rio de La Plata Craton; SF = Sao Frisco Craton. (Modified from Gray *et al.* (2006)).

2.1.1. GEODYNAMIC EVOLUTION IN THE DAMARA AREA

The belts in the Damara Orogen and the Dom Feliciano belt in southern America evolved through intercontinental rifting, continental break up, spreading and reversal of plate motion and finally subduction and continental collision in the orogenic cycle leading to the amalgamation of the Gondwana supercontinent.

A schematic plate reconstruction of the Damara orogen from 780 to 480 Ma, as suggested by Gray *et al.* (2006), is presented in figure 5. There are many uncertainties regarding relative positions of the cratons as well as the presence and widths of oceans. The dimension of the Khomas Ocean has particularly been debated (e.g. Kroner (1977), Barnes and Sawyer (1980) and Martin and Porada (1977)).

The start of continental breakup between the Rio de la Plata craton (what today is South America) and the Congo and Kalahari craton has been constrained to a maximum age of 741 ± 6 Ma based on single zircon ages of low-grade metamorphosed rhyolites (Frimmel *et al.* 1996). The opening of the Adamastor and Khomas oceans are suggested by Gray *et al.* (2006) to have been contemporary with the breakup, but are a topic of debate. Prior the continental breakup, intracontinental rifting and rhyolitic volcanism occurred (5.a.).

Ocean closure and subduction was first initiated in the northern Adamastor Ocean, about 655 Ma (figure 5.b.) whereas opening continued in the south. The subduction direction is suggested to be eastward. Spreading or passive margins occurred elsewhere in the orogen with corresponding sedimentation.

Between 580-550 Ma eastward subduction started in the southern Adamastor Ocean at the same time as northward subduction of the oceanic plate between the Congo and Kalahari craton occurred, i.e. the closure of the Khomas Ocean (figure 5c). The north Adamastor Ocean developed into the Kaoko belt, with peak metamorphism and a transpression phase that started about 580 Ma. This predates the final closure of the belts developed from the southern Adamastor Ocean and the Khomas Ocean (Goscombe *et al.* 2005). For the Khomas Ocean (the Damara belt) final basin closure occurred between 510-495 Ma and for the south Adamastor Ocean (the Gariep belt) it occurred between 550 and 540 Ma (Gray *et al.* 2006).

What is referred to as the Pan African Orogenesis (Damara orogenic event in Namibia) is broadly bracketed between 580 and 500 Ma Gray *et al.* (2006) (figure 5.c, d and e) with final movements through 480 Ma. It coincides with the intense and widespread Kuunga Orogeny that united Gondwana about 530 Ma (figure 4).

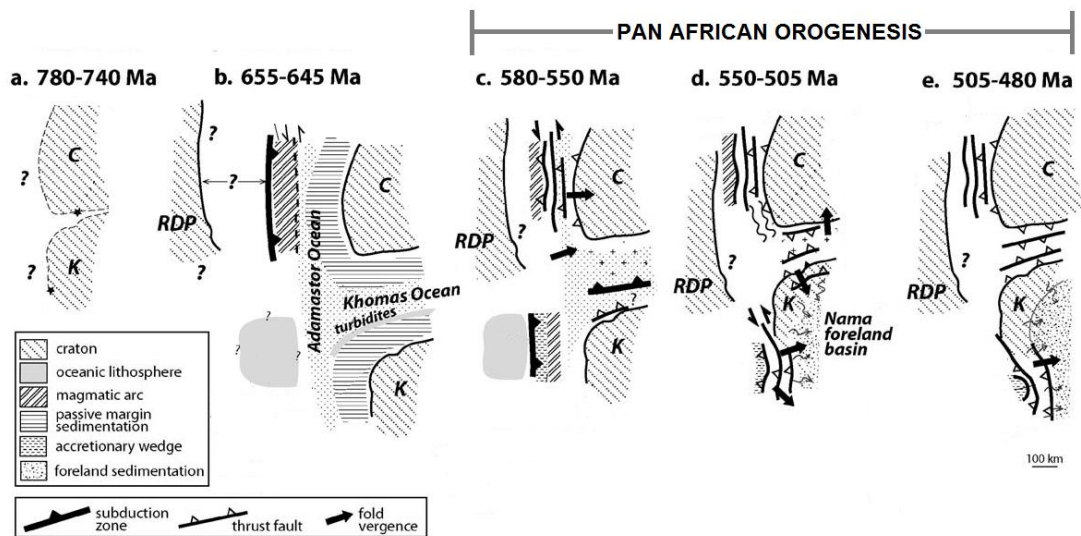


Figure 5. Schematic plate reconstruction of the Damara orogenic evolution involving the Congo (C), Kalahari (K) and Rio de la Plata (RDP) cratons. See text for description of each sequence. (Modified from Gray *et al.* (2006)).

2.2. REGIONAL SETTING; THE SOUTH ZONE OF THE DAMARA BELT

The Damara belt is divided into several zones on the basis of stratigraphy, grade of metamorphism, structure, etc. Figure 6 and 7 shows the zones of the Damara belt, from north to south: Northern Zone (NZ), Central Zone (CZ), Southern Zone (SZ), Southern Margin Zone (SMZ) and Southern Foreland (SF) (Gray *et al.* 2008). The Okahandja Shear Zone (OkSZ) (or Okahandja Lineament Zone (OLZ)) is the dividing line between CZ and SZ. In earlier descriptions the area was regarded as a wider zone which together with the SZ was referred to as the Khomas trough (or Khomas complex) suggested to be a remnant of the Khomas Ocean (Breitkopf and Maiden 1988). The MAB occurs about 10 km from the southern edge of the SZ (figure 6). A cross-section across of the Damara belt is shown in figure 7 and the location is indicated by the line A-A' in figure 6.

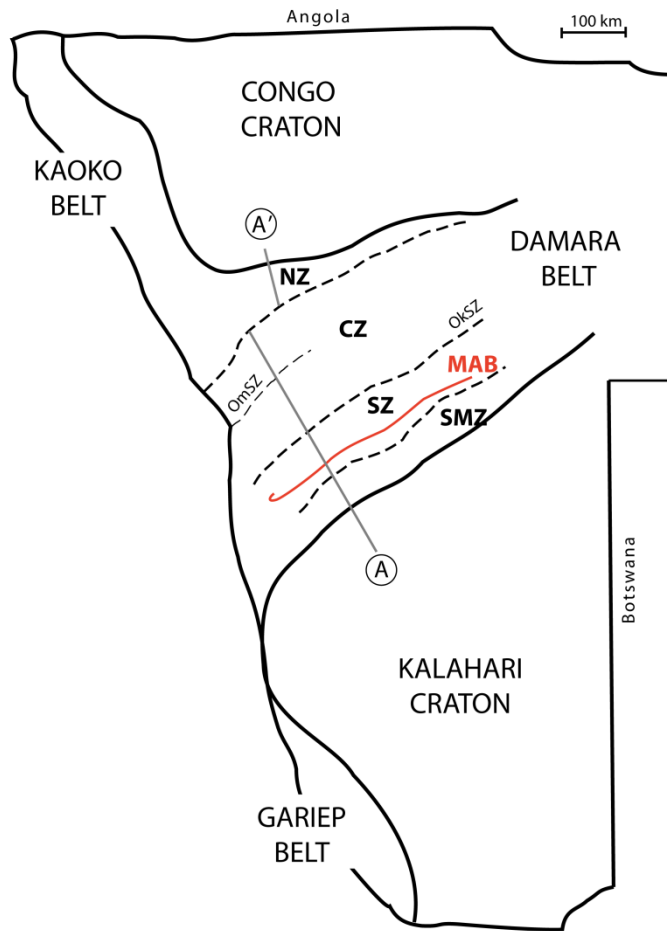


Figure 6. Map of Namibia showing the major belts and cratons and the different zones within the Damara Belt. The line A-A' show the position for the cross-section in figure 7. NZ: Northern Zone; CZ: Central Zone; OmSZ: Omaruru Shear Zone; OkSZ: Okavango Shear Zone; SZ: South Zone; SMZ: Southern Margin Zone. (Modified from Gray *et al.* (2008)).

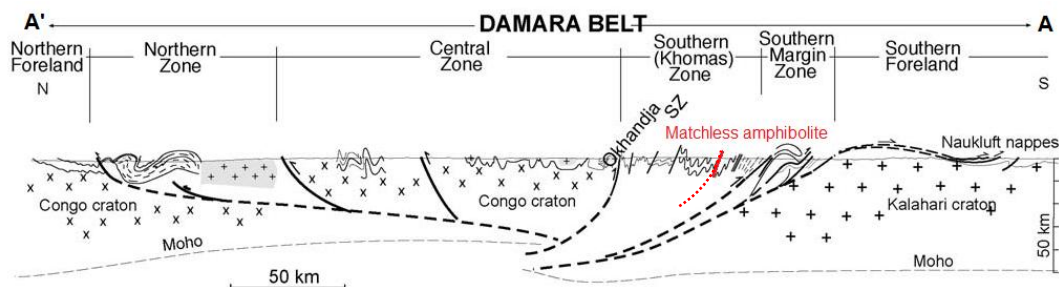


Figure 7. Simplified cross-section through the Damara Orogen, location of the profile is shown in figure 6. (Modified from Gray *et al.* (2006)).

2.2.1. STRATIGRAPHY

A simplified stratigraphy of the southern parts of the Damara belt is shown in table 1. The oldest stratigraphic unit in the Damara belt is the Nosib group and occurs in all zones, except the in SZ. The Nosib group consists of rift-related siliciclastic sediments of quartzite, conglomerates and arenites. U-Pb and Pb-Pb zircon ages from the upper Nosib group constrains the minimum age to approximately 750 Ma (Frimmel *et al.* 1996, Gray *et al.* 2008). The Kudis subgroup of the Swakop group is limited to the SMZ and consists of extensive marine sediments.

2.2.1.1. The Khomas Subgroup

The lowest formation in the Khomas Subgroup is the Chous Formation which is the most important marker in the sequence. Although it is variable across the orogen the deposition of Chous sediments marks a period of widespread crustal disturbances and local erosion of lower Damara rocks. The

origin of the sediments was first proposed to be glacial and glaciomarine but it has been disputed and it is suggested to originate from mass flow in relatively deep water. Miller *et al.* (1983) suggests that in some areas the source may be a combination of the two.

The Kuiseb Formation is present across the whole orogen and is a thick succession, at some places up to 10 km, of what have been pelites, feldspathic siltstones, sandstones and graywackes (Miller *et al.* 1983, Schneider 1983). At some areas graded bedding is present but all other primary structures have been destroyed by metamorphism and/or deformation. The mineralogy and lithological appearance changes with the metamorphic grade. In the NZ and the SZ which have undergone low-grade metamorphism, a well foliated, chlorite-muscovite-biotite schist characterizes the formation (Miller *et al.* 1983).

The sediments of the Kuiseb formation in the SZ consist of continental spreading and syn-tectonic sediments as well as passive margin sediments from the subduction and closure of the Khomas Ocean. In the remaining part of the orogen the Kuiseb Formation is only associated with spreading and continental separation (Miller *et al.* 2008).

In the SZ a difference in chemical maturity of the sediments across the zone is present. The maturity increases from the north edge of SZ southwards to about 10 km north of MAB, where the schists interbedded in the belt are characteristically less mature. South of the belt a rapid increase in maturity is observed again. The source of the differences in maturity is suggested to be differences in sedimentation processes. The schist in the north is a syn-tectonic fore-arc basin deposit overlying pre-tectonic sediments which are less mature and are deposited during spreading (Miller *et al.* 1983).

Table 1. Simplified stratigraphy table of the southern part of the Damara belt, approximate thickness in meters is given in brackets. (Modified from Barnes and Sawyer (1980) and Miller *et al.* (1983)).

Group	Subgroup	Formation	Lithology
Swakop	Khomas (14050)	Kuiseb (10000)	Schistose quartz-feldspar-mica metagreywacke and metapelite, garnet cordierite gneiss. Minor marble, quartzite, amphibole schist, marl, calc-silicate rock, skarn, graphitic schist and migmatite. (MAB)
		Auas (2400)	Quartzite, graphitic schist, quartz-mica schist, marble, conglomerate, amphibolite.
		Chous (1650)	Mixtite, pebbly schist, quartz-mica schist, quartzite, conglomerate. Dolomite, iron formation, amphibolites, calc-silicate rock, various turbiditic rocks and migmatite.
	Kudis	Hakos (2000)	Quartzite, minor turbiditic schist and quartzite.
		Blaukrans (900)	Graphitic schist, quartz-mica schist, marble, quartzite, conglomerate.
		Corona (400)	Marble, quartz-mica schist, graphitic schist, conglomerate, quartzite.
Nosib (11200)		Kamtas (6200)	Feldspathic quartzite and arkos – often pebbly, conglomerate.
		Duruchaus (5000)	Fissile metashale, micaceous metasiltstone, thin micaceous sandstone and arkose, conglomerate, meta-evaporites, albitolite, dolomite, quartz-mica schist.

2.2.2. STRUCTURE

The Khomas complex is continuous not only considering its stratigraphy but also the structure. In the northern SZ the structures are upright and then become south-east vergent and isoclinal towards southeast. The intensity of deformation increases in a south-easterly direction to such degree that close to and south of the MAB all older structures are overprinted and only a single composite NW-dipping foliation parallel to the bedding can be recognized (Miller *et al.* 2008).

2.2.3. METAMORPHISM, DEFORMATION AND COOLING AGES

The Kaoko, Gariiep and Damara belt all show separated and distinct deformational and cooling histories as recorded by individual $^{40}\text{Ar}/^{39}\text{Ar}$ samples (Gray *et al.* 2006). Figure 8 shows the deformation, metamorphism and cooling histories in the Damara belt and for the different zones within it. Regional cooling to temperatures of 300-350 °C occurred between 500-485 Ma in the SZ. Peak deformation/metamorphism in the CZ occurred at 530-500 Ma with thrusting onto the Kalahari craton from 495 Ma through 480 Ma (Gray *et al.* 2006).

The central Damara belt consists of a high-T/low-P, granite-dominated belt flanked by the N, the SZ and the SMZ that all have intermediate T/P metamorphism. The SZ underwent peak temperatures of 600 °C and pressures of 10 kbar (Gray *et al.* 2008).

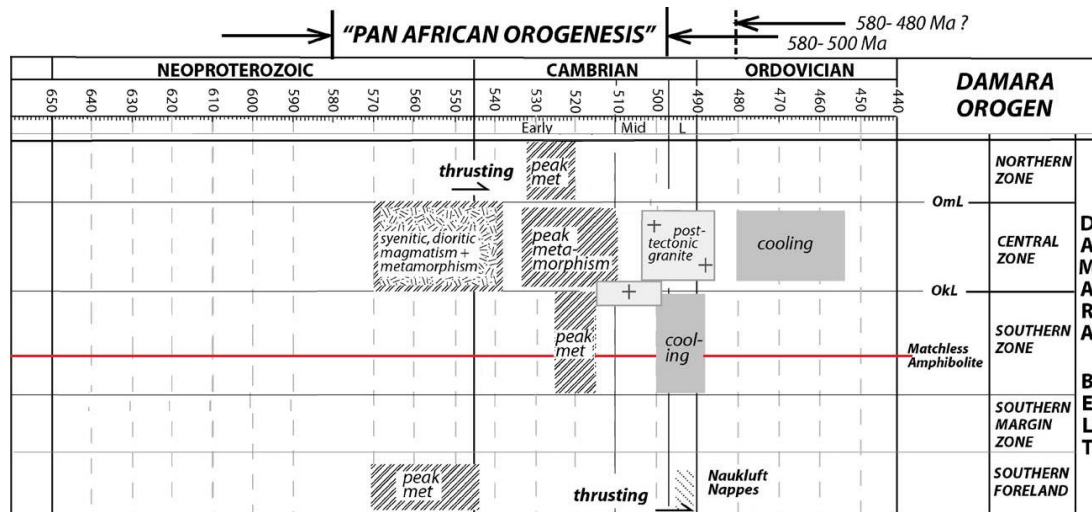


Figure 8. Time-space diagram showing the main magmatic, metamorphic and cooling events in the different belts in the Damara Orogen. (Modified from Gray *et al.* (2006)).

2.3. MATCHLESS AMPHIBOLITE BELT (MAB)

2.3.1. TECTONIC SETTING AND LITHOLOGY

The MAB is a remnant from the continental breakup and formation of the Khomas Ocean and consists of deformed and metamorphosed mafic volcanic and intrusive rocks (Breitkopf and Maiden 1988). The different mafic rocks are: amphibolite, gabbro, amphibolite schist and chlorite schist (Klemd *et al.* 1987) that are generally concentrated in two zones, 200-500 meter apart. The mafic rocks lie as layers and lenses within the Kuiseb schist and the thickness varies from about 3 km in the Windhoek area to half that size in the southwest. The number of amphibolite bands within the belt varies from a single up to ten bands in different areas (Killick 2000).

2.3.2. PETROGRAPHY AND GEOCHEMISTRY

The main constituents of the mafic rocks in the MAB are hornblende and/or actinolite, plagioclase and in many places also epidote. Minor and accessory minerals are chlorite, quartz, apatite, rutile and/or sphene and an opaque phase. Locally, minor biotite, calcite and garnet may occur (Breitkopf and Maiden 1988).

Breitkopf and Maiden (1988) analyzed the chemical composition of 52 samples of the metamorphosed mafic rocks from MAB. The samples were collected at three localities in the western, central and eastern part of the belt. Their result showed that the degree of fractional crystallization decreases from the west to the east along the belt. When plotted in TiO_2 versus Fe^*/MgO diagram (figure 9) almost all western samples plot within continental flood basalt (CFB) area whereas the eastern samples plot in the mid ocean ridge basalt (MORB) except one that plot in the overlapping field. For the central area the samples plot within MORB or in the overlapping area, except for one outlier.

The observed geochemical difference along the belt suggest that the western part was a depositional basin above a thinned continental crust whereas in the eastern part continental breakup occurred and an oceanic crust had formed (Breitkopf and Maiden 1988).

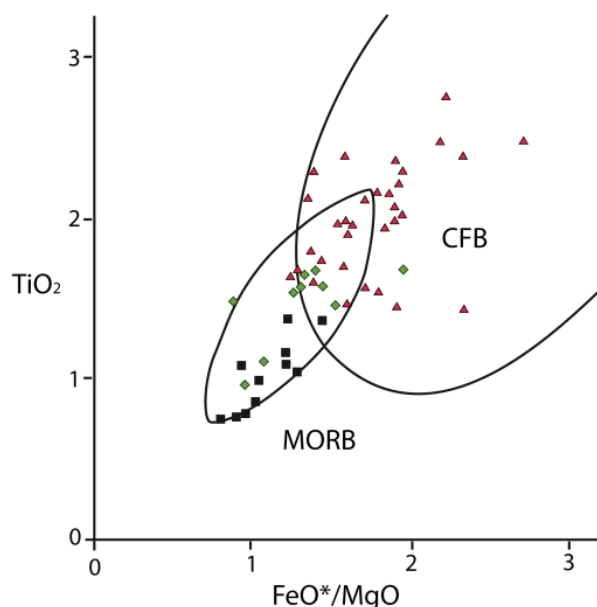


Figure 9. Plot of TiO_2 versus $\text{FeO}(\text{total})/\text{MgO}$ for 52 samples of the mafic rocks of the MAB. Red triangles: western samples; green diamonds: central samples; black Squares: eastern samples. MORB = mid-ocean ridge basalt, CFB = continental floor basalt. (Plot after Fodor and Vetter (1984), figure modified from Bretkopf and Maiden (1988)).

2.3.3. MINERALIZATION

The cupreous metal deposits along the MAB are interpreted as Besshi-type, volcano-exhalative sulfide deposits (VMS). The discriminating properties of a Besshi type deposit is that they are all enclosed in a sequence of clastic sedimentary rock and basalts in a marine environment with the host rock usually being clastic. The deposits form by exhalation on the sea floor as stratiform lenses and sheet-like accumulations, with comprehensive sedimentation occurring at the same time (Schoeman 1996). The ore assemblage is dominated by pyrite and/or pyrrhotite with significant amounts of Cu and Zn and minor amounts of Au and Ag.

Along MAB the metal deposits clusters in four areas which Killick (2000) interpreted as the location of palaeovolcanic centres. The clusters are: Gorop-Hope, Niedersachsen, Matchless and Otjihase (figure 2). Klemm *et al.* (1989) states that the beds of quartzite and magnetite quartzite associated with the mineralizations represent exhalative precipitation of chert and ferruginous chert in the vicinity of the vent system. The massive sulfide ores occurs in layers or lenses, disseminated or in stringer mineralization. The disseminated mineralization is believed to have been introduced below the seafloor and subjected to hydrothermal alteration in unconsolidated sediments (Killick 2000). In the Matchless mine (Klemm *et al.* 1987) and the Otjihase (Goldberg 1976) areas the massive ore are found within so called shoots. This is structurally controlled zones with higher concentration of ore material. The shoots are parallel to the main mineral lineation in a NW strike.

All deposits, except some in the Gorop-Hope cluster, are located to the southeast of the belt, i.e. in the structural footwall of the belt (Breitkopf and Maiden 1988). The main sulfide mineral is pyrite and pyrrhotite with associated chalcopyrite, sphalerite and minor amounts of cubanite and molybdenite. Deformation and recrystallization textures in the ore minerals indicate that they were emplaced before deformation. The deposits are closely associated with magnetite quartzite while the opposite is not true (Goldberg 1976). In the mineralized areas magnetite quartzite is always present in the vicinity, however magnetite quartzite also occurs in areas with no mineralization.

2.4. THE MATCHLESS DEPOSIT (MINE)

The Matchless deposit is located about 40 km southwest of Windhoek. The ore deposits consist of four sulfide lenses, commonly referred to as ore shoots (Killick 2000). Three of the ore shoots was mined for copper between 1970 and 1984 and the reported grades of metals during this period were: Cu 2.12% (mean), Zn 1-2%, S 14,8%, Ag 8g/t and Au 1g/t (Cook *et al.* 1994). The mine is currently (2013) operating again in the fourth shoot called the Western extension.

2.4.1. STRATIGRAPHY

The main amphibolite horizon in the mine area is 400 m thick and incorporated in the quartz-mica schist of the Kuiseb formation. Intercalated in the schist are additional amphibolite bands, layers of quartzitic rock, chlorite-rich schist and amphibole bearing schist. The sequence strikes in general to northeast and dips about 40° to the northwest (Klemd *et al.* 1987). The main copper deposits are located within sulfide bearing rocks forming the four ore shoots, located about 500 m south of the main amphibolite horizon. The three ore shoots previously mined is called the East, the West and the River shoot and are clustered together. Klemd *et al.* (1987) describe them to be approximately three meters thick, 120 meters in strike length and are plunging to the west at 30-35°.

Structurally below the ore-horizon, i.e. in the footwall, the ore grades out from massive sulfide to chalcopyrite and pyrite stringers, which all are concordant with the foliation. Laterally away from the shoots the proportion of pyrite decreases and the rock grades into normal Kuiseb schist. In the hanging wall the pattern is different; two meters away from the massive sulfide the pyrite is completely absent in the hanging wall schist. The structures in the hanging wall are randomly orientated and no clear patterns can be interpreted. The ore itself has a lot of fold structures (figure 10).

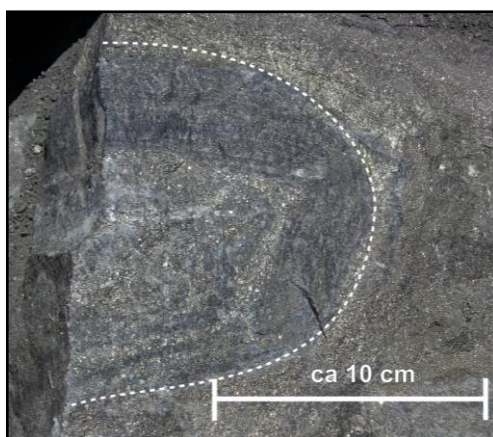


Figure 10. Fold structure in massive ore from the eastern extension ore shoot. (Photo: Cecilia Jönsson, 2013)

2.4.2. MINERALIZATION

The ore shoots are in general not homogeneous bodies but vary from massive to banded in character. Some remnant primary structures are present which have been modified by tectonic and metamorphic events. Klemd *et al.* (1987), Klemd *et al.* (1989) present a two-stage ore genesis model for the Matchless deposit. The initial exhalative deposition of sulfides was syn-genetic with the sedimentation of the Kuiseb sediments. Later pre or syn-metamorphic events led to partial remobilization of sulfides which formed in structurally controlled ore shoots. The redistribution occurred at a scale of at least decimeters according to Killick (2000). Klemd *et al.* (1987) also interpret various sulfide bands within the footwall Kuiseb schist as different pulses of hydrothermal exhalation during the ore-forming process.

3. GEOPHYSICAL THEORY

The basic theory of the magnetic, gravimetric and electric methods used during the project is presented below. An electromagnetic measurement (VLF) was also performed in the frame of the project but will only be addressed briefly and the theory section of electromagnetism is therefore omitted.

The conventions used in this text to define physical and mathematical properties are as follows: scalars (variables, parameters and constants) are given in *italic*, vectors in ***bold italic*** and units in square brackets, [], if not spelled out in the text. Unit vectors are denoted with circumflex, e.g. \hat{r} , and has the length of one (unit length).

3.1. MAGNETICS

The earth possesses a magnetic field that is essential for life on earth since it averts energetic particles emitted by the sun from hitting earth's surface. The source of the magnetic field lies mainly within the earth's liquid core. Rocks and minerals that are magnetic, or become magnetized by induction in the magnetic field, cause anomalies in the observed field. In geophysical applications these anomalies are used to obtain information of the crust, subsurface rocks and structures.

3.1.1. FUNDAMENTAL CONCEPTS AND DEFINITIONS

Magnetism can be described by potential field theory; potential field lines surround a magnetic body or around the flow of an electrical current. Magnetic poles always exist in pairs, a south (negative) and a north (positive) pole, with field lines going out from the north pole and in at the south pole (Sharma 1986).

3.1.1.1. Magnetic field strength (\mathbf{H}), flux density (\mathbf{B}) and intensity of magnetization (\mathbf{J})

A magnetic field with field strength \mathbf{H} [A/m], give rise to a magnetic flux. The flux per unit area, the flux density (sometimes referred to as the magnetic induction) is denoted as \mathbf{B} . This vector quantity can be described as "the closeness of the field lines" and is measured in volt-second (Vs) which in SI-units is expressed in Weber/m² or in Tesla [T]. In geophysical application the convention is "nanoTesla" [nT = 10⁻⁹T]. The flux density is given by:

$$\mathbf{B} = \mu\mathbf{H} \quad (1)$$

where μ is the absolute permeability of the medium on which \mathbf{H} is acting. For a non-magnetic media $\mu = \mu_0$ where μ_0 the permeability of vacuum with the numerical value of $4\pi \cdot 10^{-7}$ Ωs/m (Parasnis 1986). For any medium other than vacuum $\mu = \mu_r \cdot \mu_0$ where μ_r is the relative permeability. Introducing the magnetic susceptibility as: $\kappa = \mu_r - 1$, the flux density can be written as:

$$\mathbf{B} = \mu_0\mathbf{H} + \mu_0\kappa\mathbf{H} \quad (2)$$

The magnetic susceptibility is a characteristic constant for any magnetizable body and can for a rock be measured in field or determined in laboratory. The ratio μ_r is a pure number and so is the magnetic susceptibility. However κ is often described as fractions of "SI-unit" and in this report "μSI"=10⁻⁶ is generally used. For vacuum $\mu_r=1$ and $\kappa=0$ and equation 2 is reduced to equation 1. Any other media than vacuum has an extra magnetizing field, called the *intensity of magnetization* \mathbf{J} [A/m] induced by \mathbf{H} :

$$\mathbf{J} = \kappa\mathbf{H} \quad (3)$$

Generalized form of equation 1:

$$\mathbf{B} = \mu_0 \mathbf{H} + \kappa\mathbf{J} \quad (4)$$

(Parasnis 1986)

Both \mathbf{B} and \mathbf{H} are called magnetic field in a general use. Strictly \mathbf{H} is the measure of the output from a field-generating device and \mathbf{B} is the magnetic effect of that field. Outside a magnetic material they can be used interchangeable (Dunlop and Özdemir 2009). The earth magnetic field is denoted as \mathbf{F} and corresponds to \mathbf{B} in equation 4.

An intensity of magnetization can exist in certain materials even in the absence of an external magnetic field. This is called remanent magnetization (or just remanence) and is denoted J_r . The resultant J is the vector sum of J_r and J_i , where J_i is the induced magnetization. The importance of remanence in rocks and resultant magnetic field is further discussed in section 3.1.4.

3.1.2. DIA- AND PARAMAGNETISM

The magnetic response in a material depends on its magnetic properties which ultimately are determined by the atomic structure in the element. Materials can be divided into different classes depending on the response in a magnetic field. In diamagnetic materials a net opposed magnetic field will be produced in response to an external applied field. The individual current loops in the atom will align with the applied field but the orbital procession causes a weak opposite directed magnetic moment in each atom. Examples of diamagnetic minerals with weak and negative susceptibility are quartz, calcite and forsterite. Since the magnetic susceptibility is extremely weak any other form of magnetism, if present, will dominate. Diamagnetism is temperature independent (Dunlop and Özdemir 2009).

Every odd-numbered element has at least one electron with an unpaired spin and therefore a permanent magnetic moment. In a magnetizing field a partial alignment due to the resultant dipole moment arises. This is called paramagnetism and is one to two orders of magnitude larger than the diamagnetic effect. The paramagnetic susceptibility is temperature dependent and increased temperature lead to thermal disordering and a decrease of the magnetic susceptibility. More pronounced paramagnetic effect occurs in the transitions elements such as Fe, Co and Ni with multiple unpaired electrons. Examples of paramagnetic minerals are pyrite, amphiboles and biotites (Dunlop and Özdemir 2009).

3.1.3. FERRO-, ANTIFERRO- AND FERRIMAGNETISM

The magnetic response of rocks is dominated by ferro-, antiferro- and ferrimagnetic minerals. In contrast to dia- and paramagnetic materials these elements can retain a remanent magnetization in the absence of an external magnetic field (Dunlop and Özdemir 2009).

In ferromagnetic materials the moments of neighboring atoms are coupled parallel and the induced magnetization is parallel to the applied magnetizing field (figure 12.A). The spin moments of unpaired electrons couple magnetically with each other in small magnetic domains (size of about $1\mu\text{m}$) which give rise to a strong magnetization, two to three orders of magnitude larger than for the paramagnetic effect.

For ferromagnetic materials the intensity of the induced field increases linearly and is reversible if a weak external field is applied. For stronger fields the magnetization follows a hysteresis curve shown in figure 11. If the applied field is strong enough the magnetization will reach a saturation point, J_s , where no more magnetization can take place. Once the H-field is reduced after saturation only some magnetic domains return to former orientations and therefore a remanent magnetization will be left in the material. To remove the remanent magnetization a negative H-field, H_c , has to be applied. The intensity of magnetization of ferromagnetic materials decrease with increasing temperature, and at a critical temperature (T), the “Curie temperature” that is different for different materials, it completely disappears (Sharma 1986).

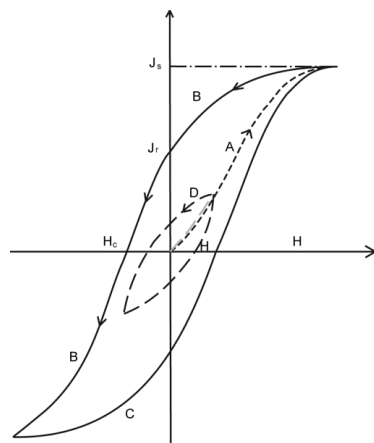


Figure 11. Hysteresis loop showing the cycle of magnetization of a ferromagnetic substance reaching saturation in the sequence A, B and C. The cyclic curve D, represent magnetization without saturation. (Modified from Sharma (1986)).

Antiferromagnetic elements are substances with susceptibilities comparable to paramagnetic material but with a non-linear temperature dependency. In these materials two sub-lattices with magnetic moments are orientated parallel to each other but with opposite directions (figure 12.B). Hematite is the most important anti-ferromagnetic rock forming mineral. In theory an antiferromagnetic material has no remanence, but if a field is applied perpendicular to the sublattices these will be deflected and a weak remanence will arise (Dunlop and Özdemir 2009).

Ferrimagnetism is a type of anti-ferromagnetism where the magnetic coupling is anti-parallel but with one of the two anti-parallel moments stronger than the other (figure 12.C). Practically all the constituents giving rise to high magnetization in rocks are ferrimagnetic. The most common magnetic minerals and their type of magnetism are listed in table 2.

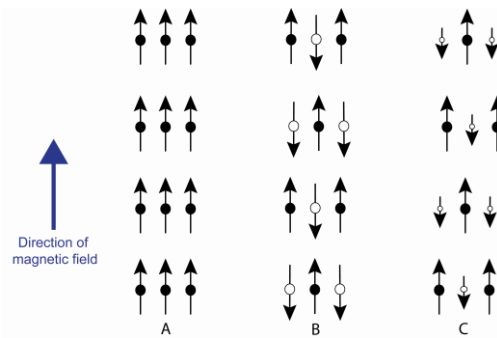


Figure 12. Illustration of magnetic moments in an atom for A: ferromagnetic, B: antiferromagnetic and C: ferrimagnetic crystals. (Modified from Sharma (1986)).

Table 2. Examples of minerals/elements of different magnetic classes. *In pure form, ilmenite is considered paramagnetic. (From Hunt *et al.* (1995) and Balsley and Buddington (1958)).

	Mineral/element	Composition
Ferromagnetic metals	iron	Fe
	nickel	Ni
Antiferromagnetic oxides	hematite	$\alpha\text{-Fe}_2\text{O}_3$
	Ilmenite*	FeTiO_3
Ferrimagnetic oxides	magnetite	Fe_3O_4
	maghemite	$\gamma\text{-Fe}_2\text{O}_3$
Ferrimagnetic sulfides	pyrrhotite	Fe_7S_8
		Fe_9S_{10}

3.1.4. MAGNETIC SUSCEPTIBILITIES AND REMANENT MAGNETIZATION OF ROCKS

The magnetic susceptibility of a rock is controlled by the type of minerals present, their concentration, grain size and their distribution. Yet the primary factor is the volume percent of magnetite (Balsley and Buddington 1958).

Remanent magnetization can be acquired in a rock in several different ways, both by primary and secondary processes. Primary remanent magnetization is attained when an igneous rock cools and solidifies from above the Curie temperature of its minerals (thermoremanent magnetization). For sedimentary rocks primary remanent magnetization is produced from the settling of magnetized particles to form consolidated sediments (Parasnis 1986). Secondary remanent magnetization in a rock is acquired after its formation during e.g. metamorphism and especially thermal metamorphism.

The ratio between intensity of remanent (J_r) and induced magnetization (J_i) is called the Königsberger ratio, Q , and is a dimensionless quantity. In the interpretation of magnetic anomalies it is important not only to consider that J_r may exceed J_i but also that the direction of J_r plays an important role as the remanent magnetization can enhance or counteract the induced magnetization (Reynolds 2011).

3.2. THE EARTH MAGNETIC FIELD

The origin of the magnetic field at the earth's surface has been a subject of discussion throughout history. The current model to describe the rise of the magnetic field is based upon two large dynamos in the liquid outer core that couples with each other and induces a magnetic field. The precise nature of the forces driving the dynamos is still to be explained. Changes in the magnetic field have been recorded within hundreds of years, a timescale much shorter than geological processes occurring in the crust or mantle. (Sharma 1986, Reynolds 2011).

3.2.1. THE MAIN DIPOLE FIELD

To a first approximation the magnetic field of the earth can be described by a dipole field generated by a dipolar electromagnet located at the centre of the earth with an angle of 11.5° to the rotation axis. The axis of this dipole magnet intersects the earth's surface at two points which are referred to as the geomagnetic poles. The position where the magnetic field is directed vertically is called the magnetic pole and does not coincide with the geomagnetic pole (figure 13), none of which coincide with the geographic poles. The position of both the geomagnetic (i.e. the tilt of the magnet) and the dip poles positions has changed through time. A circle on the earth's surface perpendicular to the dipole axis midway between the two is referred to as the geomagnetic equator. The line where the inclination is observed as zero is called the magnetic equator and does not have a circular form nor coincides with the geomagnetic equator (figure 13) (McElhinny 1973).

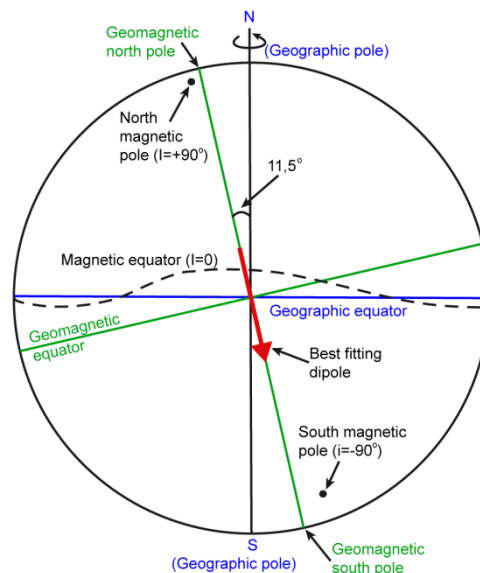


Figure 13. Illustration of the distinction between the magnetic, geomagnetic and geographic poles and equators. (Modified from McElhinny (1973)).

At any point on the earth surface a magnetic needle will orientate itself into a position determined by the geomagnetic field, F . The spatial distribution and intensity of the magnetic field is described mathematically by a model called the International Geomagnetic Reference Field (IGRF). The constants are updated every fifth year. IGRF makes it possible to relate magnetic surveys around the world to a common reference field (Reynolds 2011).

3.2.2. VARIATIONS IN THE MAGNETIC FIELD

Natural variation in the magnetic field occurs at time scales from daily to hundred year cycles. The scale of daily variations in the intensity of the field can vary between tens of nanotesla during a “normal magnetic day”, to several hundred over couple of hours in a “disturbed magnetic day”. The variations are caused by changes of the current in the ionosphere. The disturbed days are associated with magnetic storms which in turn are related to increased solar activity in a sunspot cycle (Sharma 1986). The diurnal variations can have considerable effect on the magnetic survey, during a “disturbed day” measurements should not be carried out due to the difficulties of correction. Long time variations that occur over centuries and decades are called secular variations and are not considered during field measurements since they are negligible (Reynolds 2011).

3.3.GRAVIMETRICS

In gravimetric surveying differences in gravity are measured at different locations in order to identify subsurface rock density variations. There are several factors causing changes in gravity, e.g. the positions of the sun and the moon tides, the altitude of measurement and the latitude. In geological work differences in density is used for classifying and identifying rock units. The method was first used in hydrocarbon exploration but instrumental developments have made the operation easier, faster and more accurate, which has lead to numerous applications of gravimetric surveys today.

3.3.1.BASIC PRINCIPLES

The basis of the gravity method is Newton's law of gravitation that states that the force of attraction between any two point bodies is directly proportional to the product of the masses and inversely proportional to the square distance, r , between the center of mass of the two bodies (equation 5).

$$\mathbf{F} = G \cdot \frac{m_1 \cdot m_2}{r^2} \cdot \mathbf{r} \quad (5)$$

G is the gravitational constant with the value $6.67 \cdot 10^{-11} \text{ Nm}^2/\text{kg}^2$. The force on a body at the earth's surface is given by replacing m_1 in equation 5 with the mass of the earth, M_E , and r with the radius of the earth, R . The earth is not a point mass but by approximating it with a homogenous sphere one can consider all mass to be located in a point at its centre. The force acting on a body is also given by Newton's second law of motion:

$$\mathbf{F} = m\mathbf{a} \quad (6)$$

where \mathbf{a} is the acceleration [m/s^2]. At the earth's surface the force due to the gravitational acceleration, \mathbf{F}' , is given by replacing \mathbf{a} with the gravitational acceleration, \mathbf{g}' . By combining Newton's two laws the gravitational acceleration \mathbf{g}' can be expressed as:

$$\mathbf{g}' = \frac{\mathbf{F}'}{m} = \frac{GM_E}{R^2} \cdot \mathbf{R} \quad (7)$$

The value of \mathbf{g}' varies about 0.7% between the equator and the poles. The variations is due to the fact that earth is not a perfect sphere, but flattens at the poles which yields a shorter \mathbf{R} and therefore a larger \mathbf{g}' compared to a position at the equator (Reynolds 2011).

A fictional¹ centrifugal force seen in the rotating frame of reference (the earth's surface) is introduced as \mathbf{F}_c (figure 14). The force is directed radially outward from the axis of rotation and is proportional to the distance from the rotation axis and the square of the angular velocity (Benson 1996). \mathbf{F}_c has to be considered in gravity measurements reducing the force due to centrifugal acceleration, see the vector addition in figure 14. The resultant is denoted gravity force, \mathbf{F}_g , with the resultant gravity \mathbf{g} . It is the gravity \mathbf{g} [m/s^2] that is measured in gravity surveys.

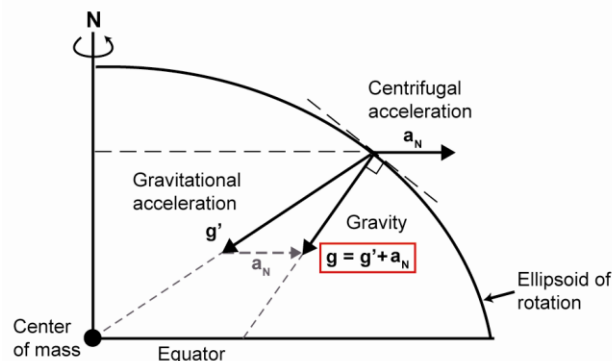


Figure 14. Representation of the resultant force due to gravity- and centrifugal force acting on a body at earth's surface. (Modified from Reynolds (2011)).

¹ Fictional in the sense that the force is not the result of a physical interaction but from the circular motion, i.e. the acceleration, of the reference frame.

In geophysical applications the unit *milligal* (mGal) is often used (Gal in honor of Galileo) or gravity unit, g.u for the gravitational acceleration. The conversion between the different units is shown in box 1.

$$\begin{aligned} 1 \text{ m/s}^2 &= 100 \text{ Gal} = 1 \cdot 10^5 \text{ mGal} = 1 \cdot 10^6 \text{ g.u} \\ 1 \cdot 10^{-5} \text{ m/s}^2 &= 1 \cdot 10^{-3} \text{ Gal} = 1 \text{ mGal} = 10 \text{ g.u.} \end{aligned}$$

Box 1

3.3.2. GRAVITATIONAL POTENTIAL AND REFERENCE FIELD

A point mass can be seen to have a surrounding attractive potential field which is directed towards the center of mass. The field can be represented by equipotential surfaces. The strength of the potential U , is defined as the work required to move a unit of mass from infinity to a position P at a distance r from the point mass (Parasnis 1986), mathematically expressed as:

$$U = \int_{\infty}^r F dr = -\frac{G \cdot m}{r} \quad (8)$$

The concept of potential is important considering a reference surface of the earth. The geoid comprises an equipotential surface where the acceleration due to gravity is orthogonal to the surface everywhere (Reynolds 2011). Another reference surface is the surface of a rotating ellipsoid similar to the earth's shape. The two surfaces will not in general coincide, see figure 15. In gravity application it is the geoid that is used as reference.

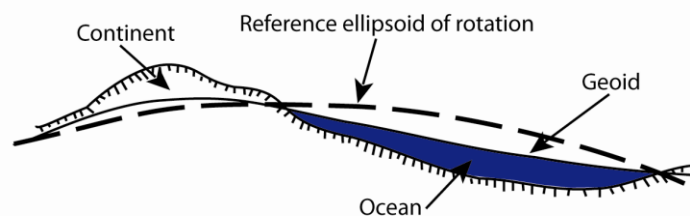


Figure 15. The difference between the reference ellipsoid of rotation and the geoid in relation to the earth's surface (not to scale). (Modified from Reynolds (2011)).

3.3.3. ROCK DENSITIES

The aim in gravity surveying is to relate gravity anomalies to different rock types, their structure and relation to each other. The density of rocks is most often determined from surface rock samples, which may be weathered or dehydrated, and not truly represent what is below ground. Error in density of the involved rocks is one of the most significant errors in gravity interpretation (Reynolds 2011).

The bulk density of rocks is determined by three different factors: the grain density of the rock-forming minerals, the porosity and the fluid in the pore spaces. It is important to separate bulk density and grain density as well as dry and wet bulk density, especially for sedimentary rocks. Dry refers to a fully moisture free state whereas wet is when the specimen is fully saturated with water. Either case is in practice difficult to obtain.

There is a range of densities for each rock type and the ranges are overlapping (figure 16). Some general trends can be observed in figure 16. Sedimentary rocks have, with some exceptions, lower density compared to igneous and metamorphic rocks, for igneous rocks the density increases with decreasing silica content. For metamorphic rocks increased metamorphism give increased density. Variations in density for a metamorphic rock may change over short distances and show greater variations within the same rock mass (Reynolds 2011).

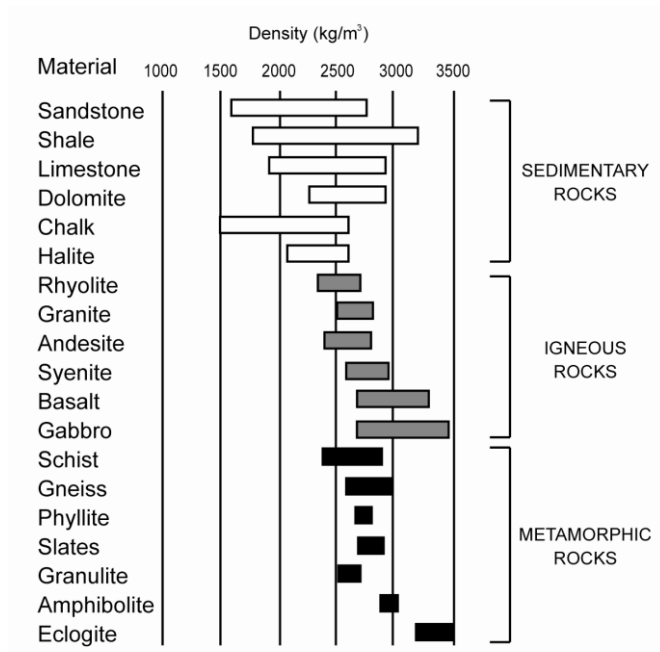


Figure 16. Density range for different rock types. (Modified from Reynolds (2011)).

3.3.4. DENSITY AND VOLUME MEASUREMENT

Volume and density determination of rock samples is based on Archimedes principle: “Any object, wholly or partially immersed in a fluid, is buoyed up by a force equal to the weight of the fluid displaced by the object”, equation 9. The magnitude of the buoyant force, F_B [N] is equal to the mass difference of weighing the sample in air and fully immersed in a water tank times the gravitational acceleration, g' (equation 10).

$$F_B = \rho_f \cdot V \cdot g' \quad (9)$$

$$F_B = m_a - m_w \cdot g' \quad (10)$$

The volume V [m³] for the sample is calculated by combining equation 9 and 10 into:

$$V = \frac{m_a - m_w}{\rho_f} \quad (11)$$

where ρ_f is the density of the fluid into which the sample is immersed (i.e. water), m_a and m_w is the mass of the sample weighted in air and immersed in water, respectively. The density of water is temperature dependent and should be kept constant. The value for ρ_f of water at a temperature of $25 \pm 1^\circ\text{C}$ is $997,1 \pm 0,3 \text{ kg/m}^3$ (Puranen *et al.* 1993). The density for the sample ρ [kg/m³] is then obtained by:

$$\rho = \frac{m_a}{V} \quad (12)$$

3.4. THE SELF POTENTIAL (SP) ELECTRICAL METHOD

The self potential or spontaneous potential (SP) method is one of the oldest geophysical methods, developed as early as 1830 (Reynolds 2011). The technique is based upon the existence of different electrical potentials between different locations in the ground. When two electrodes are put into the ground and connected by an electrical conductor (cable) an electrical current will flow between them which may be detected by a sensitive voltmeter. Under normal conditions it ranges between a few millivolts to tens of millivolts. Over sulfide mineralizations (containing pyrite, chalcopyrite and other good electronic conductors) or above graphite bearing rocks, voltages of several hundred millivolts up to a volt have been observed (Parasnis 1966).

Although the method is easy to apply, needs quite simple equipment and is relatively fast to execute in field and thereby of low cost, it is today not widely used (Nyquist and Corry 2002). This may be due to a history of unsatisfactory repeatability combined with insufficient models to explain the observed features. Although questions remain about the source mechanism for SP, it has proven to be a very successful method, especially in sulfide deposits prospecting. Corry (1985) showed an easily attainable standard of reproducibility in SP data on a 13 km survey line.

3.4.1. DIFFERENT THEORIES OF THE SELF POTENTIAL PHENOMENA

Electrical self potential arises from a range of mechanisms which broadly can be divided into two classes; 1) background potentials and 2) mineralization potentials. The background potentials range from less than a millivolt to a few tens of millivolts that may be positive or negative (Parasnis 1966). The background potentials arise from several well understood mechanisms such as: diffusion and membrane potentials, bioelectric potentials, streaming potentials.

The mineralization potentials are always negative and one order of magnitude larger than the background potentials. Several different models have been proposed to explain the phenomena but the mechanism is still not completely understood. One of the most cited models is the *geo-battery model* presented by Sato and Mooney (1960). They proposed that the ore body could be compared with a battery. Oxidation processes are dominant in the lower part of the ore body, below the water table and a reducing environment is present above forming an electrochemical half-cell. The ore body permits flow of electrons which implies that the upper surfaces become negatively charged, hence, a negative potential is measured above the ore body (Reynolds 2011). This model however fails to explain several observed features, outlined in a paper by Corry (1985), such as the amplitude of the anomalies, large gradients, lack of a positive pole etc.

Nyquist and Corry (2002) postulate an alternative model, the *redox SP model*, where the wire between the electrodes, and not the ore body, completes the circuit between oxidizing and reducing zones. No current will flow unless the electrodes are placed in separate environments where the difference in redox potential² will allow spontaneous reactions.

A third model suggested by Hamilton *et al.* (2008) accounts for the presence of SP anomalies over both disseminated and massive sulfide bodies, or any other polarizable substance. In analogy with the geo-battery model each isolated sulfide grain develops a SP cell around it. This is driven by a slight oxidation-potential difference between the ends of the grain (figure 17). The individual grains can be seen as batteries stacked in series with additive voltages, and thereby no theoretical upper limit for the voltage. The work of Hamilton and Hattori (2008) on a forest ring³, with no known mineralization present, showed that redox gradient and SP anomalies are spatially correlated.

² Redox potential is an intrinsic property of a chemical species and is a measure of the tendency for a substance to acquire electrons (measured in volts).

³ Forest ring are large (commonly more than 500 meters) circular feature of stunted tree growth in boreal forests.

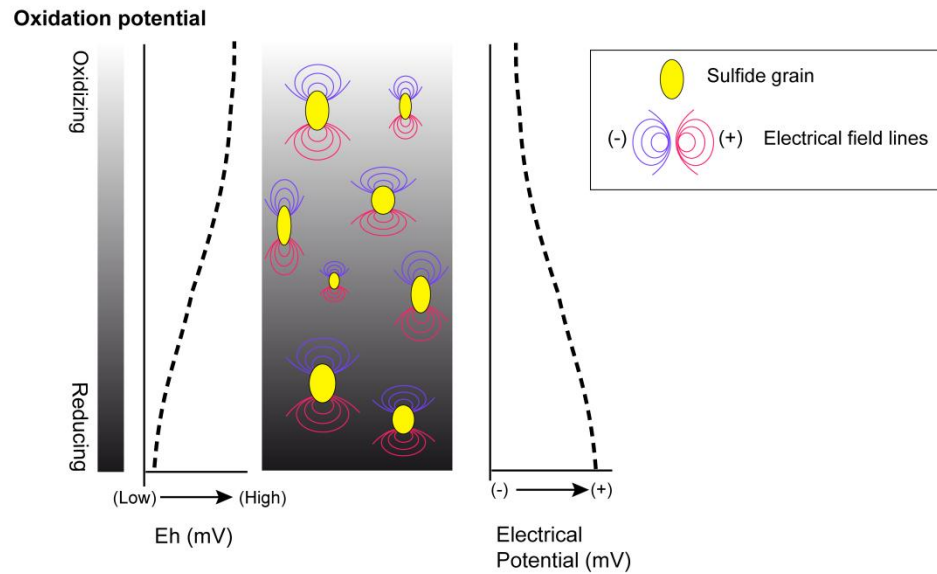


Figure 17. Development of electrical dipoles around individual sulfide grains in a strong redox gradient. (Modified from Hamilton *et al.* (2008)).

4. DESCRIPTION OF INSTRUMENTS AND FIELD APPLICATIONS

4.1. MAGNETOMETER

A magnetometer is used to identify magnetic bodies and objects. The magnetometer measures the amplitude of the earth magnetic. Magnetic responses from minerals and rocks enable identification of subsurface structures and bodies.

There are several different types of magnetometers with different operation techniques. The one used during this project was a resonance magnetometer of alkali vapor type: a G-859 Mining Mag cesium vapor magnetometer from Geometrics (figure 18), owned by GSN. The magnetometer is carried as a backpack and records the magnitude of the magnetic field (the sensor, A in figure 18) and the position automatically (GPS, B in figure) during surveying.

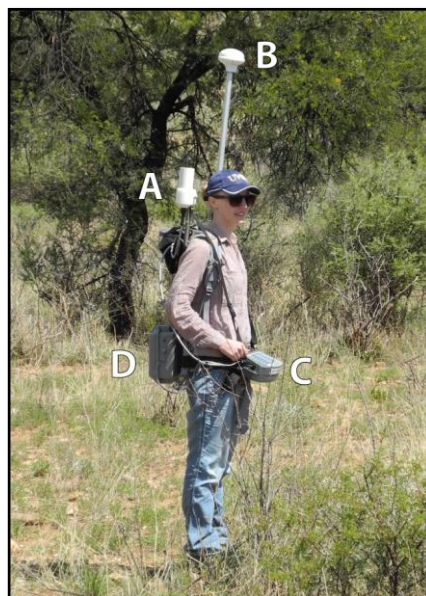


Figure 18. The G-859 Mining Mag cesium vapor magnetometer used in the project. A - sensor, B - GPS, C - monitor, D - battery case. (Photo: Carl-Axel Triumph, 2013)

4.1.1. BRIEF THEORY

The theory of operation of the cesium vapor magnetometer is based upon the theory of Zeeman splitting. The distance between different energy levels within an atom depends on the magnitude of an external (to the atom) magnetic field (Smith 1997). An external magnetic field with large magnitude yields a larger splitting of the energy levels. If the difference in energy splitting could be measured the external field could be determined. This is the fundamental concept of the optical pumping technique used in the cesium vapor magnetometer type.

4.1.2. LIMITATIONS

The magnetometer has an operating range of 18 000 to 95 000 nT and a gradient tolerance of >20 000 nT/meter. The sensitivity is 0.01 nT and the error due to changing the position of the sensor in a constant magnetic field is less than ± 0.5 nT (Geometrics 2005). The measurements performed in the present project did not pass the technical limitations of the instrument except in suspected cases of very large gradients.

Field disturbances from magnetic objects may limit the accuracy and validity of the measurements and are important to note. Magnetic noise may be caused by cars, metal sheds, power lines, metallic fences etc or metal objects on the person that perform the measurement. Disturbances may be non-avoidable and field notes with correlating coordinates are of outmost importance for later correction of data.

4.2. GRAVITY METER

The gravitational acceleration on earth varies roughly between 9.780318 and 9.832177 m/s^2 (=978031.8 and 983217.7 mGal) from the equator to the poles. Anomalies in the range of 1 to 10 mGal and sometimes even less (down to 0.1 mGal) due to density variations of rocks, are the aim of identification in gravity surveys (Parasnis 1986). From these numbers it is clear that very precise instruments are required for the measurements. Gravity is measured by a gravity meter and the position and elevation is measured by an external system in order to correct the data. The measurement is done point wise.

Gravity can be measured both absolute and relative. An absolute measurement requires a very careful experimental procedure and takes long time. For most geophysical and geological applications it is only the difference in the gravity field that is important in order to map and identify features and different rock bodies. Relative measurements are used in almost all geophysical applications due to its time efficiency and easily handled instrument, it is however possible to relate a relative survey to an absolute gravity station in order to make the measurements comparable.

The principles of the modern relative gravity meter are spring mechanics, where the extension in a spring due to the pull of gravity on a mass mounted on the spring is measured. The relative gravimeters can be divided into stable and unstable depending on their working principle. The stable is essentially a highly sensitive balance where one measures the extremely small displacement from equilibrium when the gravity changes. The unstable gravimeters are designed to measure the force necessary to bring a sensitive element back to equilibrium when displaced in a gravitational field (Sharma 1986). There are different types of stable and unstable gravimeters. The basic principle of an unstable relative gravimeter, an Autograv Scintrex CG-5 (figure 19) used in this project will be presented. The instrument used is owned by the GSN.



Figure 19. The gravity meter used in the project is of the type Autograv Scintrex CG-5. (Photo: Patrick Johansson, 2013)

4.2.1. SCINTREX AUTOGRAV CG-5

The sensitive element in the Scintrex CG-5 is based on an elastic molded quartz system. The force on a mass due to gravity is balanced by a spring and a small electrostatic force. An automated feedback circuit changes the electrostatic force on the mass to bring it back to the zero position. The feedback voltage is the measure of the relative gravity at the measurement site (Scintrex 2009, CG-5 Manual, Scintrex Limited, Concord/Ontario)

4.2.2. POSITION AND ALTITUDE DETERMINATION

Accurate altitude and position determination is of most importance in gravity surveys. To achieve an accuracy of ± 0.1 mGal the N-S position must be known within ± 10 m and the elevation within some centimeter (Reynolds 2011). The system used for altitude and position determinations were a Trimble R6/TSC 3 owned by GSN. In this study repeated position measurements at the same location did not deviate more than one meter and repeated altitude determinations yielded a discrepancy of less than one centimeter.

4.3. FIELD PROCEDURE FOR SELF POTENTIAL MEASUREMENTS

A comprehensive field manual for SP measurements is written by Corry *et al.* (1982) where different sources of disturbance (telluric currents, cultural noise, electrode problems etc) are discussed and methods for avoiding and correcting for these are presented. In this project a somewhat simplified measurement procedure was used.

The SP equipment used is showed in figure 20. It consists of two non-polarizable Pb-PbCl electrodes (1 in figure 20A and B), cable drums (2), a high impedance voltmeter (3), a geological hammer (4) and a GPS (5). The use of non-polarizable electrodes is preferred over normal metal electrodes since electrochemical reactions between the metal and the moisture in the ground can build up charges which may obscure the small natural self potential (Parasnis 1966).



A



B

Figure 20.A. (left) Equipment used for SP measurements, see text for description. **B:** (top) Close up of the non-polarizable Pb-PbCl electrode. (Photos: Cecilia Jönsson, 2013)

A base electrode is planted in neutral ground in a hole of about 0.3 m in depth and kept fixed during the measurements. The same base station should be used for the best correlation between measurement lines and days. The base electrode is connected to one end of the cable then the electrode was covered with plastic and the hole filled with soil and finally covered by branches and grass. This procedure is to ensure that the soil moisture and temperature is kept as constant as possible during the measurements as changes in these two parameters otherwise may affect the electrode potential. The rowing electrode is then placed at the measurement points along the survey lines. During a reading the electrode is shaded from the sun since ultraviolet radiation may change the electrode potential (Corry *et al.* 1982).

4.3.1. ERRORS AND LIMITATIONS

The precision and accuracy of the measurement are difficult to estimate since no repeatable measurements were done and no drift measurements of the electrodes were made. Corry (1985) states that data is seen to repeat within ± 20 mV within a range of 750 mV which may be used as guidance. The profiles were measured during different days and therefore the base station conditions may vary and thereby the potential between different days. This error is however assumed to be negligible for the purpose of the measurement.

4.4. LABORATORY EQUIPMENT FOR PETROPHYSICAL ANALYSES

Petrophysics is the study of rocks' physical properties. The following parameters were measured in this project:

- density and volume
- magnetic susceptibility
- strength of remanent magnetization

The measurements were performed at the petrophysical laboratory at SGU in Uppsala. The procedure followed SGU standards.

4.4.1. MAGNETIC SUSCEPTIBILITY

Magnetic susceptibilities were measured in a low-frequency AC bridge apparatus. The instrument is optimized to measure the susceptibility of hand specimens of maximum dimensions about 10 cm ($V=100-300$ cm³). The instrument is first balanced by a measurement without a sample. Then the sample is inserted into the coil which becomes unbalanced and changes the output voltage. The susceptibility in the direction of the coil axis is proportional to the output voltage. For a complete description of the apparatus and derivation of formulas see Report of investigation No. 28 “*Apparatus for the measurement of magnetic susceptibility and its anisotropy*” by Puranen and Puranen (1977).

4.4.2. REMANENT MAGNETIZATION

A Remanence Meter R4 (figure 21) developed by the Geological Survey of Finland was used for the remanent magnetization measurements. The space where measurements are performed is shielded with two μ -metal (nickel and iron alloy) cylinders in order to remove any disturbing magnetic field (e.g. the earth's magnetic field and local sources) from the surroundings. The sample to be measured is fitted into a box (figure 21) and fixed so that it would not change position upon turning the box.

The change of the magnitude of the magnetic field is measured with and without the sample placed in the instrument. By measuring in opposite position of the sample the induced magnetization is removed and the remanence in that direction is measured. The box with the sample is rotated into six different positions and the remanence in three orthogonal directions is obtained (Puranen *et al.* 1993).

The total intensity of the remanent magnetization J_r is given by equation 13.

$$J_r = \sqrt{J_{r,x}^2 + J_{r,y}^2 + J_{r,z}^2} \quad (13)$$



Figure 21. The Remanence Meter R4 used in the project. In front of the apparatus are the boxes in which the sample are placed. (Photo Cecilia Jönsson, 2013)

4.4.3. ERRORS AND PRECISION OF LABORATORY MEASUREMENTS

The weighing error of the setup is maximum 0.1 grams for a typical block of $m_a = 500$ g and $V = 200$ cm³, the relative maximum error of repeated density and volume estimates is about 0.1% according to Puranen *et al.* (1993). For dry porous samples the densities are systematically underestimated.

Repeated measurements were done on four samples. Two of them had relative maximum error smaller than 0.1% while the other two had a relative error less than 2% for the volume and density measurements. The larger relative error than stated by Puranen *et al.* (1993) is probably due to the high porosity of these samples. For the susceptibility, all repeated measurements were within 10 percent of each other. The error in the remanence measurement is larger for all samples. One sample can be disregarded as the value is below the detection limit of 30 mA/m. For the other samples the error is 10-15%, some of the error may be caused by the sample is not located in the same position in the box during the measurements.

5. METHOD

5.1. DATA PROCESSING

Data processing is here considered to consist of quality assurance of the data as well as the subsequent processing of the results in order to facilitate interpretation.

5.1.1. MAGNETIC DATA

Quality assurance of magnetic data is necessary to remove all contributions to the observed field other than those caused by the subsurface sources. This process was divided into three steps:

- Removal of zero values and outliers
- Removal of data based on observed disturbance features
- Diurnal correction

A processing routine was written in *MATLAB R2012b* by MathWorks and the data were visually examined and additional filters were applied in the program *Oasis Montaj* by Geosoft Inc.

Erroneous data, such as zero values and single extreme values, are readily identifiable in the raw data. The source for these errors is unknown but it was observed that extreme single values often occur at the start and end of a survey line. It is possible that some of the zero values are due to a too large gradient in the magnetic field, i.e. larger than the gradient tolerance of the magnetometer. This was considered by comparison between the location of errors (not related to start and stop) and airborne magnetic data.

During the field measurements the locations of disturbance features were noted in order to be able to correct for this in retrospect. Examples of disturbances are gates, metal waste on ground and power lines nearby. The values of the magnetic data on these locations were controlled, i.e. did or did it not yield a deviation in the field, and the magnitude was compared to what would be expected from the airborne magnetic data.

5.1.1.1. Diurnal correction

A diurnal correction was performed which was based on data from the Tsumeb magnetic station, a base station recording the total intensity of the earth magnetic field every minute. The station is located about 400 km north-northeast of the Matchless mine area. The diurnal variation at the measurement site was assumed to be same as at the Tsumeb magnetic station. A reference value of 25 550 nT (average total magnetic field value in Tsumeb) was selected and the deviation from this value calculated and correction applied on the ground measured magnetic data.

Test of the diurnal correction showed that a larger discrepancy was obtained on diurnal corrected data compared to uncorrected at locations measured repeatedly but on different days. A possible explanation to this is that the difference in diurnal variations between the Matchless Mine area and the Tsumeb area are greater than assumed. Further processing and filtering to facilitate interpretation were therefore done on non diurnal corrected data.

5.1.2. REDUCTION OF GRAVITY DATA

Before analysis of gravity data can be done, several processing steps have to be applied to eliminate all other factors than the density as a source for gravity variations. Factors affecting the gravity reading are both due to instrumental errors and of natural causes. Some corrections are automated in the instrument while other corrections are made by means of the software *Oasis Montaj* version 7.2.1, 2010 by Geosoft Inc, with the *Gravity and Terrain Correction* extension. A short description of the corrections performed on the data is presented below.

5.1.2.1. Drift

Long term drift in the elastic system in the gravimeter is an unavoidable error caused by creep in the quartz spring. The drift is considered to be linear (SCINTREX 2009) and can easily be corrected by making measurements at a reference location at the start and end of each surveying day.

5.1.2.2. Earth tide correction

The earth tide correction corrects for the gravity differences due to the position of the moon and the sun that cause deformation of the earth. The correction is generated in the software of the gravimeter based on the Longman formula (Longman 1959, SCINTREX 2009). The operator enters the latitude, longitude and the difference in time to GMT into the gravity meter before the start of surveying to obtain the correction.

5.1.2.3. Latitude correction

Latitude correction is necessary in order to remove the effect of the decreasing gravity from the poles towards the equator. The decrease in gravity is due to the increasing distance between the earth's centre and its surface. The effect of increase in gravity due to more mass below is also present but much smaller. The net effect is a decreasing gravity with decreasing latitude (Parasnis 1986).

5.1.2.4. Free-air correction

The gravity decreases with increasing elevation due to a larger distance to the center of mass of the earth (equation 14). The free-air correction, C_F , is the difference between the gravity measured at a reference plane (usually the geoid) and at an elevation h [m], with no rock mass in between and is given by:

$$C_F = \frac{2 \cdot g_0 \cdot h}{R} \quad (14)$$

where g_0 is the gravity at the reference level and R is the earth's radius (Sharma 1986).

5.1.2.5. Bouguer correction

The Bouguer correction corrects for the attractive force due to the increased rock mass between the gravity station and the reference surface, normally the geoid. The rock mass is treated as a horizontal slab with thickness equal to the elevation difference. The gravity attraction is then:

$$C_B = 2\pi \cdot G \cdot \rho \cdot h \quad (15)$$

where ρ is the density of the rock mass and G is the gravitational constant (Sharma 1986). The combined effect of the free-air and Bouguer correction is that the gravity decreases by approximately 0.2 mGal/m (Sharma 1986). The corrections are automatically performed by the Geosoft executable for gravity data in *Oasis Montaj*.

5.1.2.6. Terrain correction

The Bouguer correction assumes a horizontal slab meaning that the effect of the topography around the measurement point is not taken into account. A measurement done in a valley will be affected by the surrounding hills due to an attractive, somewhat upward directed, gravitational force. The same argument is valid if the measurement is done on a hill, but then the valley corresponds to a mass deficiency (figure 22) (Sharma 1986). To correct for this effect a terrain correction based on a digital elevation model (DEM) is performed. The DEM used in this project was 30×30m.

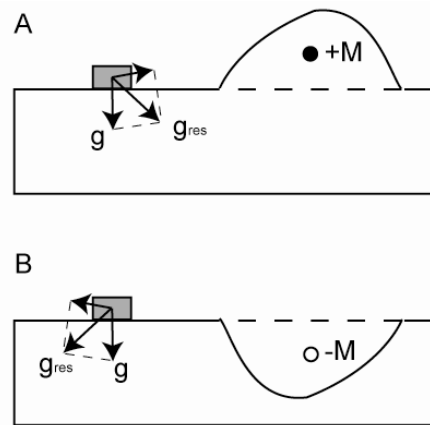


Figure 22. Principle of terrain correction with A) mass excess and B) mass deficiency.

5.1.2.7. Regional trend

Once all the above described corrections are made a gravity anomaly map can be produced. The accuracy depends on measurement point density and the complexity of the mass variations. If there is a regional trend in the data this can be calculated and subtracted in order to enhance near surface anomalies. For trend corrections the gravity at a large scale must be known to obtain a good basis for the correction.

5.1.3. PRESENTATION OF GEOPHYSICAL DATA

5.1.3.1. Gridding

Gridding and interpolation of the discrete geophysical data is necessary to be able to visualize data in a continuous manner (on a map) and to facilitate interpretation. The geographical distribution of the data can be in lines, a mesh or in a random manner, depending on the survey type. In order to interpolate between the data points a grid with a specified cell size is created. The cell size should be determined so that the resolution of the original dataset is not lost and at the same time a continuous surface is obtained. The best interpolation method to use for the data depends on the distribution. In the present project the minimum surface curvature gridding was used. The method is described by Dunlop and Özdemir (2009). The interpolation surface is analogous to a surface passing through each data point in the smoothest possible manner i.e. with a minimal curvature.

5.1.3.2. Filters

Gravity and magnetic potential-fields represent the sum of anomalies caused by sources at different depths, from the earth's surface to the core. Deep bodies produce long-wave responses and shallow bodies can produce both long and short wave-lengths. In order to resolve near-surface anomalies the long-wave regional field should be removed.

All processing was performed by means of the software *Oasis Montaj* by Geosoft Inc. with the MAGMAP extension. For mathematical simplicity and speed of operation the filters are applied within the wave-number domain (Fourier). The data is pre-processed in order to be conform to the fundamental maxims of the processing and then transformed to the wave number domain and whereafter a filter (or several filters) is applied. Thereafter the data is transformed back to the space domain and visualized.

5.1.3.3. Upward continuation and residual

An upward continuation filter can in a simplified view be seen as if the measurement is moved to a higher level, i.e. the data at the actual observation point is extrapolated upward. This filter removes or minimizes the effect of short wavelengths originating from shallow sources. By subtracting the upward continuation grid from the original grid the result is a grid of the *residual* field showing the response from shallow sources (Jacobsen 1987). The residual is a common practice to present both gravity and magnetic data.

In section 6 the magnetic and gravimetric data is presented as a 500 meter residual. The original grid is extrapolated by means of upward continuation to 1000 m. This grid is subtracted from the original grid and the residual is obtained. The residual is approximately seen as the response from the top 1000

meters below the ground but with an average main contribution from the top 500 meters, thereby the convention of designating it as 500 meter residual.

5.1.3.4. Reduction to pole

The shape and amplitude of an anomaly due to a magnetic body depends on the strength and direction of the earth magnetic field inducing a response in the magnetic body (and the strength and direction of the remanent magnetization possibly present in the body). This results in different amplitude and shape of the magnetic anomalies from identical magnetic bodies depending on where on earth the measurement is done. In order to globally compare data as well as remove skewness of anomalies a “reduction to pole filter” is applied. The transformation gives the shape of the anomaly as if it was measured at the North Pole with a field inclination of 90° . The processing also moves the anomalies to lie directly over the source and thereby correlation and comparison with other geophysical data and geological information can be conducted. The numerical calculation of the reduction to the pole processing is presented by Baranov and Naudy (1964).

5.1.3.5. Tilted derivative (TDR)

The tilt angle is defined as the ratio of the first vertical derivative to the horizontal gradient of the potential field. This measure identifies the location of both shallow and deep magnetic or gravimetric sources. The property is positive over the source and negative elsewhere and zero at, or near, the edges of the causative body. This filter is advantageous in identifying deeper sources with smaller amplitudes since it uses ratios and not absolute values. For magnetic data the processing should be applied on a reduced to the magnetic pole filtered grid to obtain the most correct position of the magnetic bodies. The method is described and compared with other filters by Miller and Singh (1994).

5.2. BACKGROUND GEOPHYSICAL DATA

Literature studies combined with study of airborne geophysical material supplied by the GSN were conducted prior to field work. The geophysical data consist of airborne magnetic and radiometric data, supplemented by several ArcGIS layers of geological features (rock types, dykes, structures and mineralizations) and other geographical information (figure 23).

All maps presented are shown in the WGS84 UTM 33S coordinate reference system, and with north directed straight up. The outline of Friedenau farm is included in most maps to facilitate comparison between different maps. The small rectangle within the farm area outlines the area operated by the mining company (old boundary).

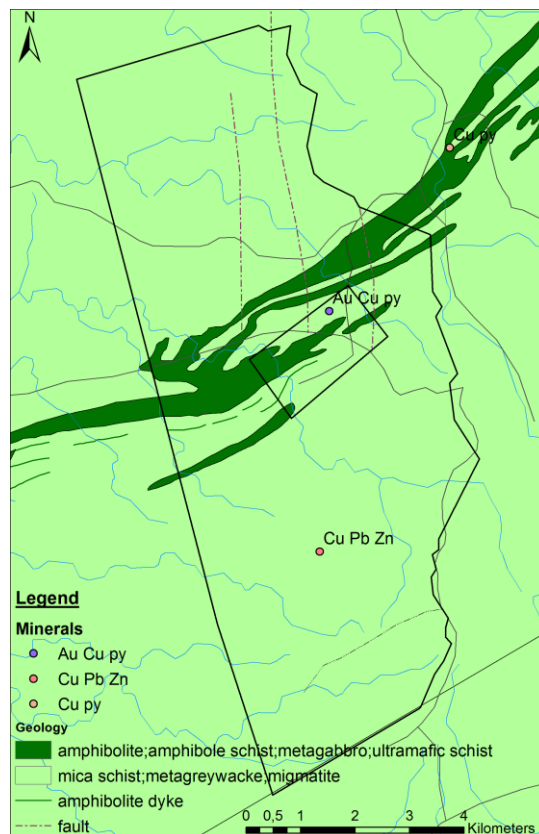


Figure 23. Geological and geographical background material of the area of study. The black polygon is the outline the area of Friedenau Farm, the rectangle within the polygon show an old boundary for the area operated by the mining company.

5.2.1. AIRBORNE GEOPHYSICAL DATA

Airborne geophysical magnetic and radiometric data were kindly provided by the GSN. The airborne data was produced as a part of the High Resolution Airborne Geophysical Programme (Hutchins *et al.* 1997). The survey was conducted along parallel N-S lines with a 200 meter separation and an approximate point distance of 7 meters along the lines. The ground clearance was between 80-100 meters.

The magnetic anomaly map for the whole MAB is shown in figure 24. The magnetic response within the study area is shown in more detail in figure 25. The magnetic field in this area indicates a positive regional gradient from the south-southeast to the north-northwest.

Figure 26 is a ternary map showing the relative abundance of the elements potassium, thorium and uranium. The concentration of all elements are shown as a gradient between black and white, where white is high concentration and black is low. The MAB clearly stands out as a low concentration feature indicated by the black trail in figure 26.

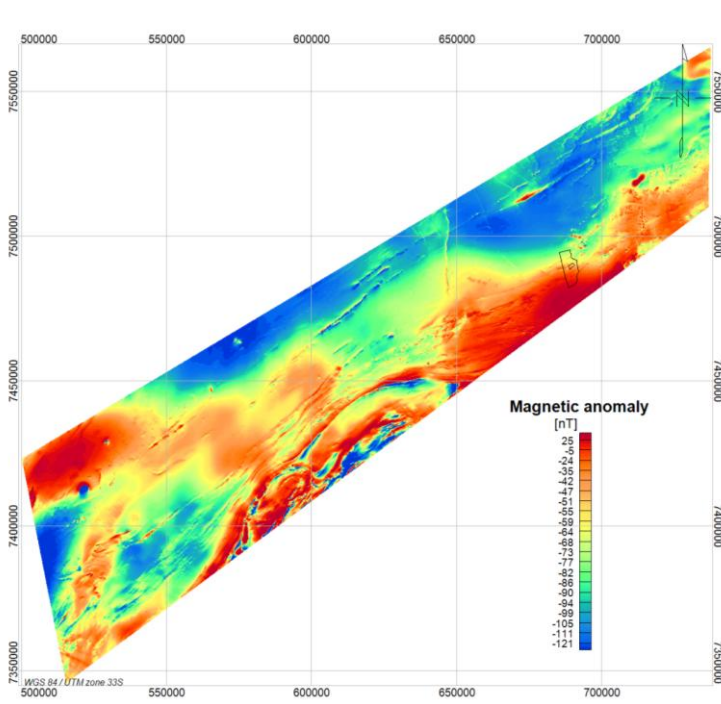


Figure 24 (top) Magnetic anomaly map over the whole area of the MAB. The outline of Friedenau farm is included as reference. Data supplied by GSN.

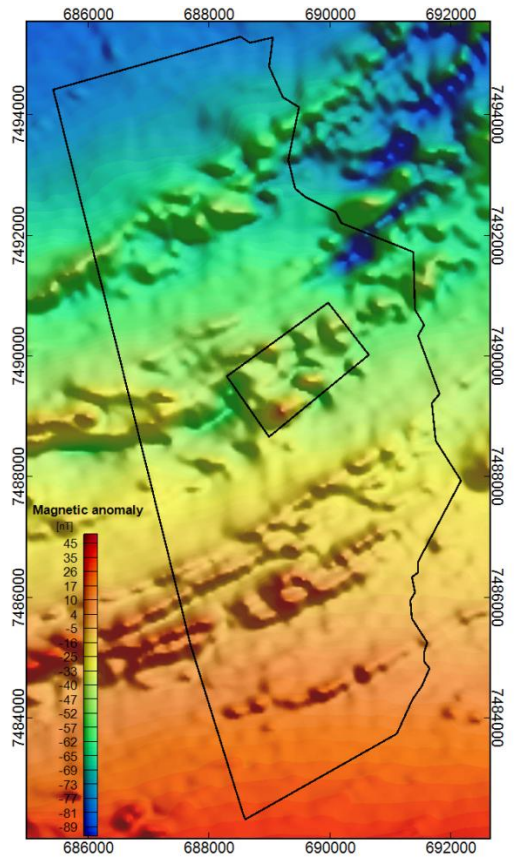


Figure 25 (right). Shaded magnetic anomaly map over the Friedenau Farm (black outline). Data reduced to pole. NB different range of colors in the scale compared to figure 24. Data supplied by GSN.

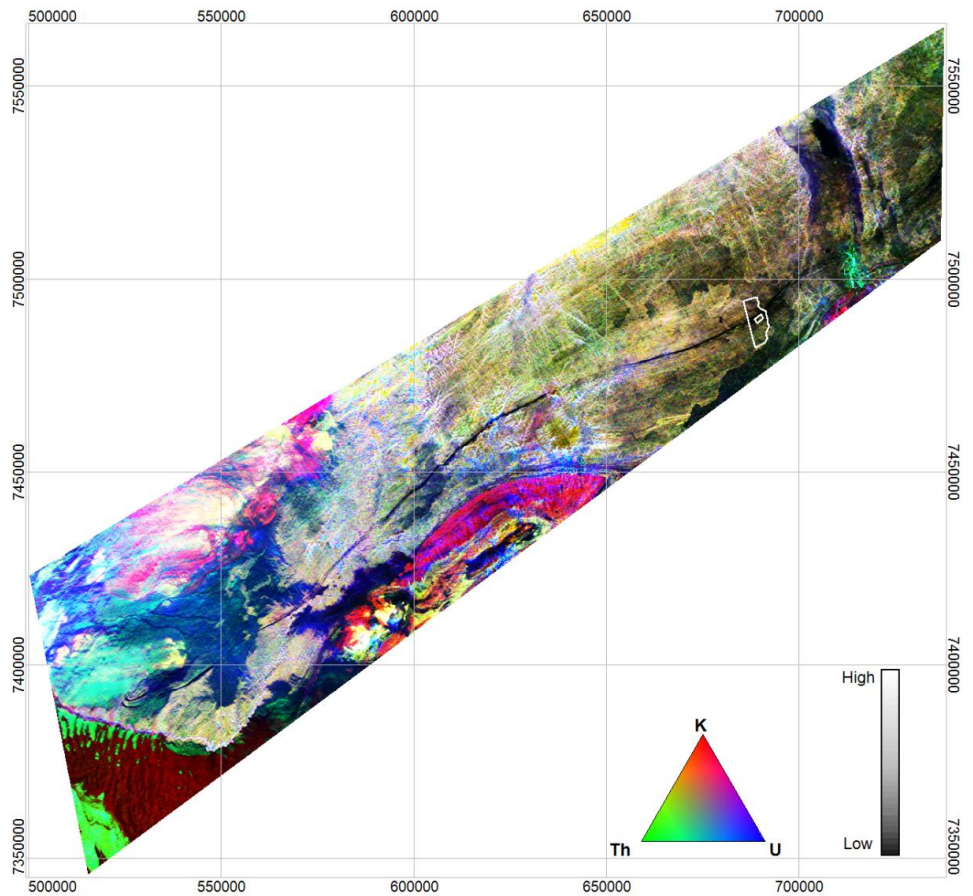


Figure 26. Ternary radiometric map showing the relative abundance of K, Th and U. The amphibolite belt is a low radiating feature seen as a black almost continuous trail. The outline of the Friedenau farm is shown in white as reference.

5.3. FIELDWORK DESCRIPTION

The field survey was carried out in collaboration with the staff from the SGU and the GSN. In total 12 people were involved in the collection of field data. The measurements took place during a five week period from April to May 2013. The collection of data was part in the collaboration and training project of the operation of instruments, in particular the gravity meter and the position and altitude system but also the other techniques used. The training program also consisted of short lectures and computer processing of data.

Ground magnetic measurements were carried out along two almost north-south striking profiles, approximately 11 km in length, called East and West hereinafter. The survey mode was continuous recording with a time interval of five second which corresponds to a point distance between 2 and 7 meters, depending on walking pace. Along the East profile electromagnetic (VLF) measurements with a point distance of 50 meters, was also performed. Locations of the profiles and VLF measurement points are shown in figure 27.

Regional gravimetric measurements were carried out with a point distance between 100 and 500 meters. The point distribution is shown in figure 28. The measurement time was set to 30 or 60 seconds and the height of the gravity meter over ground was kept constant 17 cm for all points.

Detailed ground magnetic measurements were performed in an area in between the old and the new mine. Five profiles, each 1.5 km, long, with a line separation of 100 m were measured with the magnetometer. Along the three most easterly profiles (profile 3-5) electrical measurements (SP) were undertaken with a point distance of approximately 50 meters (figure 29).

Field observations and rock sampling were carried out parallel with the measurements. In total 27 observations were done and 22 samples collected from 21 of these sites (figure 30). Since the rocks in the area are heavily weathered, eight "fresh" samples from the mine (western extension) were collected with the shortcoming of not knowing exact position of these. The samples consisted both of material from the ore and representatives of the surrounding schists. Four remnant drill cores were collected as reference material to be compared with the weathered samples. Thin sections were prepared and identification of main minerals was performed to aid the classification of the rocks.

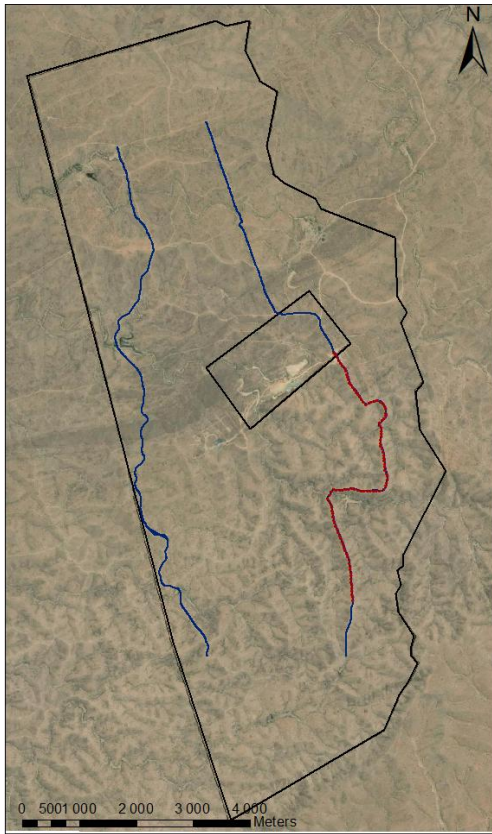


Figure 27. Magnetic measurements along two profiles: East and West, shown in blue. The VLF measurement along part of the East profile is shown by red dots.

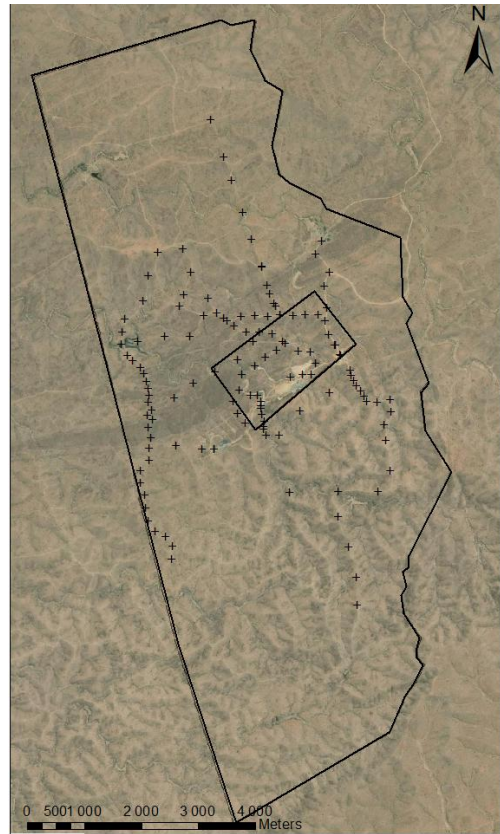


Figure 28. The distribution of gravity measurement points (+).



Figure 29. Detailed magnetic profiles 1-5 (west to east) and location of the SP measurements (turquoise triangles).

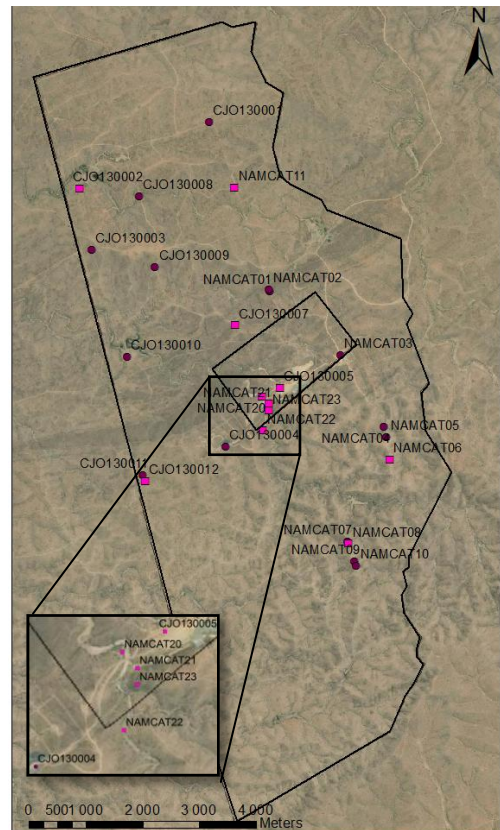


Figure 30. Location of observations (round dark purple dots) and sample locations (square bright pink markers). Observation CJO130006 is located outside of the map, along the road between Windhoek and the Matchless Mine area.

6. RESULT

6.1. ROCK CLASSIFICATION AND PETROPHYSICAL RESULTS

A summary of the classification of the rock samples based on petrophysical data and thin-section study is presented in table 3. The full description of all observations and related samples are presented in Appendix 1

From field and laboratory measurements of magnetic susceptibility it is evident that the amphibolite or amphibolite/gabbro does not have a high magnetic signature in general. Only one sample of amphibolite (CJO130007) out of eight has high susceptibility (24040 μ SI) but low remanence. High susceptibilities and Q-values were found in three samples; magnetite quartzite (NAMCAT23A), schist (NAMCAT6) and meta-arenite (NAMCAT11). Notable variations of the density and magnetic susceptibilities occur within each classed rock type (table 3).

Table 3. Rock-type classification and results from the petrophysical analysis.

ID	D (kg/m ³)	K (μ SI)	J (mA/m)	Q
Cu-ore				
NAMCAT17	4502	4150	20	0.11
NAMCAT18	3988	710	20	0.69
NAMCAT19	3912	2090	10	0.14
Magnetite quartzite				
NAMCAT23A	2760	199660	185230	22.64
Amphibolite				
CJO130005	3010	1020	0	0.12
CJO130007	2829	24040	60	0.06
Amphibolite/metagabbro				
NAMCAT12	2970	1760	130	1.82
NAMCAT13	2966	750	10	0.21
NAMCAT20	2953	700	10	0.19
NAMCAT21	2932	610	0	0.17
CJO130006	2970	690	0	0.05
DRILLCORE04	2995	620	10	0.46
Schist				
NAMCAT6	2731	14569	6730	11.28
NAMCAT8	2788	600	20	0.61
CJO130002	2705	320	0	0.25
CJO130012	2711	840	30	0.8
NAMCAT23B	2496	960	20	0.63
Mica schist				
NAMCAT14	2806	500	0	0.24
CJO130009	2662	250	0	0.32
DRILLCORE01	2780	1260	20	0.39
NAMCAT22	2726	600	10	0.32
DRILLCORE02	2941	390	20	1.11
Chlorite mica schist				
NAMCAT15	2771	390	0	0.21
NAMCAT16	2785	350	0	0.32
Meta-arenite				
NAMCAT11	2602	7600	2790	8.95

6.2. GRAVITY

The gravity data is presented as a Bouguer anomaly map and as a 500 m residual map in figure 31 A and B respectively. A distinct gradient with increasing values from southeast to northwest is present in (figure 30A). This corresponds to increasing mass excess towards the northwest. The residual map shows near surface mass excess in the central western part that correlates with the fold hinge of the MAB.

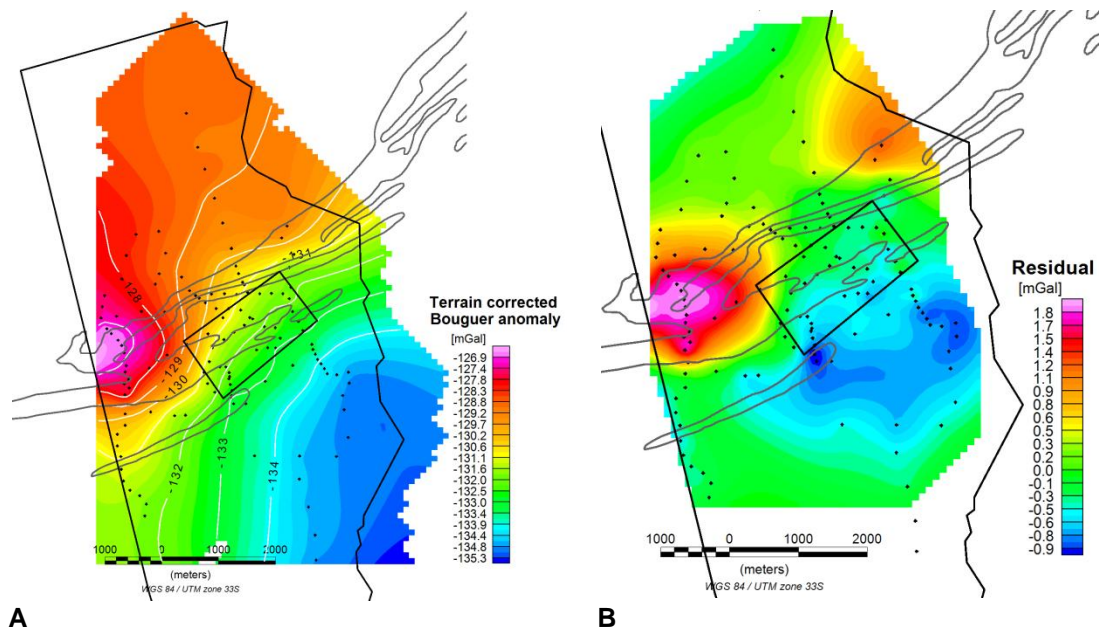


Figure 30. Black dots show the distribution of measurement points. Gray polygon is the outline of the MAB. **A:** Bouguer anomaly map. **B:** 500 meter residual map.

6.3. MAGNETIC HORIZONS

The ground magnetic responses along the East and West profiles are shown in figure 31.A. No obvious correlation is seen between the mafic rocks of the MAB and the magnetic signature. Several, both large and small amplitude anomalies are found along the profiles. The anomaly with the largest amplitude, in the south part of the western profile, is recorded over a horizon which further east has a known mineralization (figure 31.C).

The ground magnetic and airborne measured magnetic responses cannot be compared directly however the location of the sources of the anomalies can be compared. The location of the sources (or the indication of their location) responsible for magnetic anomalies in the different data sets is shown in figure 31.B. The correlation is considered to be good. The ground magnetic data resolve more details and give the magnitude of the near surface magnetic sources.

The results from the detailed measurements are shown as profiles in figure 33 and as a grid in figure 34. Four large positive anomalies are seen in three of the profiles. In figure 35 the comparison between a detailed geological map and the ground magnetic anomalies show a good correlation between strong positive magnetic anomalies and mapped outcrops of magnetite quartzite. Detailed figures of the magnetic responses from the East, the West and detailed profiles (1-5) are found in Appendix 2 and a comparison of airborne and ground magnetic data in Appendix 3.

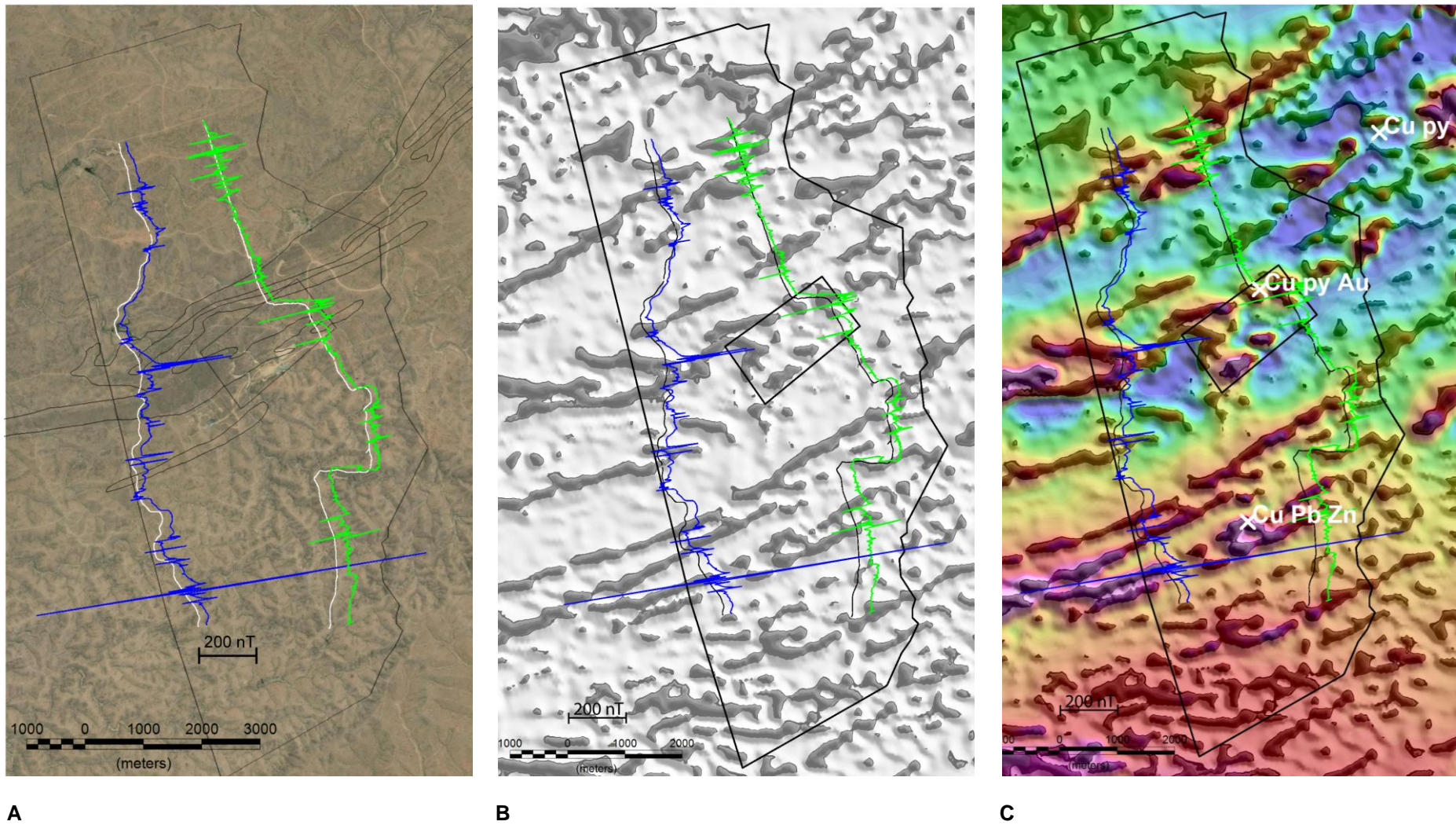


Figure 32. The magnetic response plotted along the East and West profiles. The measurement lines are shown in white in A and in black in B and C. The lines represent the baseline of 28 500 nT of the readings. **A:** The outline of the MAB is shown as reference. The MAB is also visible as a darker streak in the aerial photo. **B:** TDR filter applied on 500 m residual reduced to pole airborne magnetic data. Locations of the sources of large and small anomalies are shown in gray. **C:** Airborne magnetic data presented as a composite of an anomaly map and a TDR map. (Both maps based on 500 m residual and reduced to pole data). The reading along the East and West profiles are shown as well as known mineralization (white crosses) within the area.

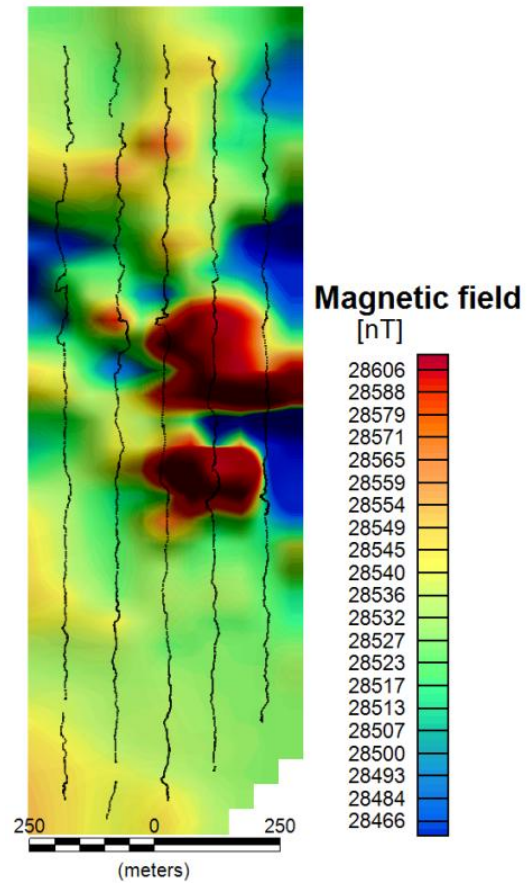
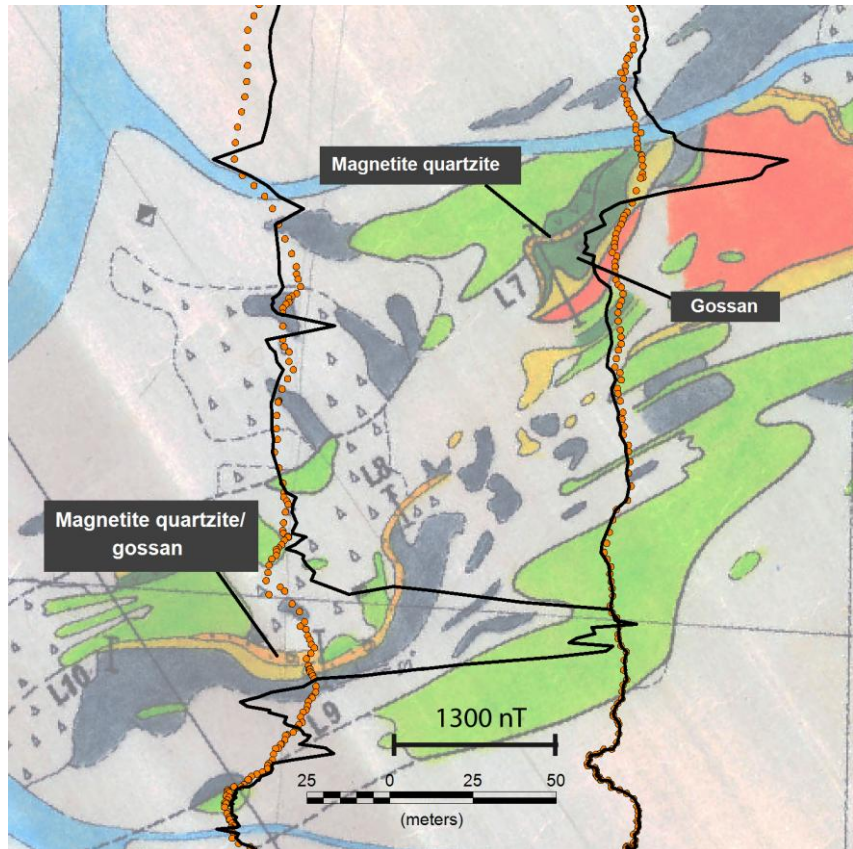


Figure 34. The total magnetic field from detailed measurements shown as grid. Profile traces in black.

Figure 33 (above). The total magnetic field based on detailed ground magnetic measurement plotted along the measured profiles. The profile traces (black lines only visible under the large responses in orange) represent the baseline of value 28 500 nT. The blue lines show the outline of the MAB, the black box show the outline of figure 35 and the white ellipse shows the anomalies that are further discussed in the section 9.3.

Figure 35 (right). The magnetic anomalies placed on top of bedrock map. The outline of the figure is shown in figure 33. The black lines show the magnetic field reading, orange dots show the measurement points. Geological units of interest are specified.



6.4. SULFIDE MINERALIZATION

Results from the SP measurements are shown in figure 36. Large negative (several hundred millivolts) responses correlate with mapped location of gossans.

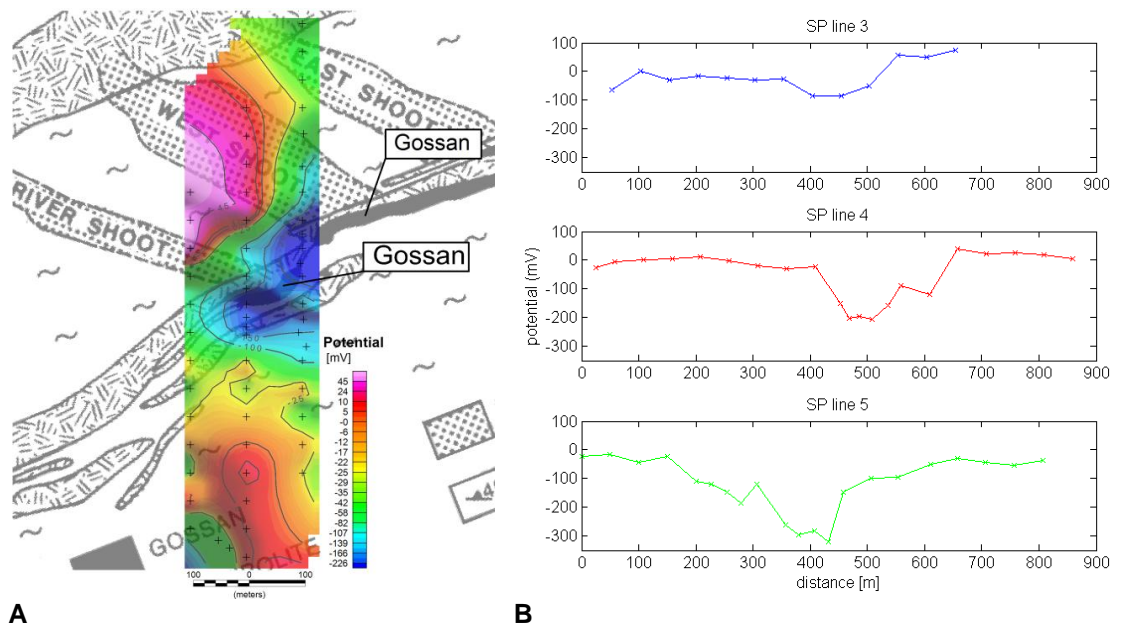


Figure 36. The results of SP measurements **A**: Result presented as a map with crosses showing the measurement locations, profile 3 to 5 is numbered from west to east (same as numbering as magnetic profiles). **B** profiles, x = 0 in the south.

7. STRUCTURAL AND LITHOLOGICAL MODEL

A three dimensional model at regional scale of the geological and geophysical units within the survey area was constructed as a part of this project. The purposes with the model are:

- Build and visualize geological units based on magnetic and gravimetric data
- Test existing structural model of the belt against geophysical data

7.1. DESCRIPTION

The model was constructed and evaluated in *ModelVision 12.0* by Pitney Bowes Software Pty Ltd. The modeling process is completely user controlled which means that the position, density and magnetic susceptibility of all the bodies are altered by the user. The gravimetric and magnetic field yielded by these bodies were calculated and compared with the corresponding measured data. Parameters of the bodies were altered until a satisfactory fit between the response from the model and the measured data was obtained.

The data that was used in the modeling was airborne magnetic, regional gravity and petrophysical data. To a lesser extent also ground magnetic data was used to test the validation of the regional model against the high resolution ground magnetic data.

Eight different geological units with different densities and/or magnetic susceptibilities were constructed. The identification of the different units was initially based on sampling. More units were added and all units were altered geometrically and petrophysically during the modeling process to obtain a geological model explaining the geophysical signatures. All geological units, their densities and susceptibilities as well as the corresponding colors in figure 37 are shown in table 4.

The background was set to represent low susceptibility schist that is dominating in the area. The density and magnetic susceptibility values were determined on the basis of the average values from the petrophysical data of this rock type. The density was set to 2.740 kg/m^3 and the susceptibility to $600 \mu\text{SI}$.

In total 27 bodies with a simple geometry were constructed. The majority consists of thin tabular bodies to represent thin sheets in the schist with strike and dip concordant to the belt after Klemd *et al.* (1987). The body representing the MAB was constructed from the mapped outline of the belt and extended 30 km at depth. The large depth extent is based on the assumption that the lateral extension of the belt (350 km) is reflected in its depth extension. The density was set to the average value of the collected amphibolite and amphibolite/metagabbro samples. One body is referred to as “waste area” for which the magnetic response is correlating with the basin of an old mining waste deposit and is not considered a geological feature located in the bedrock.

Magnetic bodies identified from TDR-filtered airborne magnetic data were given a depth extension relating to the lateral extension seen in the data. The model yielded two types of “magnetic schist”; one with higher magnetic susceptibilities and one with lower (table 4).

7.2. MODEL RESULT

The resulting model is shown in figure 37. The figure shows the model in perspective; the profile-lines lie along the ground and in a NNW-SSE strike. The gravity and magnetic model responses along the line 3 and 5 compared with measured values are shown in figure 38.A and B. A general good agreement between modeled respond and measured airborne magnetic and gravimetric data is observed. Comparison of ground magnetic and model responses is shown in figure 38.C. All modeled profiles and their cross-sections are found in appendix 4.

To obtain a satisfactory fit to the gravitational data, a large body with 1% higher density compare to the background was inserted northwest of the belt. This body is shown as transparent with the outline in gray lines in figure 37.

Table 4. Geological units included in the model.

Name	Body Type	Susceptibility (μSI)	Density (kg/m^3)	Body color
Background	-	600	2740	
MAB	General Polyhedron	880	2900	
MAB magnetic	Tabular	5000		
Magnetite quartzite	Tabular	10000	2760	
Meta-arenite	Tabular	4000	2600	
NW body	Tabular	600	2770	
Schist 1	Tabular	1500	2740	
Schist 2	Tabular	3000	2740	
Waste area	Tabular	3500	2760	

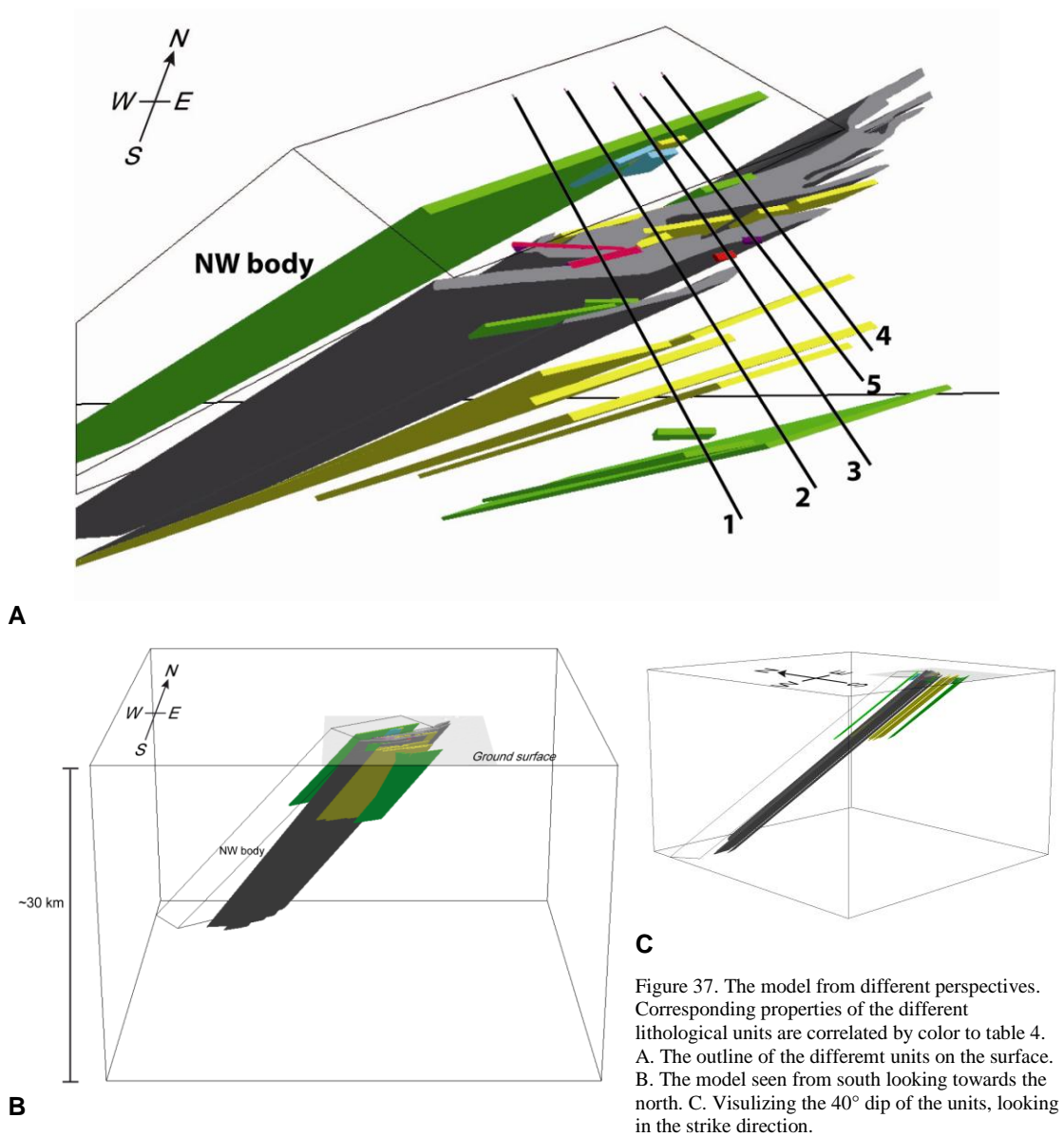
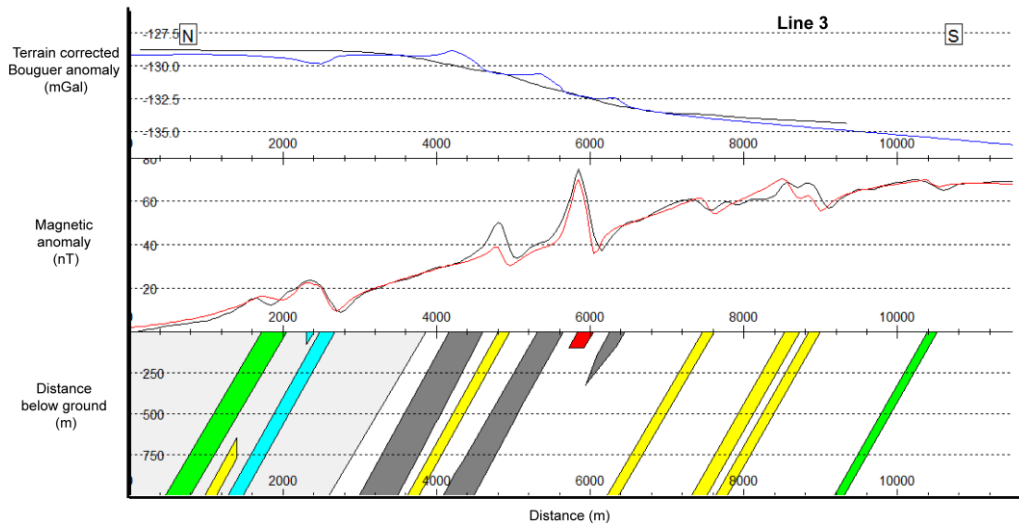
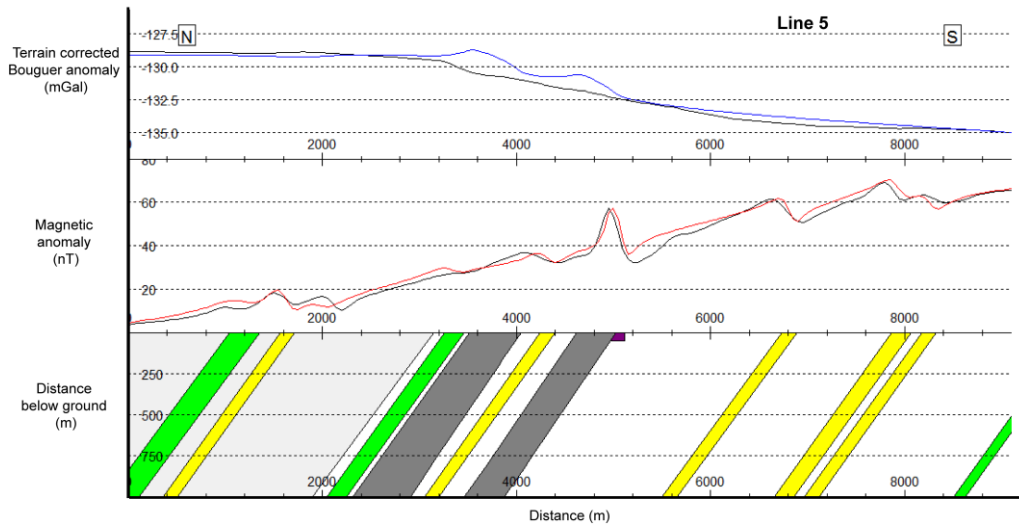


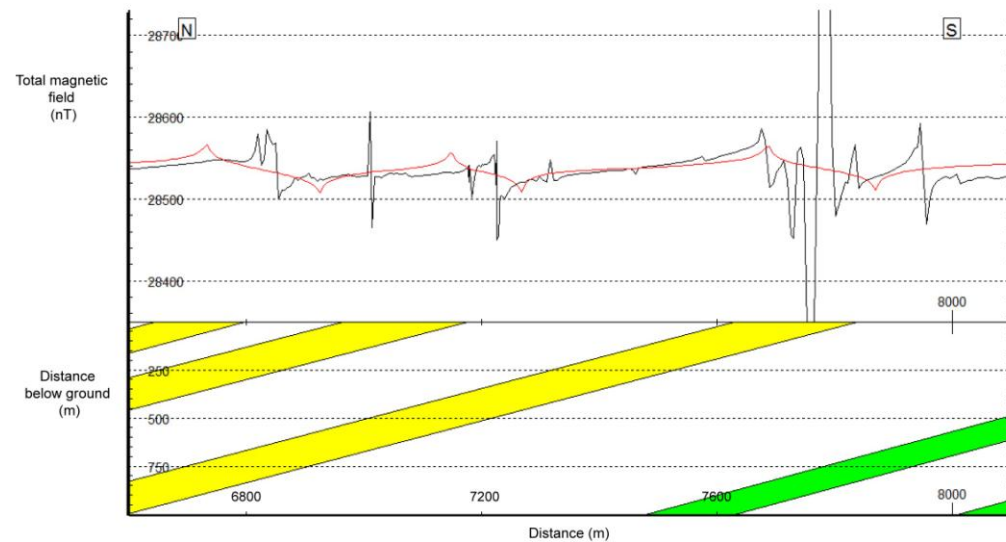
Figure 37. The model from different perspectives. Corresponding properties of the different lithological units are correlated by color to table 4. A. The outline of the different units on the surface. B. The model seen from south looking towards the north. C. Visualizing the 40° dip of the units, looking in the strike direction.



A



B



C

Figure 38. Comparison of the model response and measured values. The uppermost sections in the diagrams show the gravity responses from the model (blue line) and the measured values (black line). The middle sections show the modeled magnetic response (red line) compared to the airborne magnetic data (black line). The bottom sections show a cross section of the model along the lines (the location is shown in figure 37A). NB! Different scales in x and y, the dip is 40° in all figures. **A:** profile 3 **B:** Profile 5. **C:** Model response compared with ground magnetic measurements along a section of East ground magnetic profile.

7.3. DISCUSSION OF LIMITATIONS AND VALIDNESS OF THE MODEL

In the process of constructing a model no unique solution to the observed data exists, instead several different models can be constructed to fit the same data set. The lack of uniqueness is always an uncertainty present in a model. The quality and quantity of the data, as well as the knowledge and skills of the user determine the reliability of the final model.

A main constrain in the constructed model is that the effect of remanent magnetization is not included. Samples with high remanence do exist in the area in different rock types (table 3). However no directional measurements were done on these samples. To incorporate the remanence in the model therefore requires further assumptions and is not considered for the present purpose.

The magnetic and density properties used for the modeled bodies are based on a relatively few samples and are only used as guidance. The quality of the samples is considered relative poor due to extensive weathering of most of the samples. These drawbacks are however not of crucial matter since it is the relative differences between the bodies that are modeled.

The density and magnetic data that the response of the model is compared to is considered good. The airmagnetic data is of high quality with dense sampling and has been shown during this project to correlate with ground magnetic data. The quality of the gravity data is good but the density of measurements varies and so does the information one is able to obtain from it. In high sampling areas the confidence of the model is high.

The model suggests a density difference between the NW and SE of the MAB in the area. The difference is approximately 1%. This suggested trend cannot be confirmed by the petrophysical data since only one sample (CJO130002) of schist is collected north of the belt. I consider a slight difference in the densities of the bulk bedrock at the different sides of the belt to be a probable explanation to the density difference suggested by modeling. From the petrophysical analysis it is evident that the density differs in the schists. A slightly higher concentration of the heavier type schist in the NW is enough to explain the gradient in the gravity field. The rock sampling and measurements of gravity should be denser to be able to secure this question.

The existing structural model of laterally extensive sheets dipping about 40 degrees towards NW is shown to be supported by geophysical data.

8. DISCUSSION

Every geophysical method has its advantages and disadvantages considering the information they may provide of the geological units below the ground surface. By comparing indications from different geophysical anomalies information of subsurface rocks and structures are obtained.

8.1. MASS EXCESS; GRADIENT AND FOLD HINGE

The gravity measurement was successful in the identification of the mafic rocks of the MAB. From the modeling result we conclude that the belt alone cannot to be responsible of the gradient in the gravity data (figure 39A). A probable explanation of the observed gradient is that a density difference is present between the schist southeast and northwest of the belt. When tested in the model a good fit was obtained (figure 39B). A difference of 1% is enough to explain the gradient, in the area of study.

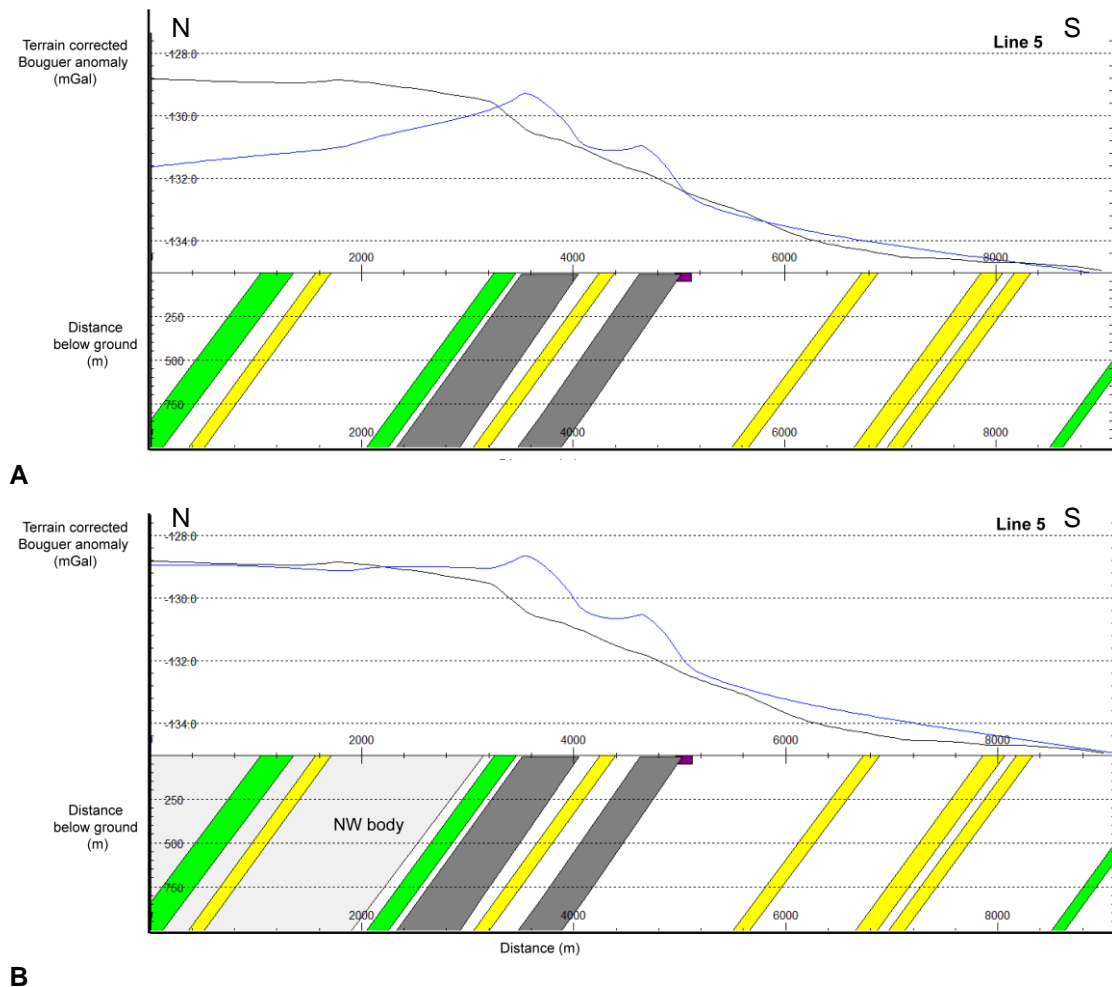


Figure 39. A. The modeled response (blue line) compared to gravity data (black line) over line 5 with same density of the schist on both sides of the belt. A clear discrepancy is seen. B Same as A but with a body (light gray) inserted NW of the belt with a 1% higher density compared to the background.

The residual map shows a near-surface mass excess that is interpreted to be related to increased mass around the fold hinge of the belt. Here the measurement points are relatively dense and therefore the data is regarded reliable. The anomaly is somewhat offset towards NW in relation to the outline of the belt. This can be explained by the 40° dip of the belt to the NW but also by the less weathered rocks below the surface which have higher densities. Most of the mass excess is therefore shifted northwest with regard to the outline of the belt.

The reason that the belt does not appear as a continuous mass excess following the mapped outline of the MAB is thought to be a combination of too sparse measurement points as well as compositional and geometrical variations along the belt. To be able to map the outline of mafic rocks within the belt a gravity survey with point distances of approximately 40 m is required.

8.2. MAGNETIC SIGNATURES

The high Q-values found in three samples show that remanence exist in different geological units and will complicate interpretation of magnetic data. Depending on the direction of the remanence the magnetic anomalies seen in airborne and ground magnetic measurements may be altered. Measurements of the remanence direction can be obtained by taking oriented samples in field. During field measurements it is however impossible to determine if remanent magnetization is present or not. Three orientated samples were taken which did not show any or very low remanence. Thus the effect of remanent magnetization was not incorporated in the model calculation.

A regional gradient in the magnetic field is seen in the airborne magnetic data and can also be detected in the ground magnetic measurement, especially along the eastern profile. The source of the gradient is situated at greater depth but some effect is seen in near-surface regions. The gradient is weakly observable in the 500 meter residual map.

The error in the ground magnetic data due to non-diurnal corrected data is considered negligible, since the anomalies are at least one order of magnitude larger than the diurnal differences. However some notches in the data can be seen due to different days of measurements.

Comparison between airborne and ground magnetic measurement is used for verification of the two datasets. The measurements are performed at different elevations and with different point distances and therefore are not directly comparable. However, the indication of the location of causative bodies in the two different sets of data should be, and is, the same along the eastern and western profiles (Appendix 3).

The cause of the linear extensive magnetic horizons, seen in the airborne magnetic data and verified in the ground magnetic data (figure 32B and C) are suggested and modeled to be due to magnetic horizons within the schist. That such units exist is confirmed by some samples collected within the area. The horizons are in the order of 10 to 80 meters wide and lie at or close to the surface as indicated by the narrow and sharp anomalies in the ground magnetic data. More detailed studies of the shapes of the anomalies and modeling of the causative bodies' location and their geometrical form can be performed on the current data set, but considered out of the scope for this project.

The identification of laterally extensive magnetic horizons in the schist leads to new questions upon the source of this feature. Can it be related to primary depositional processes and/or later deformation and metamorphism? The minerals responsible for the anomalies can be either pyrrhotite or magnetite or both, and may vary in concentration along the belt. For detailed studies of the anomalies denser sampling and analysis of the magnetic minerals responsible for the anomalies is required.

The anomaly located in the very south of the West profile is of special interest for two reasons; firstly the anomaly has the largest amplitude of those recorded along the West and East profiles. The shape of the amplitude is also reversed compared to what is observed in most other anomalies, i.e. the positive part of the asymmetrical anomaly is towards the north and the negative part to the south. Secondly, the anomaly lies in the vicinity of mineralizations of Cu, Pb and Zn type (figure 32C). This deposit is also classified as stratabound and lies within the same structural horizon as the large magnetic anomaly indicated in the airborne data. Is there possible a connection between large magnetic anomaly and the location of mineralization?

The MAB does not appear as a continuous high magnetic susceptibility feature but the analysis of the magnetic field and the study of the magnetization of the collected samples reveal heterogenic distributed high magnetic signatures of the MAB. It is known that the composition varies along and within the belt. The compositional variation and generic process responsible for the variation is still an issue to be considered.

There is a close correlation between the large amplitude magnetic anomaly and observations of magnetite quartzite (figure 35). However some discrepancies may be seen. The most eastern profile (profile 5 in figure 35) does not pass directly over the magnetite quartzite horizon but still reveals an anomaly of high amplitude. The reason might be that the mapping and/or rectification of the map is not accurate. Or as I consider likely, that the magnetite quartzite horizon continues at depth in a northeast direction. This would also explain the smaller amplitude compared to the left anomaly along profile 4 (Figure 35).

There are two large positive anomalies in the order of several thousands nT in the ground measurements that are located outside the frame of the detailed geological map. The anomaly in profile 2 has the largest amplitude measured within the complete area. The locations of these anomalies are indicated by a white ellipse in figure 33. The anomalies are found at the approximate location of the West ore shoot and nearby the mapped outline of the MAB. The large amplitude and narrow shape of the anomalies indicate that the sources are at, or close to, the surface. A high concentration of magnetite and pyrrhotite within or in the vicinity to the ore is therefore not considered to be a possible source. The depth to the ore at this location is estimated to about 150 m. No anthropogenic objects that could be responsible of magnetic disturbance were observed in field at, or close to, the anomalies. However metallic objects on the ground were observed at a distance of 40 m from the anomaly along profile 4, but the distance is considered too large to yield any response in the data.

8.3. IDENTIFICATION OF SULFIDE MINERALIZATION

The negative anomalies of the SP measurement clearly coincide with the gossan (figure 36). It is known that SP give large negative anomalies over sulfide bodies in a redox-environment. Due to the incomplete understanding of the SP phenomena is it difficult to discuss the precise nature of the SP anomalies. However, it is evident that the large negative anomalies correlate to the upper part of known ore shoots. A possible correlation of magnetite quartzite and SP anomaly also needs to be considered.

The self potential-effect due to magnetite is not completely known, not in general nor in this specific situation. Parasnis (1966), who is one of few authors mentioning the effect, states: “... *above some sulphide bodies, notably those containing pyrite, chalcopyrite and pyrrhotite, and above graphite they may attain values as high as several hundred millivolt to a volt... Large voltages have also been reported over pyrolusite, psilomelane⁴, magnetite and anthracite coal.*” Heiland (1946) state that pyrite shows the strongest SP although it is not the only mineral that exhibits the SP property and also mentions magnetite as an example.

I propose that the SP anomaly in the area is due to the sulfides present in a redox-environment. An oxidizing-environment at the surface of the ore is observable as a gossan. The shoots over which the anomalies are recorded have been mined, the shape and mass of the remaining sulfides in the shoots are unknown and therefore the effect due to this is uncertain. The observed readings from the SP survey can be explained by figure 17. The largest negative anomaly is recorded at the top of the ore body in the most oxidizing environment. No strong negative anomalies are seen vertically above the buried ore due to the redox-gradient is smaller here compare to at the surface of the body (compare with the redox-potential curve on the left side of figure 17).

8.4. ELECTROMAGNETIC METHODS

The electromagnetic method, VLF, did not yield any interpretable data as the signal to noise ratio was too low. This is due to the lack of appropriate VLF radio-transmitters. The location of transmitters, the signals of which were strong enough were unfavorable in relation the strike direction of the MAB. If this specific method would be considered to be used in the area, a local set-up of a transmitter is necessary.

If EM-methods could be used, an indication which of either of the minerals pyrrhotite or magnetite is the source of magnetic anomalies in the schist. Pyrrhotite is a fairly conducting mineral compared to the surrounding and an anomaly in the VLF would probably appear. There are several other electromagnetic instruments and systems available on the market that would be applicable in the area. Many of them would produce more reliable data than the VLF system.

⁴ Manganese oxide (authors note)

9. FURTHER STUDIES

This project was a first attempt to test ground geophysical methods in the selected area of the MAB. Further studies are suggested to gain more information of the geology in the area and to resolve issues that have become apparent through this study.

The results from our survey show that the potential for the SP method to find new sulfide mineralizations in the area is good. In order to increase the understanding of the SP phenomena in this specific area, and in general, measurements are suggested to be performed over other known sulfide deposits that are not mined. Measurement over magnetite quartzite, where it is known that no sulfide mineralization is present, is also proposed to resolve the issue of the SP response and magnitude due to magnetite.

Both regional and detailed gravity surveys are proposed. The aim of a regional survey would be to determine the long-wave differences in density and identify if the difference is regional or local. A regional gravity survey would also reveal structures of the belt and the surrounding rocks. Detailed gravity surveys over the belt would give more information of the shape and depth extension of the belt as well as identifying compositional differences along the belt.

There are several magnetic anomalies within the area the sources of which could not be identified. This concerns both the anomalies observed in the schist and in the amphibolite. More detailed modeling on the data that has been collected is possible with follow up in field and additional sampling. Analysis and study of the magnetic mineralogy is suggested with the purpose to relate geophysical features to geology and to increase the overall understanding of the belt.

The strong magnetic anomaly in the southern part of the West profile is of special interest since mineralizations are recorded within the same magnetic horizon. Understanding of the relation between the magnetic minerals and the mineralization may facilitate future prospecting along the MAB.

The remanent magnetization of the magnetite and pyrrhotite is also suggested to be studied in more detail. If the direction of the remanent magnetization varies along the belt essential changes in the characteristics of the magnetic signature of the host rock may occur. This is important since the magnetite quartzite and pyrrhotite bearing rocks often are related to ore bodies.

10. CONCLUSIONS

A three-dimensional model of a limited area of the MAB is shown in figure 37. According to this model the bulk bedrock in the area consists of a schist that has 1% higher density NW of the belt compared to the SE. The MAB consists of mafic rocks with considerably higher densities than the surrounding rock units, and with a magnetic susceptibility that is generally low but somewhat increased compared to the background values of the model. Within the belt lenses of mafic rocks with very high susceptibilities exists.

There are two types of magnetic horizons within the bulk schist. These rock units have the same densities as the surrounding rocks but they have considerable higher (twice or five times as large) magnetic susceptibilities compared to the bulk schist. These units are often laterally very extensive and have an approximate shape of thin sheets. Lenses of meta-arenite are interbedded in the schist; this rock unit has lesser density than the background but higher magnetic susceptibility. All the different lithological units have the same strike SW-NE and dip 40° towards NW, as the MAB. In addition there are units of magnetite quartzite which are not concordant to the belt and have a very limited depth extension.

Of all tested ground geophysical methods only the VLF method did not yield any applicable information for the MAB within the study area. The gravity measurements identified the mafic rocks of the MAB and gave new information of the bulk densities of the bulk rocks at different sides of the belt. The ground measured magnetic data show a good correlation of the location of the sources to the magnetic anomalies in the airborne magnetic data. The ground magnetic measurements resolve the magnetic signals in much more detail and single anomalies in the airborne data is shown to consist of up to four different anomalies from the ground measurement. The airborne magnetic data is sufficient for creating a regional model of the belt, for detailed modeling ground magnetic data as well as

measurements of the orientation of remanent magnetization is necessary to obtain a reliable model. Remanent magnetization is present in both the magnetized amphibolites as well as in the sedimentary rocks.

Under the prevailing conditions the Self Potential method is successful in the area of locating sulfide bodies. More studies are nonetheless required for a more comprehensive understanding of the cause of the SP-phenomena and the contribution from magnetite.

The objective for this project was successfully achieved:

- i. Four different ground geophysical methods were tested and evaluated.
- ii. Different geophysical properties were identified in both the schist and the amphibolite.
- iii. A three-dimensional model was constructed on the basis of the collected data, demonstrating the structural build-up of the MAB in the project area.

11. ACKNOWLEDGEMENTS

There have been a lot of people contributing to this work through involvement in the MeetingPoints Mining project. I am grateful for all of your contributions, both large and small.

Thanks to the personnel at the SGU office in Lund for providing me with an office space and a pleasant work environment during the process of writing this thesis. Thanks to Anders Gustavsson for help with the petrophysical analysis and Philip Curtis for support with the visualization of the model, at SGU in Uppsala.

Without the involvement of the GSN and the Weatherly International Plc Namibia, providing access to the mine area, this project would not have been possible. A special thanks to the geophysical division at the GSN for the warm welcome, assistance and of course all the hard work in and out of field; Dave Hutchins, Nortin Titus, Ivor Kahimise, Tjipekapora T. Katjuongua, Simeon Shilamba, Ronneliah Mako Sitali and Andries Johannes, as well as Job Schikongo at Weatherly Namibia at the Matchless Mine for the guidance in field.

Special regards to Rune Johansson, project manager at MeetingPoints Mining for giving me the opportunity to be a part of the project. Thanks to Erik Jonsson, Mats Thörnelöf and Sven Aaro at SGU for all assistance, in and out of field, discussions and the help throughout the work of the thesis. Mats Thörnelöf carried out the VLF measurement which is greatly acknowledged. Sven Aaro introduced me to the gravity method in theory and practice. I would also like to thank my supervisor at Lund University, Anders Scherstén, for his guidance through the process. I would like to express great appreciation to Carl-Axel Triumpf for taking the role as supervisor although not stated as such and for the introduction to the SP method. Thanks for your commitment and for the humor everything was performed with. Lastly I would like to express my greatest appreciation to my main supervisor Lutz Kübler for the uncountable hours of assistance in every part throughout this work. Thanks for always having an open door (phone line or chat), for the numerous discussions and your patient support.

12. REFERENCES

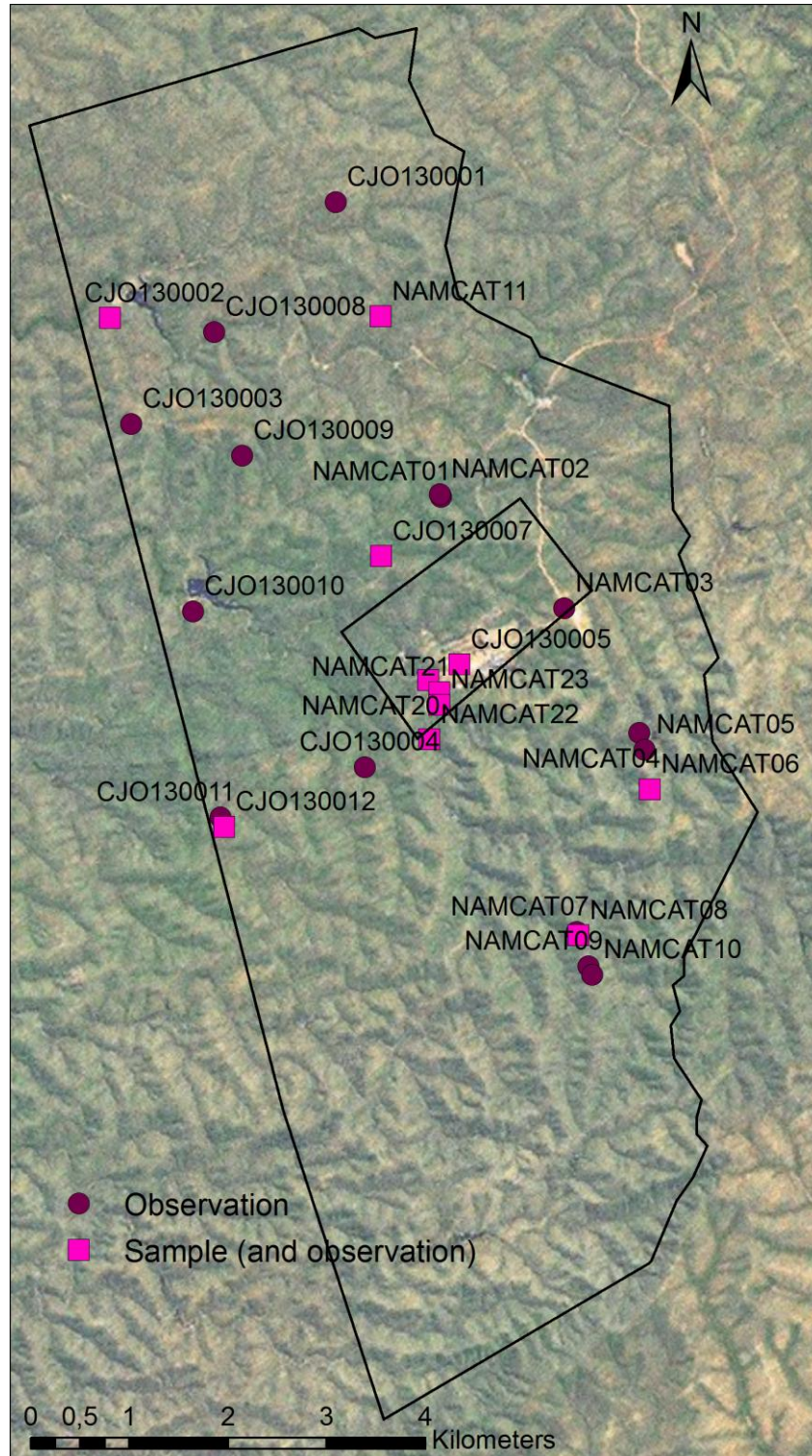
- Balsley, J. R. and A. F. Buddington (1958). "Iron-titanium oxide minerals, rocks, and aeromagnetic anomalies of the Adirondack area, New York." Economic Geology **53**(7): 777-805.
- Baranov, V. and H. Naudy (1964). "Numerical calculation of the formula of reduction to the magnetic pole." Geophysics **29**(1): 67-79.
- Barnes, S.-J. and E. W. Sawyer (1980). "An alternative model for the Damara Mobile Belt: Ocean crust subduction and continental convergence." Precambrian Research **13**(4): 297-336.
- Benson, H. (1996). University Physics, Wiley.
- Breitkopf, J. H. and K. J. Maiden (1988). "Tectonic setting of the Matchless Belt pyritic copper deposits, Namibia." Economic Geology **83**(4): 710-723.
- Cook, N. J., R. Klemd and M. Okrusch (1994). "Sulphide mineralogy, metamorphism and deformation in the Matchless massive sulphide deposit, Namibia." Mineralium Deposita **29**(1-15).
- Corry, C. E. (1985). "Spontaneous polarization associated with porphyry sulfide mineralization." Geophysics **50**(6): 1020-1034.
- Corry, C. E., G. T. DeMouilly and M. T. Gerety (1982). Field Procedure Manual for Self-Potential Surveys. Zonge Engineering & Research Organization.
- Dunlop, D. J. and Ö. Özdemir (2009). 8 - Magnetizations in Rocks and Minerals. Treatise on Geophysics. G. Schubert. Amsterdam, Elsevier: 277-336.
- Fodor, R. V. and S. K. Vetter (1984). "Rift-zone magmatism: Petrology of basaltic rocks transitional from CFB to MORB, southeastern Brazil margin." Contributions to Mineralogy and Petrology **88**(4): 307-321.
- Frimmel, H. E., U. S. Klötzli, P. R. Siegfried and S. University of Cape Town. Dept. of Geological (1996). "New Pb-Pb single Zircon age constraints on the timing of neoproterozoic glaciation and continental break-up in Namibia."
- Geometrics, I. (2005). G-859 MINING MAG Cesium Vapor Magnetometer - Operation Manual.
- Goldberg, I. (1976). "A preliminary account of the Otjihase copper deposit, South West Africa." Economic Geology **71**(1): 384-390.
- Goscombe, B., D. Gray, R. Armstrong, D. A. Foster and J. Vogl (2005). "Event geochronology of the Pan-African Kaoko Belt, Namibia." Precambrian Research **140**(3-4): 103.e101-103.e141.
- Gray, D. R., D. A. Foster, B. Goscombe, C. W. Passchier and R. A. J. Trouw (2006). "⁴⁰Ar/³⁹Ar thermochronology of the Pan-African Damara Orogen, Namibia, with implications for tectonothermal and geodynamic evolution." Precambrian Research **150**(1-2): 49-72.
- Gray, D. R., D. A. Foster, J. G. Meert, B. D. Goscombe, R. Armstrong, R. A. J. Trouw and C. W. Passchier (2008). A Damara orogen perspective on the assembly of southwestern Gondwana. **294**: 257-278.
- Hamilton, S. and K. Hattori (2008). "Spontaneous potential and redox responses over a forest ring." Geophysics **73**(3): B67-B75.
- Hamilton, S., K. Hattori and Brauner K. (2008). Redox-induced spontaneous polarization as a cause of large self potential anomalies over disseminated sulphides and other buried features. KEGS Symposium, Canadian Exploration Geophysical Society meeting. Toronto.
- Heiland, C. A. (1946). Geophysical Exploration. New York, Prentice-Hall, inc.

- Hunt, C. P., B. M. Moskowitz and S. K. Banerjee (1995). Magnetic properties of rocks and minerals. Rock Physics & Phase Relations: A Handbook of Physical Constants. Washington, DC, AGU. **3**: 189-204.
- Hutchins, D. G., S. C. Milner and E. Korkiakoski (1997). Regional Airborne Geophysics and Geochemistry: A Namibian Perspective. Fourth Decennial International Conference on Mineral Exploration. A. G. Gubins, Proceedings of Exploration 97: 779-792.
- Hutchins, D. G. and R. Wackerle (2007). The High Resolution Airborne Geophysical Survey Programme of Namibia: A Success Story in Promoting Mineral Exploration. Fifth Decennial International Conference on Mineral Exploration.
- Jacobsen, B. H. (1987). "A case for upward continuation as a standard separation filter for potential-field maps." Geophysics **52**(8): 1138-1148.
- Killick, A. M. (2000). "The Matchless Belt and associated sulphide mineral deposits, Damara Orogen, Namibia." Communs geological Survey of Namibia **2000**(12): 73-80.
- Klemd, R., K. J. Maiden and M. Okrusch (1987). "The Matchless copper deposit, South West Africa/Namibia; a deformed and metamorphosed massive sulfide deposit." Economic Geology **82**(3): 587-599.
- Klemd, R., K. J. Maiden, M. Okrusch and P. Richter (1989). "Geochemistry of the Matchless metamorphosed massive sulfide deposit, South West Africa/Namibia; wall-rock alteration during submarine ore-forming processes." Economic Geology **84**(3): 603-617.
- Kroner, A. (1977). "Precambrian mobile belts of southern and eastern africa — ancient sutures or sites of ensialic mobility? a case for crustal evolution towards plate tectonics." Tectonophysics **40**(1–2): 101-135.
- Kröner, A. and R. J. Stern (2005). AFRICA | Pan-African Orogeny. Encyclopedia of Geology. C. S. Editors-in-Chief: Richard, L. R. M. Cocks and R. P. Ian. Oxford, Elsevier: 1-12.
- Longman, I. M. (1959). "Formulas for computing the tidal accelerations due to the moon and the sun." Journal of Geophysical Research **64**(12): 2351-2355.
- Martin, H. and H. Porada (1977). "The intracratonic branch of the Damara Orogen in South West Africa II. Discussion of relationships with the Pan-African mobile belt system." Precambrian Research **5**(4): 339-357.
- McElhinny, M. W. (1973). Palaeomagnetism and plate tectonics, Cambridge university press.
- Miller, H. G. and V. Singh (1994). "Potential field tilt—a new concept for location of potential field sources." Journal of Applied Geophysics **32**(2–3): 213-217.
- Miller, R. M., H. E. Frimmel and G. P. Halverson (2009). Chapter 5.3 Passive Continental Margin Evolution. Developments in Precambrian Geology. A. N. S. H. E. F. Claudio Gaucher and P. H. Galen, Elsevier. **Volume 16**: 161-181.
- Miller, R. M. G., T. Becker and G. Survey (2008). The Geology of Namibia: Neoproterozoic to lower palaeozoic, Ministry of Mines and Energy, Geological Survey.
- Miller, R. M. G., S. A. C. f. Scientific and I. Research (1983). The Pan-African Damara Orogen of South West Africa/Namibia, Geological Society of South Africa.
- Nyquist, J. and C. Corry (2002). "Self-potential: The ugly duckling of environmental geophysics." The Leading Edge **21**(5): 446-451.
- Parasnis, D. S. (1966). Mining Geophysics, Elsevier Publishing Company.
- Parasnis, D. S. (1986). Principles of applied geophysics, Chapman and Hall.
- Puranen, M. and R. Puranen (1977). Apparatus for the measurement of magnetic susceptibility and its anisotropy. Report of investigation. Geological Survey of Finland. **No. 28**.

- Puranen, R., K. Sulkanen, A. Poikonen, R. Nissinen, P. Simelius and L. Harinen (1993). User's manual for computerized petrophysics laboratory. Instrumentation Report.
- Reynolds, J. M. (2011). An introduction to Applied and Environmental Geophysics.
- Sato, M. and H. M. Mooney (1960). "The electrochemical mechanism of sulfide self-potentials." Geophysics **25**(1): 226-249.
- Schneider, A. (1983). The Chemical Composition of the Common Metamorphic Sediments of the Damara Orogen. Intracontinental Fold Belts. H. Martin and F. Eder, Springer Berlin Heidelberg: 655-677.
- Schoeman, P. (1996). Overview and comparison of Besshi-type deposits: ancient and recent. MSc Dissertation, Rhodes University.
- SCINTREX (2009). CG-5 Scintrex Autograv System, Operation Manual.
- Sharma, P. V. (1986). Geophysical Methods in Geology. New York, Elsevier Science Publishing Co., Inc.
- Smith, K. (1997). Technical Report M-TR91, Cesium Optically Pumped Magnetometers, Basic Theory of Operation.

APPENDIX 1 – OBSERVATION AND SAMPLE DESCRIPTIONS

Coordinate reference system: WGS84 UTM 33S



ID: NAMCAT01

Observation

Observation date: 2013-04-11**Coordinates:**

E 689235

S 7490910

Locality description:**Description**

Object: outcrop

Rock type: schist

Structure:

Texture:

Grainsize:

Color:

Strike:

Dip:

Comments:

Magnetic susceptibility, in situ measurement on outcrop

Measurement no:	1	2	3	4	5	6	7	8	9
Mag. susc (μ SI):	184	196	150	296	131	174	252	253	

ID: NAMCAT02

Observation

Observation date: 2013-04-11**Coordinates:**

E 689227

S 7490933

Locality description:**Description**

Object: outcrop

Rock type: amphibolite

Structure:

Texture:

Grainsize:

Color:

Strike:

Dip:

Comments: Occurs as lenses in shist

Magnetic susceptibility, in situ measurement on outcrop

Measurement no:	1	2	3	4	5	6	7	8	9
Mag. susc (μ SI):	611	8890	651	699	831	742	528	351	568

ID: NAMCAT03

Observation

Observation date: 2013-04-11**Coordinates:**

E 690378

S 7489858

Locality description:**Description**

Object: boulder

Rock type: Cu-ore

Structure:

Texture:

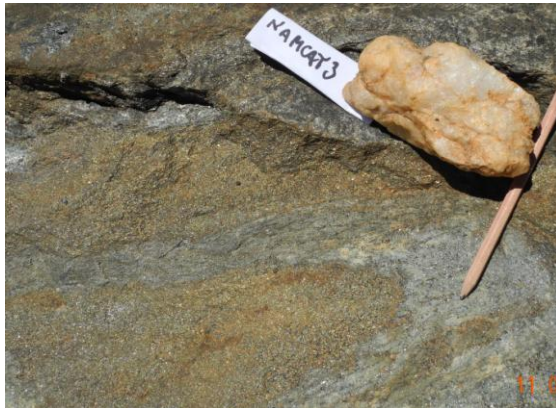
Grainsize:

Color:

Strike:

Dip:

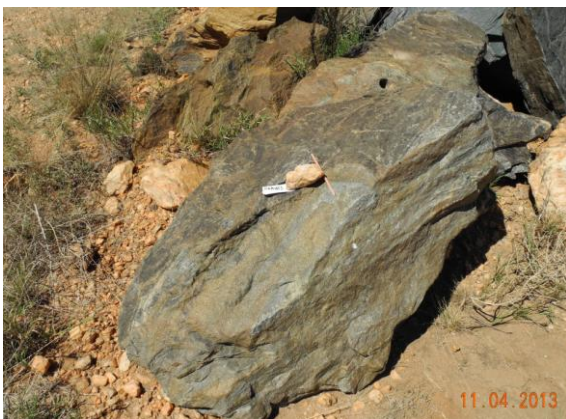
Comments:



Carl-Axel Triumpf, 2013

Magnetic susceptibility, in situ measurement on outcrop

Measurement no:	1	2	3	4	5	6	7	8	9
Mag. susc (μ SI):	319	244	227	216	383	182	233	227	



Carl-Axel Triumpf, 2013

ID: NAMCAT04

Observation

Observation date: 2013-04-11**Coordinates:**

E 691067

S 7488687

Locality description:**Description**

Object: outcrop

Rock type: schist

Structure: schistosity

Texture:

Grainsize:

Color: dark colored

Strike:

Dip:

Comments: Intensely folded with quartz-pebbles or boudins.



Carl-Axel Triumf, 2013

Magnetic susceptibility, in situ measurement on outcrop

Measurement no:	1	2	3	4	5	6	7	8	9
Mag. susc (μ SI):	256	273	283	225	314	206	270	331	



Carl-Axel Triumf, 2013



Carl-Axel Triumf, 2013

ID: NAMCAT05

Observation

Observation date: 2013-04-11**Coordinates:**

E 691116

S 7488526

Locality description:**Description**

Object: outcrop

Rock type: schist

Structure: schistosity

Texture:

Grainsize:

Color: light colored

Strike:

Dip:

Comments: Strongly weathered. Flat outcrop.



Carl-Axel Triumf, 2013

Magnetic susceptibility, in situ measurement on outcrop

Measurement no:	1	2	3	4	5	6	7	8	9
Mag. susc (μ SI):	240	5450	2750	5010	6550	4030	4560	6210	

ID: NAMCAT06

Observation and sample

Observation date: 2013-04-11**Coordinates:**

E 691160

S 7488158

Locality description:**Description**

Object: outcrop
 Rock type: schist
 Structure: schistosity
 Texture: equigranular
 Grainsize: medium grained
 Color: light colored
 Strike:
 Dip:
 Comments: Strongly weathered



Anders Gustafsson, 2013

Magnetic susceptibility, in situ measurement on outcrop

Measurement no:	1	2	3	4	5	6	7	8	9
Mag. susc (μSI):	747	395	1070	234	334	401	6430	3040	

Petrophysical measurements

Volume (cm^3)	Density (kg/m^3)	Mag. susc (μSI)	J (mA/m)	Q-value
175.7	2731	14569	6730	11.28



Carl-Axel Triumf, 2013



Carl-Axel Triumf, 2013

ID: NAMCAT07

Observation

Observation date: 2013-04-12**Coordinates:**

E 690459

S 7486835

Locality description:**Description**

Object: outcrop in road

Rock type: mica schist

Structure: schistosity

Texture:

Grainsize:

Color:

Strike: 265°

Dip: 50°

Comments:



Carl-Axel Triumf, 2013

Magnetic susceptibility, in situ measurement on outcrop

Measurement no:	1	2	3	4	5	6	7	8	9
Mag. susc (μ SI):	304	306	306	3130	152	291	145	305	287

ID: NAMCAT08

Observation and sample

Observation date: 2013-04-12**Coordinates:**

E 690474

S 7486805

Locality description:**Description**

Object: outcrop

Rock type: schist

Structure: schistosity, folded

Texture:

Grainsize: medium grained

Color: dark colored

Strike: 250° (255°)

Dip: 40° (20°)

Comments: Strike and dip are given for schistosity and fold axis (in brackets). Schist with thin layers (less than 5 mm) of quartz and potassiumfeldspar, also boudins of quartz up to 0.2 m thick.



Anders Gustafsson, 2013

Magnetic susceptibility, in situ measurement on outcrop

Measurement no:	1	2	3	4	5	6	7	8	9
Mag. susc (μSI):	278	209	238	295	278	162	392	249	347

Petrophysical measurements

Volume (cm ³)	Density (kg/m ³)	Mag. susc (μSI)	J (mA/m)	Q-value
110.0	2788	600	20	0.61



Carl-Axel Triumf, 2013



Carl-Axel Triumf, 2013

ID: NAMCAT09

Observation

Observation date: 2013-04-12**Coordinates:**

E 690566

S 7486517

Locality description:**Description**

Object: outcrop in road

Rock type: mica schist

Structure:

Texture:

Grainsize:

Color:

Strike:

Dip:

Comments:

Magnetic susceptibility, in situ measurement on outcrop

Measurement no:	1	2	3	4	5	6	7	8	9
Mag. susc (μ SI):	164	110	114	173	181	121	64	166	186

ID: NAMCAT10

Observation

Observation date: 2013-04-12**Coordinates:**

E 690596

S 7486436

Locality description:**Description**

Object: outcrop near road

Rock type: schist

Structure:

Texture:

Grainsize:

Color:

Strike:

Dip:

Comments: Schist within layers (<5 mm) of quartz and potassiumfeldspar.



Carl-Axel Triumpf, 2013

Magnetic susceptibility, in situ measurement on outcrop

Measurement no:	1	2	3	4	5	6	7	8	9
Mag. susc (μ SI):	330	394	188	230	252	202	262	216	318



Carl-Axel Triumpf, 2013



Carl-Axel Triumpf, 2013

ID: NAMCAT11

Observation and sample

Observation date: 2013-04-12**Coordinates:**

E 688691

S 7492599

Locality description:**Description**

Object: boulders of local origin at road

Rock type: meta-arenite

Structure: weak schistosity, mica rich

Texture: equigranular

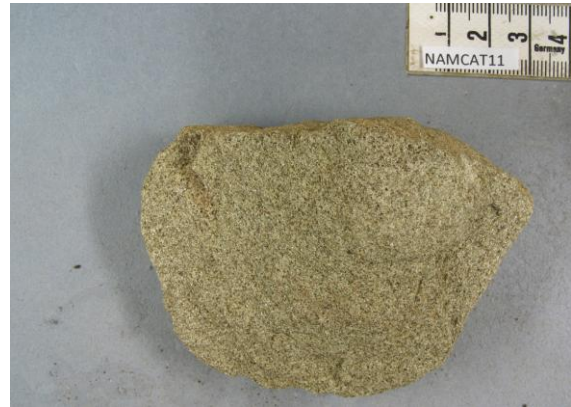
Grainsize: fine grained

Color: light colored

Strike: 265°

Dip: north

Comments: This rock type is also found in an small outcrop in the road. Very brittle.



Anders Gustafsson, 2013

Magnetic susceptibility, in situ measurement on outcrop

Measurement no:	1	2	3	4	5	6	7	8	9
Mag. susc (μSI):	5120	4870	4720	6110	4420	5820	6100	5110	

Petrophysical measurements

Volume (cm ³)	Density (kg/m ³)	Mag. susc (μSI)	J (mA/m)	Q-value
149.4	2602	7600	2790	8.95



Carl-Axel Triumf, 2013



Carl-Axel Triumf, 2013

ID: NAMCAT12

Observation and sample

Observation date: 2013-04-12**Coordinates:**

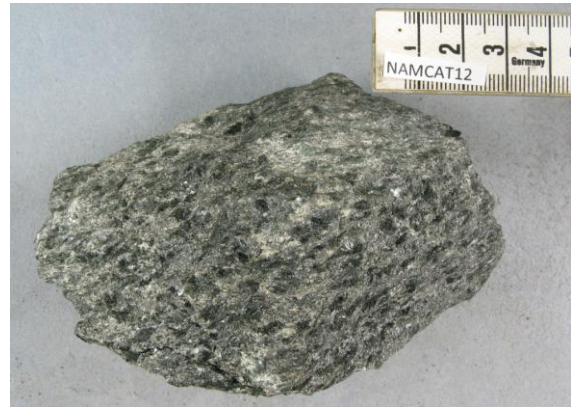
E -
S -

Locality description:

From waste rock dump, exact location from below ground is not known.

Description

Object: waste rock dump
 Rock type: amphibolite/metagabbro
 Structure: foliated
 Texture:
 Grainsize: coarse medium grained
 Color: dark gray
 Strike:
 Dip:
 Comments: Secondary amphibolite.



Anders Gustafsson, 2013

Magnetic susceptibility, in situ measurement on outcrop

Measurement no:	1	2	3	4	5	6	7	8	9
Mag. susc (μ SI):									

Petrophysical measurements

Volume (cm^3)	Density (kg/m^3)	Mag. susc (μ SI)	J (mA/m)	Q-value
219.7	2970	1760	130	1.82

ID: NAMCAT13

Observation and sample

Observation date: 2013-04-12**Coordinates:**

E -
S -

Locality description:

From waste rock dump, exact location from below ground is not known.

Description

Object: waste rock dump
 Rock type: amphibolite/metagabbro
 Structure: foliated
 Texture:
 Grainsize: coarse medium grained
 Color: dark gray
 Strike:
 Dip:
 Comments: Secondary amphibolite with more plagioclase compared to NAMCAT12.



Anders Gustafsson, 2013

Magnetic susceptibility, in situ measurement on outcrop

Measurement no:	1	2	3	4	5	6	7	8	9
Mag. susc (μSI):									

Petrophysical measurements

Volume (cm^3)	Density (kg/m^3)	Mag. susc (μSI)	J (mA/m)	Q-value
250.6	2966	750	10	0.21

ID: NAMCAT14

Observation and sample

Observation date: 2013-04-12**Coordinates:**

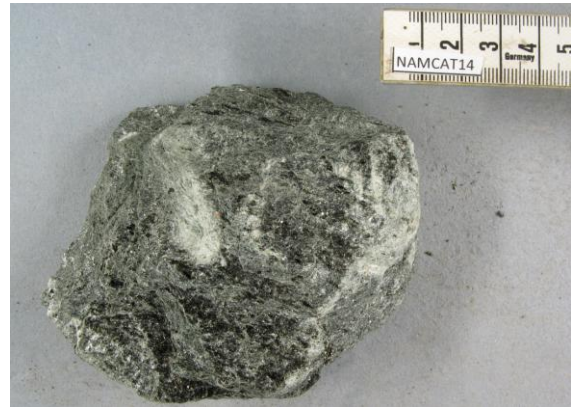
E -
S -

Locality description:

From waste rock dump, exact location from below ground is not known.

Description

Object: waste rock dump
 Rock type: mica schist
 Structure: schistosity
 Texture: equigranular
 Grainsize: medium grained
 Color: dark colored
 Strike:
 Dip:
 Comments: Mica schist with no quartz.



Anders Gustafsson, 2013

Magnetic susceptibility, in situ measurement on outcrop

Measurement no:	1	2	3	4	5	6	7	8	9
Mag. susc (μSI):									

Petrophysical measurements

Volume (cm^3)	Density (kg/m^3)	Mag. susc (μSI)	J (mA/m)	Q-value
151.4	2806	500	0	0.24

ID: NAMCAT15

Observation and sample

Observation date: 2013-04-12**Coordinates:**

E -
S -

Locality description:

From waste rock dump, exact location from below ground is not known.

Description

Object: waste rock dump
 Rock type: chlorite mica schist
 Structure: schistosity, with quartz lenses
 Texture: equigranular
 Grainsize: medium grained
 Color: dark colored
 Strike:
 Dip:
 Comments: Mica schist with quartz lenses. Sample is taken close to orebody.



Anders Gustafsson, 2013

Magnetic susceptibility, in situ measurement on outcrop

Measurement no:	1	2	3	4	5	6	7	8	9
Mag. susc (μSI):									

Petrophysical measurements

Volume (cm^3)	Density (kg/m^3)	Mag. susc (μSI)	J (mA/m)	Q-value
198.3	2771	390	0	0.21

ID: NAMCAT16

Observation and sample

Observation date: 2013-04-12**Coordinates:**

E -
S -

Locality description:

From waste rock dump, exact location from below ground is not known.

Description

Object: waste rock dump
 Rock type: chlorite mica schist
 Structure: schistosity, with quartz lenses
 Texture: equigranular
 Grainsize: medium grained
 Color: dark colored
 Strike:
 Dip:
 Comments:



Anders Gustafsson, 2013

Magnetic susceptibility, in situ measurement on outcrop

Measurement no:	1	2	3	4	5	6	7	8	9
Mag. susc (μSI):									

Petrophysical measurements

Volume (cm^3)	Density (kg/m^3)	Mag. susc (μSI)	J (mA/m)	Q-value
272.7	2785	350	0	0.32

ID: NAMCAT17

Observation and sample

Observation date: 2013-04-12**Coordinates:**

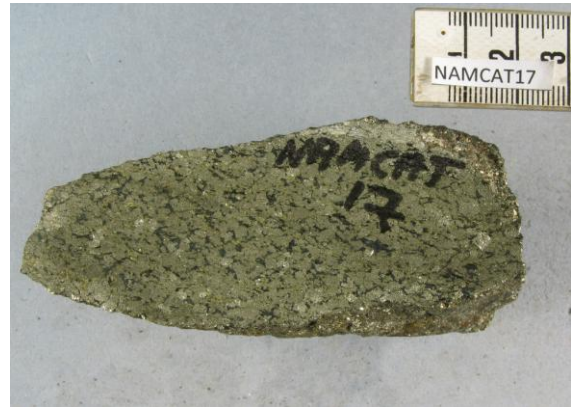
E -
S -

Locality description:

From waste rock dump, exact location from below ground is not known.

Description

Object: waste rock dump
 Rock type: Cu-ore
 Structure: massive
 Texture: equigranular
 Grainsize: medium grained
 Color:
 Strike:
 Dip:
 Comments: Sample of copper-ore.



Anders Gustafsson, 2013

Magnetic susceptibility, in situ measurement on outcrop

Measurement no:	1	2	3	4	5	6	7	8	9
Mag. susc (μSI):									

Petrophysical measurements

Volume (cm^3)	Density (kg/m^3)	Mag. susc (μSI)	J (mA/m)	Q-value
209.5	4502	4150	20	0.11

ID: NAMCAT18

Observation and sample

Observation date: 2013-04-12**Coordinates:**

E -
S -

Locality description:

From ore dump, exact location below ground is not known.

Description

Object: ore dump
 Rock type: Cu-ore
 Structure: massive
 Texture: equigranular
 Grainsize: medium grained
 Color:
 Strike:
 Dip:
 Comments: Elongated amphiboles. Sulfide changing to bornite.



Anders Gustafsson, 2013

Magnetic susceptibility, in situ measurement on outcrop

Measurement no:	1	2	3	4	5	6	7	8	9
Mag. susc (μSI):									

Petrophysical measurements

Volume (cm^3)	Density (kg/m^3)	Mag. susc (μSI)	J (mA/m)	Q-value
264.1	3988	710	20	0.69

ID: NAMCAT19

Observation and sample

Observation date: 2013-04-12**Coordinates:**

E -
S -

Locality description:

From ore dump, exact location below ground is not known.

Description

Object: ore dump
 Rock type: Cu-ore
 Structure: massive
 Texture: equigranular
 Grainsize: medium grained
 Color:
 Strike:
 Dip:
 Comments:



Anders Gustafsson, 2013

Magnetic susceptibility, in situ measurement on outcrop

Measurement no:

1	2	3	4	5	6	7	8	9
---	---	---	---	---	---	---	---	---

Mag. susc (μSI):

Petrophysical measurements

Volume (cm^3)	Density (kg/m^3)	Mag. susc (μSI)	J (mA/m)	Q-value
179.7	3912	2090	10	0.14

ID: NAMCAT20

Observation and sample

Observation date: 2013-04-16**Coordinates:**

E 689097

S 7489203

Locality description:**Description**

Object: outcrop
 Rock type: amphibolite/metagabbro
 Structure: massive
 Texture: uneven grained
 Grainsize: medium grained
 Color: dark colored
 Strike:
 Dip:
 Comments:



Anders Gustafsson, 2013

Magnetic susceptibility, in situ measurement on outcrop

Measurement no:	1	2	3	4	5	6	7	8	9
Mag. susc (μ SI):	405	365	425	366	388	159	432	564	

Petrophysical measurements

Volume (cm^3)	Density (kg/m^3)	Mag. susc (μ SI)	J (mA/m)	Q-value
219.5	2953	700	10	0.19



Carl-Axel Triumf, 2013



Carl-Axel Triumf, 2013

ID: NAMCAT21

Observation and sample

Observation date: 2013-04-17**Coordinates:**

E 689200

S 7489088

Locality description:**Description**

Object: outcrop
 Rock type: amphibolite/metagabbro
 Structure: massive
 Texture: uneven grained
 Grainsize: medium grained
 Color: dark colored
 Strike:
 Dip:
 Comments:



Anders Gustafsson, 2013

Magnetic susceptibility, in situ measurement on outcrop

Measurement no:	1	2	3	4	5	6	7	8	9
Mag. susc (μ SI):	389	317	294	373	356	370	332	322	338

Petrophysical measurements

Volume (cm^3)	Density (kg/m^3)	Mag. susc (μ SI)	J (mA/m)	Q-value
188.2	2932	610	0	0.17



Carl-Axel Triumf, 2013



Carl-Axel Triumf, 2013

ID: NAMCAT22

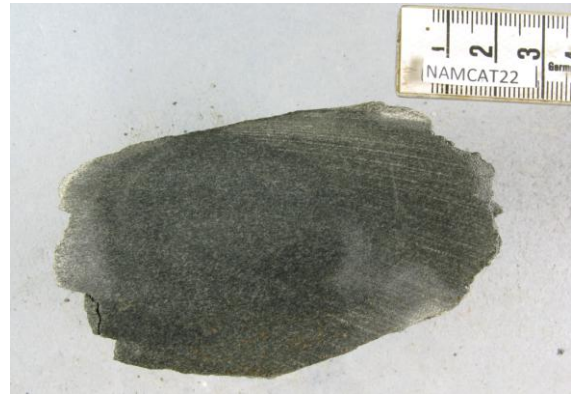
Observation and sample

Observation date: 2013-04-17**Coordinates:****E** 689102**S** 7488650**Locality description:**

Rock wall with shearzone structures such as quartz boundins and overturned fold structures

Description

Object: outcrop
 Rock type: mica schist
 Structure: quartz lenses, schistosity, shear zone
 Texture: equigranular
 Grainsize: fine grained
 Color: dark colored
 Strike:
 Dip:
 Comments: Shear zone with heterogenous deformation. Quartz boundins up to 0.5 m large and overturned fold structures. Some unaffected and heterogenous layers.



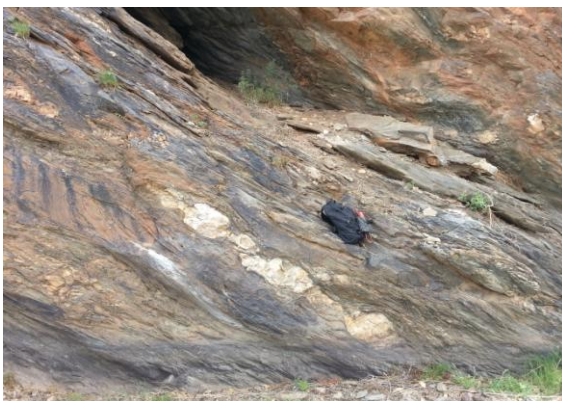
Anders Gustafsson, 2013

Magnetic suceptibility, in situ measurement on outcrop

Measurement no:	1	2	3	4	5	6	7	8	9
Mag. susc (μ SI):	313	223	198	388	194	228	373	362	

Petrophysical measurements

Volume (cm^3)	Density (kg/m^3)	Mag. susc (μ SI)	J (mA/m)	Q-value
214.5	2726	600	10	0.32



Cecilia Jönsson, 2013



Carl-Axel Triumf, 2013

ID: NAMCAT23A

Observation and sample

Observation date: 2013-04-17**Coordinates:**

E 689198

S 7488971

Locality description:**Description**

Object: outcrop

Rock type: magnetite quartzite

Structure: layered

Texture:

Grainsize: medium grained

Color:

Strike:

Dip:

Comments: Gossan outcrop with surrounding schist. Possible directional susceptibility variation over the gossan with the highest value perpendicular to layering. Extremely weathered. With magnetite and hematite.



Anders Gustafsson, 2013

Magnetic susceptibility, in situ measurement on outcrop

Measurement no:	1	2	3	4	5	6	7	8	9
Mag. susc (μ SI):	15000	50100	24700	22100	20100	496	635	2090	60300

Petrophysical measurements

Volume (cm^3)	Density (kg/m^3)	Mag. susc (μ SI)	J (mA/m)	Q-value
251.2	2760	199660	185230	22.64



Cecilia Jönsson, 2013



Cecilia Jönsson, 2013

ID: NAMCAT23B

Observation and sample

Observation date: 2013-04-17**Coordinates:**

E 689198

S 7488971

Locality description:**Description**

Object: outcrop

Rock type: schist

Structure: schistosity

Texture: equigranular

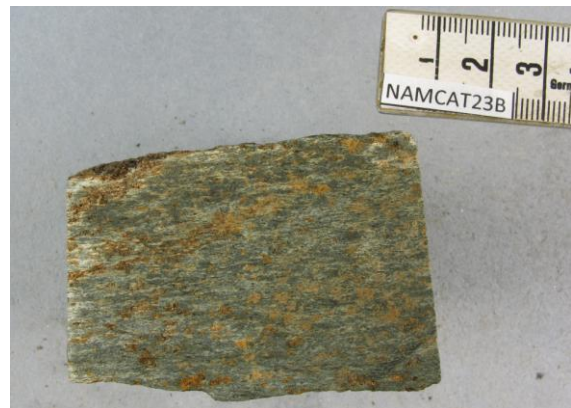
Grainsize: fine grained

Color:

Strike:

Dip:

Comments: Schist surrounding gossan. Large variations in susceptibility which might be due to heterogenous weathering of magnetite.



Anders Gustafsson, 2013

Magnetic susceptibility, in situ measurement on outcrop

Measurement no:	1	2	3	4	5	6	7	8	9
Mag. susc (μ SI):	574	490	425	363	939	830	350	596	

Petrophysical measurements

Volume (cm^3)	Density (kg/m^3)	Mag. susc (μ SI)	J (mA/m)	Q-value
118.8	2496	960	20	0.63

ID: CJO130001

Observation

Observation date: 2013-04-05**Coordinates:****E** 688286**S** 7493666**Locality description:**Small outcrop (<5m²), with blocks of same rocktype.**Description**

Object: outcrop/blocks

Rock type: schist

Structure:

Texture:

Grainsize:

Color:

Strike:

Dip:

Comments: Not a typical Kuiseb schist, no muscovite.

Magnetic susceptibility, in situ measurement on outcrop

Measurement no:	1	2	3	4	5	6	7	8	9
Mag. susc (μSI):	141								

ID: CJO130002

Observation and sample

Observation date: 2013-04-05**Coordinates:**

E 686157

S 7492615

Locality description:

Vertical blocks of local origin.

Description

Object: outcrop/blocks

Rock type: schist

Structure: schistosity

Texture: equigranular

Grainsize: fine grained

Color: dark colored

Strike:

Dip:

Comments:



Anders Gustafsson, 2013

Magnetic susceptibility, in situ measurement on outcrop

Measurement no:	1	2	3	4	5	6	7	8	9
Mag. susc (μSI):	137	151	112	103	182				

Petrophysical measurements

Volume (cm^3)	Density (kg/m^3)	Mag. susc (μSI)	J (mA/m)	Q-value
121.4	2705	320	0	0.25



Cecilia Jönsson, 2013



Cecilia Jönsson, 2013

ID: CJO130003

Observation

Observation date: 2013-04-05**Coordinates:**

E 686344

S 7491623

Locality description:

One vertical block, possible a gossan. Quartz rich.

Description

Object: outcrop/blocks

Rock type: gossan?

Structure:

Texture:

Grainsize:

Color:

Strike:

Dip:

Comments:



Cecilia Jönsson, 2013

Magnetic susceptibility, in situ measurement on outcrop

Measurement no:	1	2	3	4	5	6	7	8	9
Mag. susc (μ SI):	908	514	325	2200	663				



Cecilia Jönsson, 2013

ID: CJO130004

Observation

Observation date: 2013-04-05**Coordinates:**

E	-
S	-

Locality description:

Sample collected from ore dump, exact location below ground is unknown.

Description

Object: ore dump

Rock type: -

Structure: layered

Texture: equigranular

Grainsize: fine grained

Color:

Strike:

Dip:

Comments: Ore dump consisting of ore material and amphibolite.



Cecilia Jönsson, 2013

Magnetic susceptibility, in situ measurement on outcrop

Measurement no:	1	2	3	4	5	6	7	8	9
Mag. susc (μ SI):	2100	201	130	104	112	384	196	159	

ID: CJO130005

Observation and sample

Observation date: 2013-04-05**Coordinates:**

E 689393

S 7489345

Locality description:

Outcrop along road in mining area.

Description

Object: outcrop

Rock type: amphibolite

Structure: strong schistosity

Texture: equigranular

Grainsize:

Color:

Strike:

Dip:

Comments: Strongly deformed and weathered.



Anders Gustafsson, 2013

Magnetic susceptibility, in situ measurement on outcrop

Measurement no:	1	2	3	4	5	6	7	8	9
Mag. susc (μ SI):	465	611	601	667	410	574			

Petrophysical measurements

Volume (cm^3)	Density (kg/m^3)	Mag. susc (μ SI)	J (mA/m)	Q-value
153.0	3010	1020	0	0.12

ID: CJO130006

Observation and sample

Observation date: 2013-04-19**Coordinates:**

E 701216

S 7501194

Locality description:Large outcrop area >20m² weathered.**Description**

Object: outcrop
 Rock type: amphibolite/metagabbro
 Structure: massive, strongly weathered
 Texture: uneven grained
 Grainsize: coarse medium grained
 Color: dark colored
 Strike:
 Dip:
 Comments: Outcrop along road between Windhoek and research area.



Anders Gustafsson, 2013

Magnetic susceptibility, in situ measurement on outcrop

Measurement no:	1	2	3	4	5	6	7	8	9
Mag. susc (μSI):	428	430	409	468	360	450	421	440	

Petrophysical measurements

Volume (cm ³)	Density (kg/m ³)	Mag. susc (μSI)	J (mA/m)	Q-value
210.7	2970	690	0	0.05



Cecilia Jönsson, 2013



Cecilia Jönsson, 2013

ID: CJO130007

Observation and sample

Observation date: 2013-04-23**Coordinates:**

E 688669

S 7490363

Locality description:

Outcrop and block standing out from the ground in an inclined fashion, along foliation plane. Large

Description

Object: outcrop
 Rock type: amphibolite
 Structure: schistosity
 Texture: equigranular
 Grainsize: fine grained
 Color: light gray
 Strike:
 Dip:
 Comments:



Anders Gustafsson, 2013

Magnetic susceptibility, in situ measurement on outcrop

Measurement no:	1	2	3	4	5	6	7	8	9
Mag. susc (μSI):	5870	525	8120	447	754	399	550	2160	8240

Petrophysical measurements

Volume (cm^3)	Density (kg/m^3)	Mag. susc (μSI)	J (mA/m)	Q-value
253.9	2829	24040	60	0.06



Cecilia Jönsson, 2013



Cecilia Jönsson, 2013

ID: CJO130008

Observation

Observation date: 2013-04-24**Coordinates:**

E 687133

S 7492473

Locality description:

Flat outcrop on road with evident planar structure.
Outcrop area about 10m²

Description

Object: outcrop, flat
Rock type: mica schist
Structure: schistosity
Texture:
Grainsize: fine grained
Color: light colored
Strike:
Dip:
Comments: With quartz lenses.



Cecilia Jönsson, 2013

Magnetic susceptibility, in situ measurement on outcrop

Measurement no:	1	2	3	4	5	6	7	8	9
Mag. susc (μSI):	610	2240	795	726	1370	5020	4150	9840	



Cecilia Jönsson, 2013



Cecilia Jönsson, 2013

ID: CJO130009

Observation and sample

Observation date: 2013-04-24**Coordinates:****E** 687378**S** 7491317**Locality description:**Outcrop and blocks of same rock type. Area about 15m² and outcrop <5m².**Description****Object:** outcrop/boulders**Rock type:** mica schist**Structure:** schistosity**Texture:****Grainsize:****Color:****Strike:****Dip:****Comments:**

Anders Gustafsson, 2013

Magnetic susceptibility, in situ measurement on outcrop

Measurement no:	1	2	3	4	5	6	7	8	9
Mag. susc (μSI):	216	207	183	204	306	147	237	222	

Petrophysical measurements

Volume (cm ³)	Density (kg/m ³)	Mag. susc (μSI)	J (mA/m)	Q-value
341.0	2662	250	0	0.32



Cecilia Jönsson, 2013



Cecilia Jönsson, 2013

ID: CJO130010A

Observation

Observation date: 2013-04-24**Coordinates:**

E 686903

S 7489869

Locality description:

Flat outcrop of mica schist with large lenses of amphibolite.

Description

Object: outcrop

Rock type: mica schist

Structure:

Texture:

Grainsize:

Color:

Strike:

Dip:

Comments: With darker lenses of amphibolite (CJO130010B)



Cecilia Jönsson, 2013

Magnetic susceptibility, in situ measurement on outcrop

Measurement no:	1	2	3	4	5	6	7	8	9
Mag. susc (μ SI):	225	329	694	638	266	2140	243	204	

ID: CJO130010B

Observation

Observation date: 2013-04-24**Coordinates:**

E 686903

S 7489869

Locality description:**Description**

Object: outcrop

Rock type: amphibolite

Structure:

Texture:

Grainsize:

Color:

Strike:

Dip:

Comments: Occurs as lenses in shist (CJO130010A)



Cecilia Jönsson, 2013

Magnetic susceptibility, in situ measurement on outcrop

Measurement no:	1	2	3	4	5	6	7	8	9
Mag. susc (μ SI):	298	515	538	553	443	344	1100	825	



Cecilia Jönsson, 2013

ID: CJO130011

Observation

Observation date: 2013-04-24**Coordinates:**

E 687134

S 7487948

Locality description:Large (>10m²) flat outcrop.**Description**

Object: outcrop, large
 Rock type: mica schist with quartz lenses
 Structure:
 Texture:
 Grainsize:
 Color: dark colored
 Strike:
 Dip:
 Comments:



Cecilia Jönsson, 2013

Magnetic susceptibility, in situ measurement on outcrop

Measurement no:	1	2	3	4	5	6	7	8	9
Mag. susc (μSI):	269	362	441	263	265	299	326		



Cecilia Jönsson, 2013



Cecilia Jönsson, 2013

ID: CJO130012

Observation and sample

Observation date: 2013-04-24**Coordinates:**

E 687169

S 7487857

Locality description:

Locality marked as anomaly during magnetic measurements. Inclined outcrops over and area

Description

Object: outcrop
 Rock type: schist
 Structure: foliated, crenulation cleavage
 Texture: equigranular
 Grainsize: fine grained
 Color:
 Strike:
 Dip:
 Comments: Strongly weathered and deformed, very hard.



Anders Gustafsson, 2013

Magnetic susceptibility, in situ measurement on outcrop

Measurement no:	1	2	3	4	5	6	7	8	9
Mag. susc (μ SI):	991	915	1360	2540	623	1460	853	940	

Petrophysical measurements

Volume (cm^3)	Density (kg/m^3)	Mag. susc (μ SI)	J (mA/m)	Q-value
182.4	2711	840	30	0.8



Cecilia Jönsson, 2013



Cecilia Jönsson, 2013

ID: DRILLCORE01

Observation and sample

Observation date: 2013-04-16**Coordinates:**

E -
S -

Locality description:

Remnant drillcore collected close to NAMCAT20,
exact location is unknown.

Description

Object: drillcore
 Rock type: mica schist
 Structure: schistosity
 Texture: equigranular
 Grainsize: fine grained
 Color:
 Strike:
 Dip:
 Comments: Fresh reference samples to compare with other collected at surface.



Anders Gustafsson, 2013

Magnetic susceptibility, in situ measurement on outcrop

Measurement no:	1	2	3	4	5	6	7	8	9
Mag. susc (μSI):									

Petrophysical measurements

Volume (cm^3)	Density (kg/m^3)	Mag. susc (μSI)	J (mA/m)	Q-value
79.2	2780	1260	20	0.39

ID: DRILLCORE02

Observation and sample

Observation date: 2013-04-16**Coordinates:**

E -
S -

Locality description:

Remnant drillcore collected close to NAMCAT20,
exact location is unknown.

Description

Object: drillcore
 Rock type: mica schist
 Structure: with quartz lenses, schistosity
 Texture: uneven grained
 Grainsize: fine to medium grained
 Color:
 Strike:
 Dip:
 Comments: Fresh reference samples to compare with other collected at surface.



Anders Gustafsson, 2013

Magnetic susceptibility, in situ measurement on outcrop

Measurement no:	1	2	3	4	5	6	7	8	9
Mag. susc (μSI):									

Petrophysical measurements

Volume (cm^3)	Density (kg/m^3)	Mag. susc (μSI)	J (mA/m)	Q-value
65.2	2941	390	20	1.11

ID: DRILLCORE03

Observation and sample

Observation date: 2013-04-16**Coordinates:**

E -
S -

Locality description:

Remnant drillcore collected close to NAMCAT20,
exact location is unknown.

Description

Object: drillcore
 Rock type: not determined
 Structure:
 Texture:
 Grainsize:
 Color:
 Strike:
 Dip:
 Comments: Fresh reference samples to compare with other collected at surface.



Anders Gustafsson, 2013

Magnetic susceptibility, in situ measurement on outcrop

Measurement no:	1	2	3	4	5	6	7	8	9
Mag. susc (μSI):									

Petrophysical measurements

Volume (cm^3)	Density (kg/m^3)	Mag. susc (μSI)	J (mA/m)	Q-value
74.7	2975	1050	30	0.64

ID: DRILLCORE04

Observation and sample

Observation date: 2013-04-16**Coordinates:**

E -
S -

Locality description:

Remnant drillcore collected close to NAMCAT20,
exact location is unknown.

Description

Object: drillcore
 Rock type: amphibolite/metagabbro
 Structure: massive
 Texture: uneven grained
 Grainsize: medium grained
 Color:
 Strike:
 Dip:
 Comments: Fresh reference samples to compare with other collected at surface.



Anders Gustafsson, 2013

Magnetic susceptibility, in situ measurement on outcrop

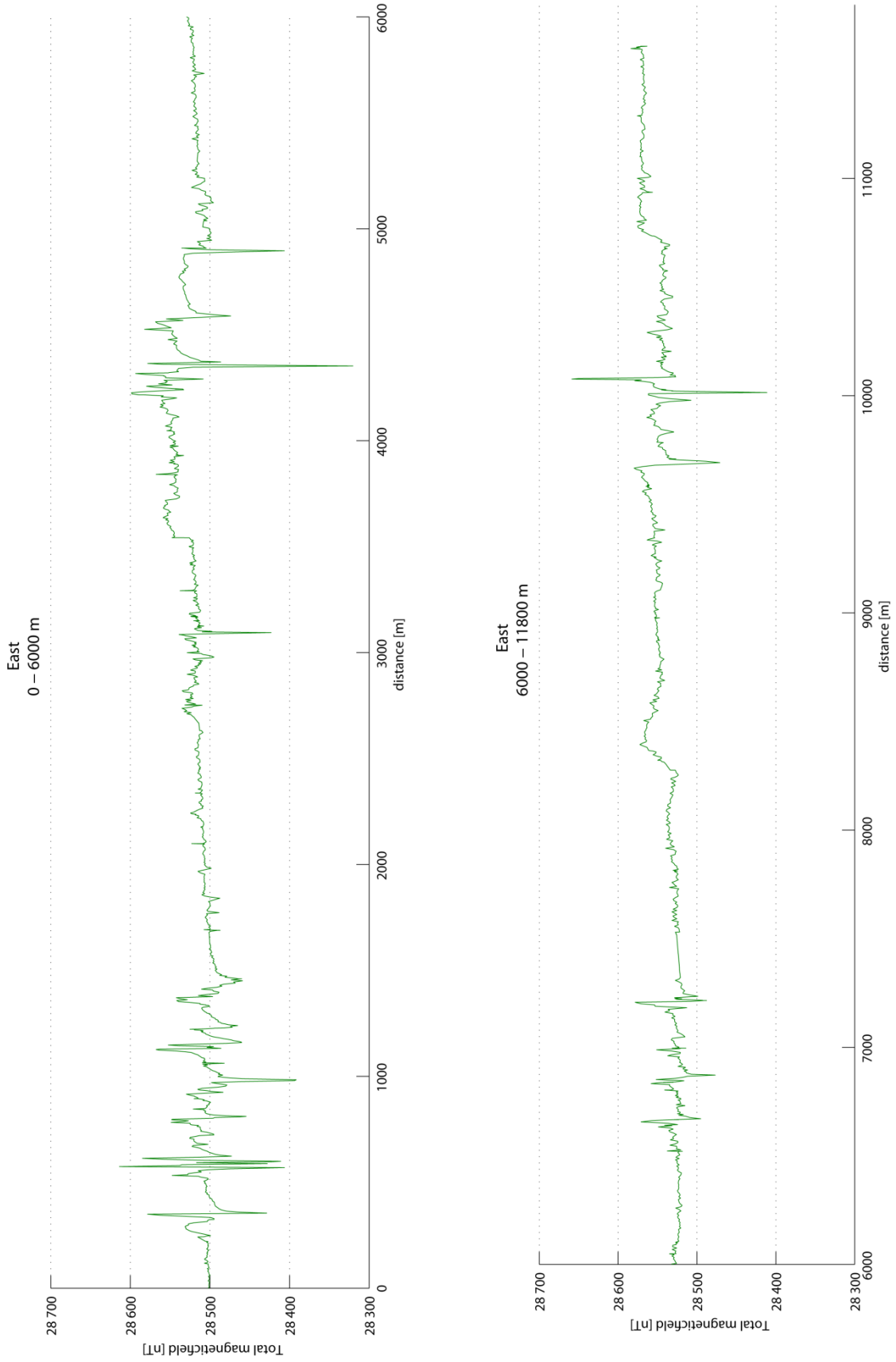
Measurement no:	1	2	3	4	5	6	7	8	9
Mag. susc (μSI):									

Petrophysical measurements

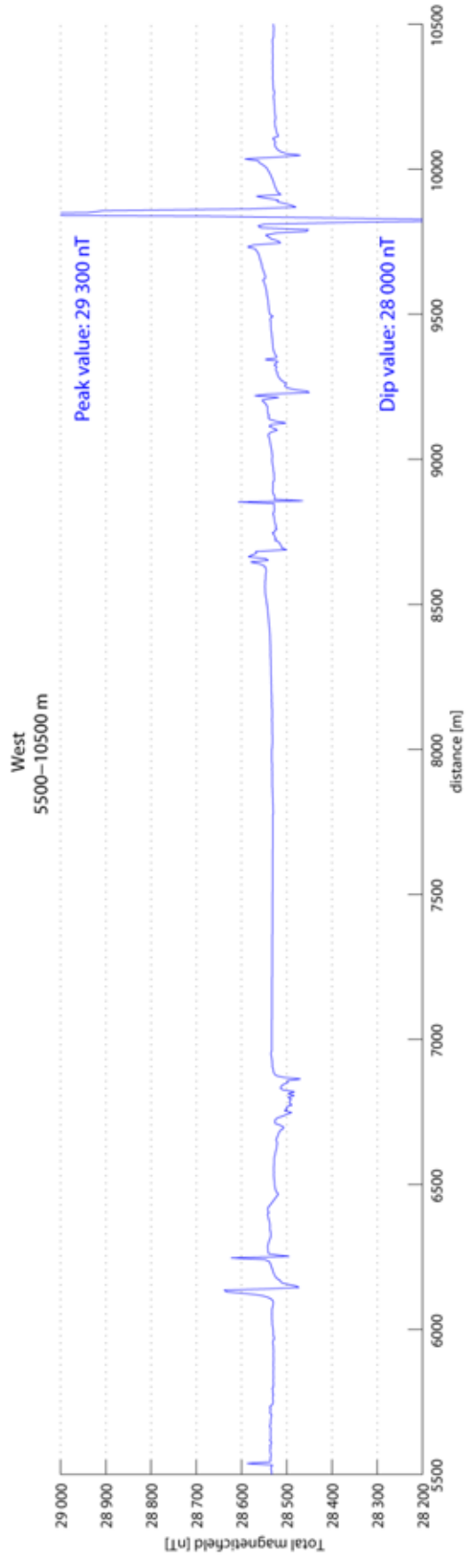
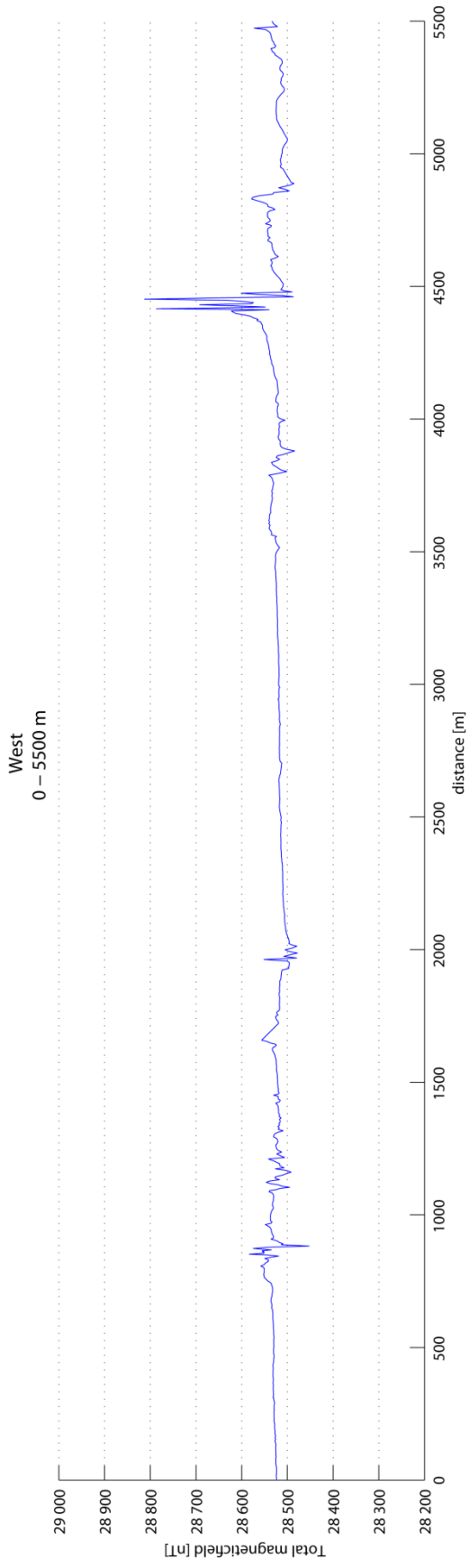
Volume (cm^3)	Density (kg/m^3)	Mag. susc (μSI)	J (mA/m)	Q-value
82.2	2995	620	10	0.46

APPENDIX 2 – GROUND MAGNETIC RESULTS

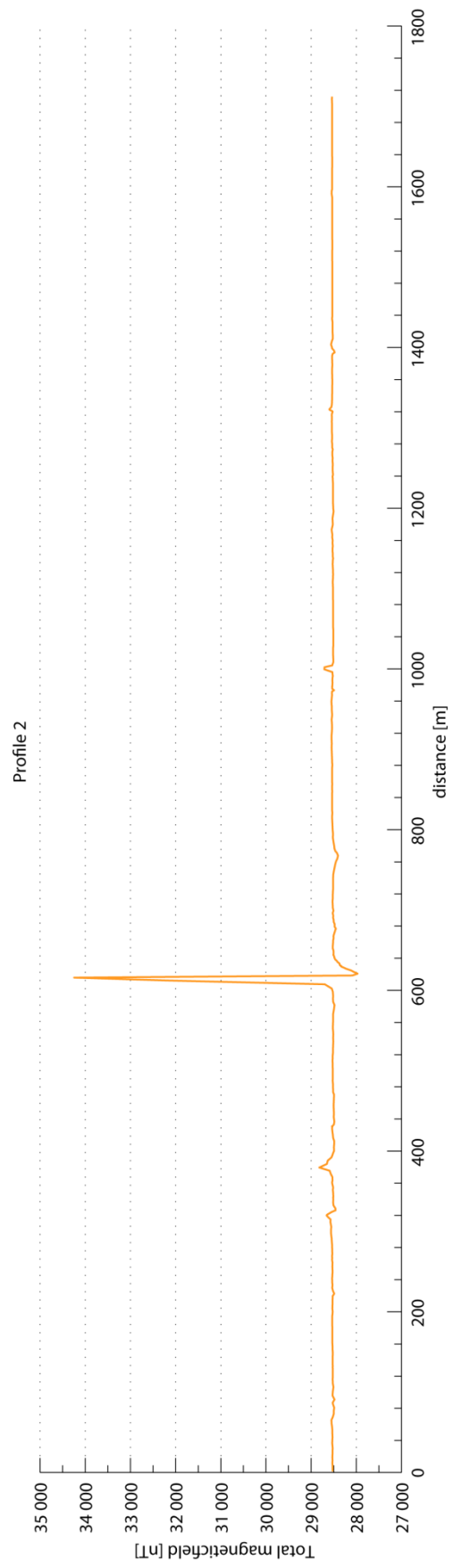
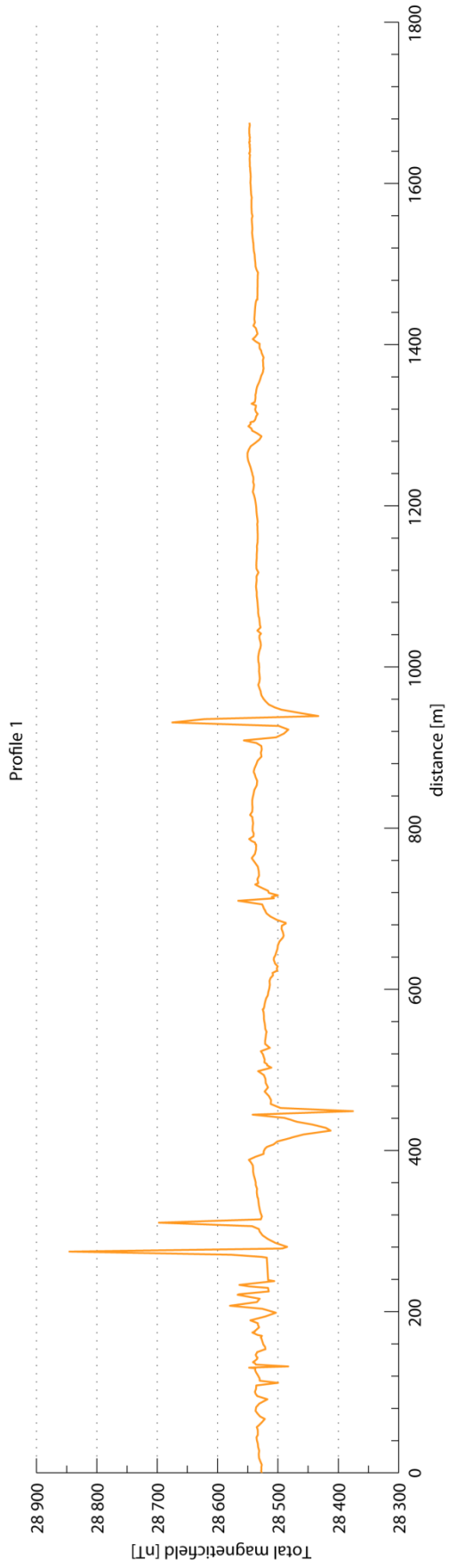
Different scales in every figure.



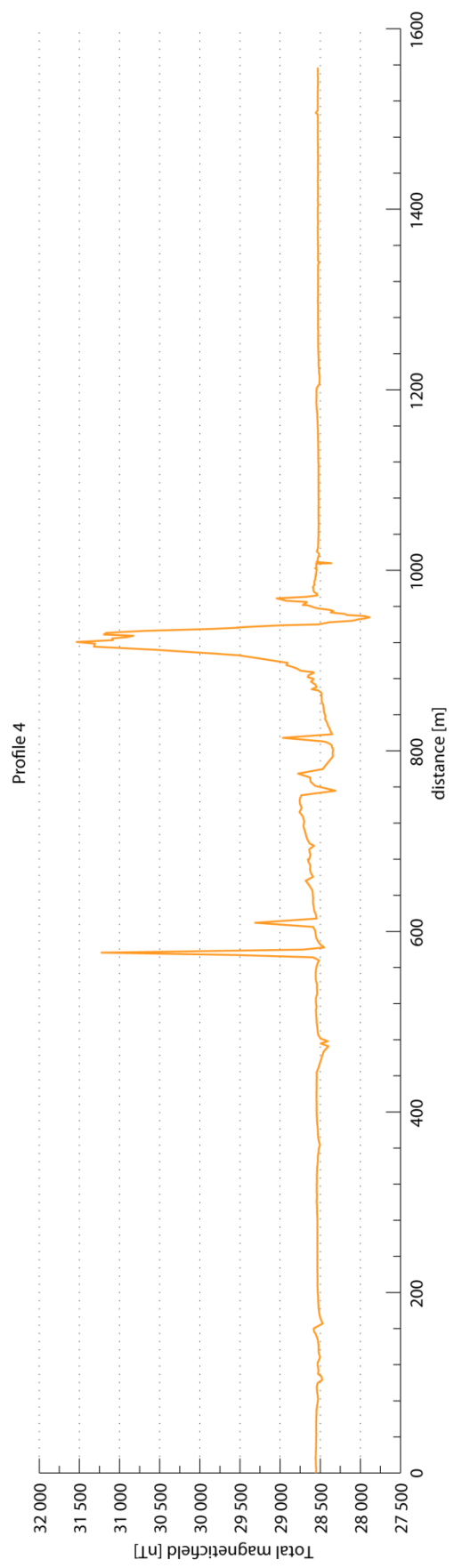
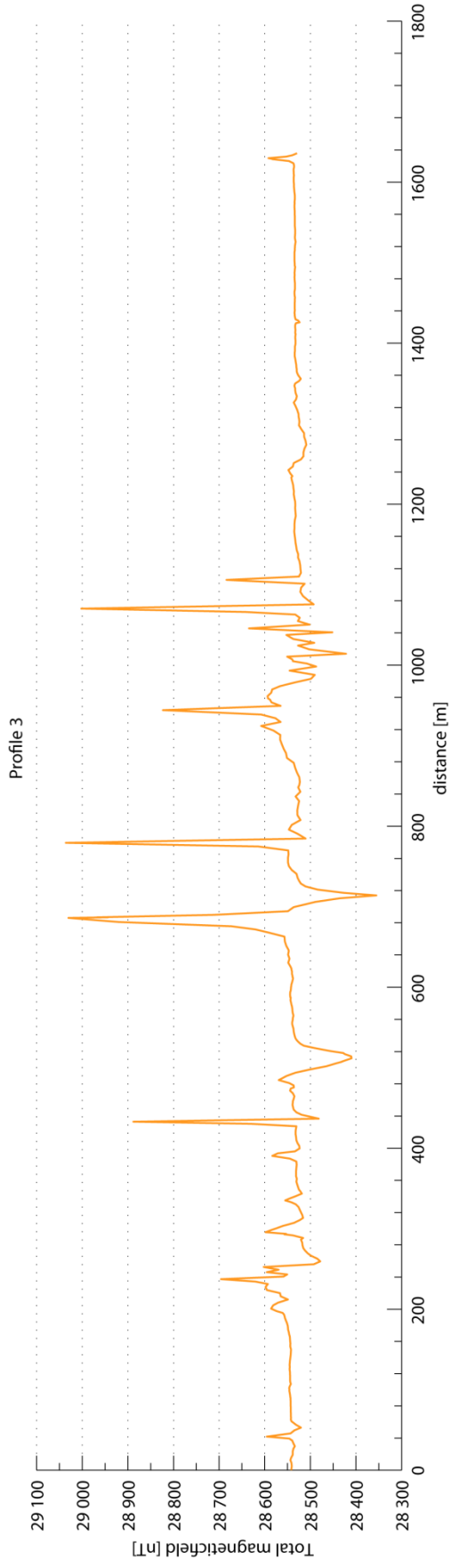
Appendix 2 – Ground magnetic results



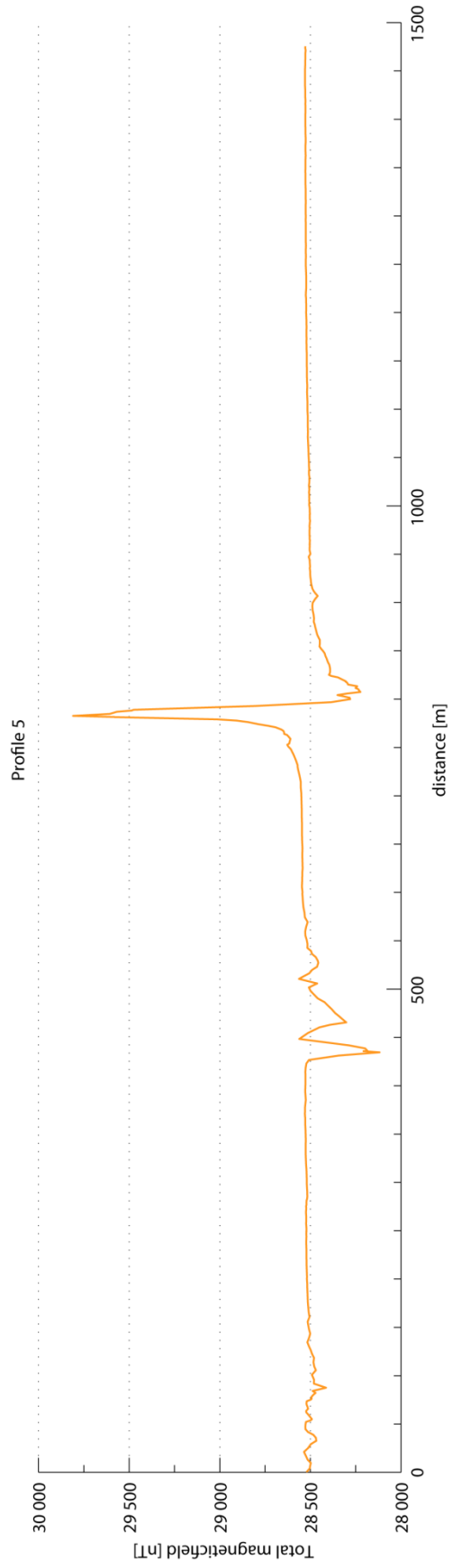
Appendix 2 – Ground magnetic results



Appendix 2 – Ground magnetic results



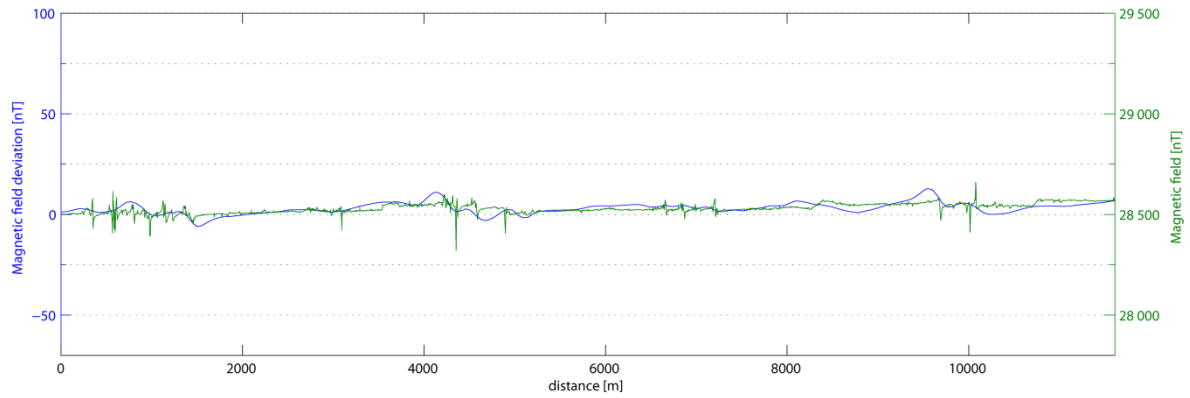
Appendix 2 – Ground magnetic results



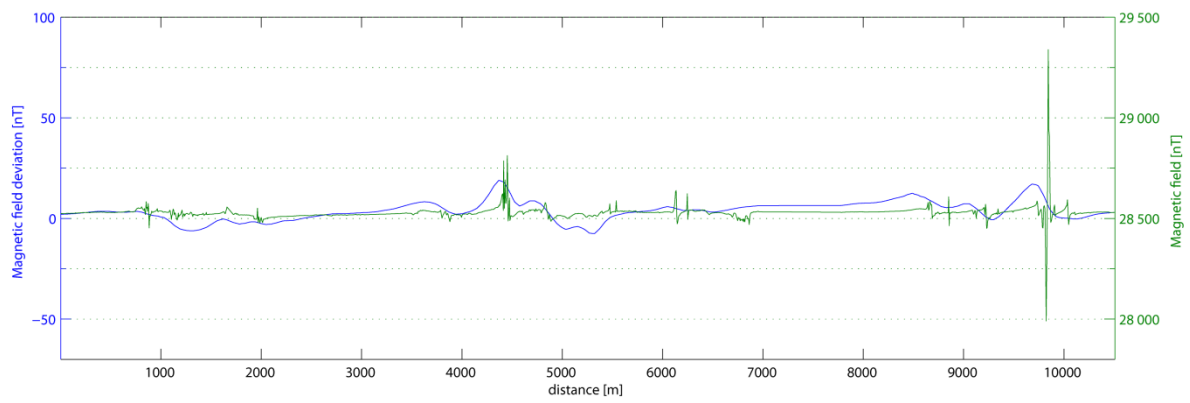
APPENDIX 3 – COMPARISON OF AIRBORNE AND GROUND MAGNETIC DATA

Same vertical scales in all figures.

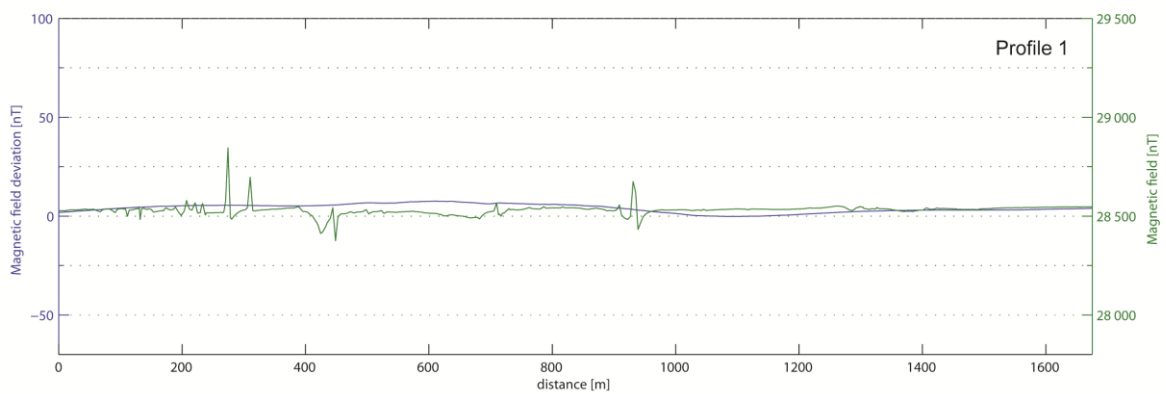
East profile:



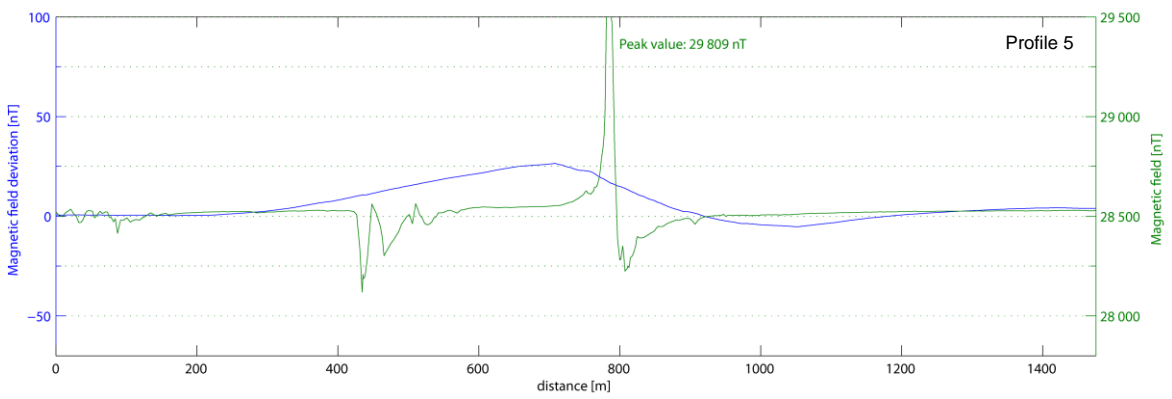
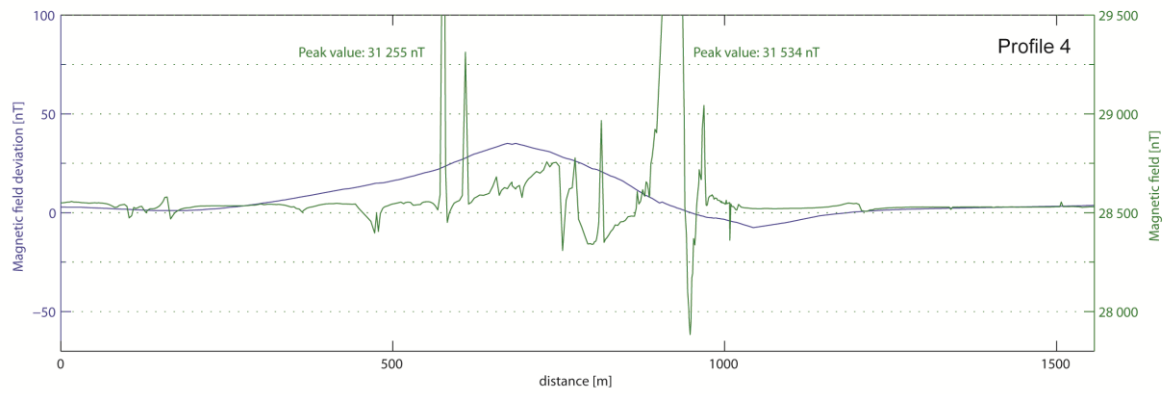
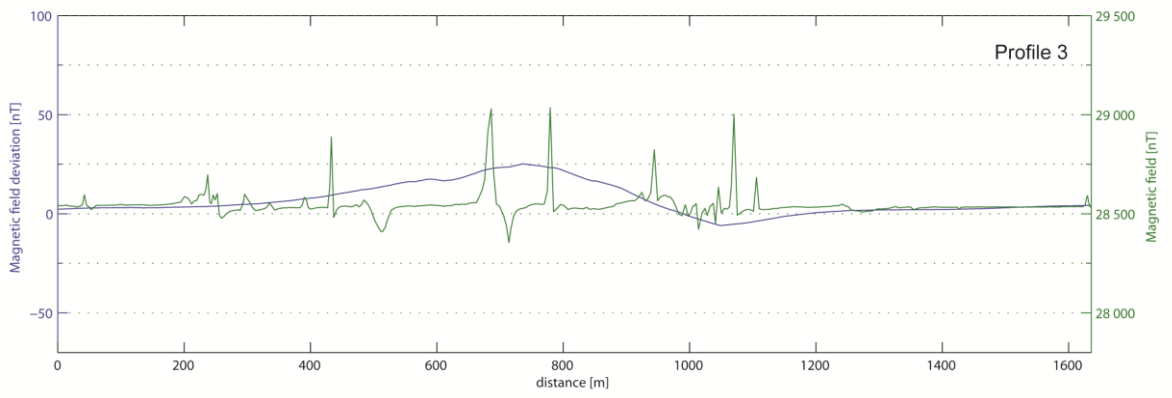
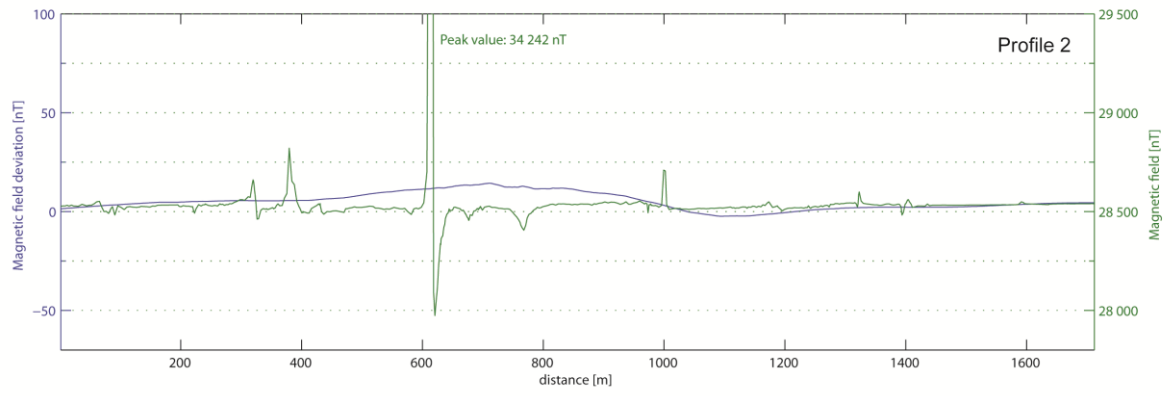
West profile



Detail profiles:



Appendix 3 – Comparison of airborne and ground magnetic data



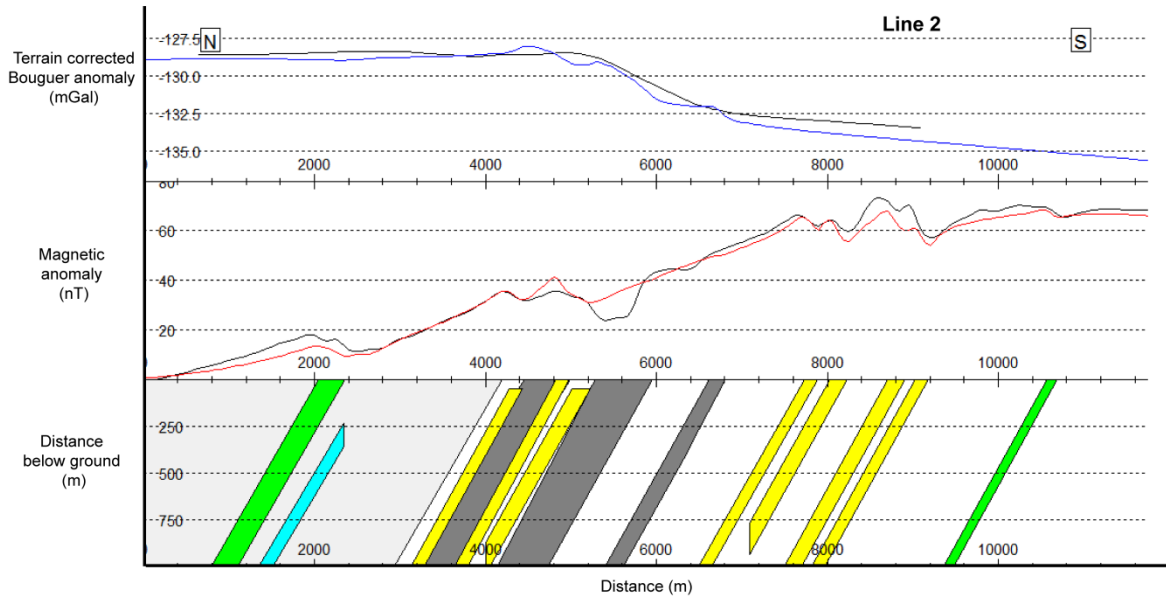
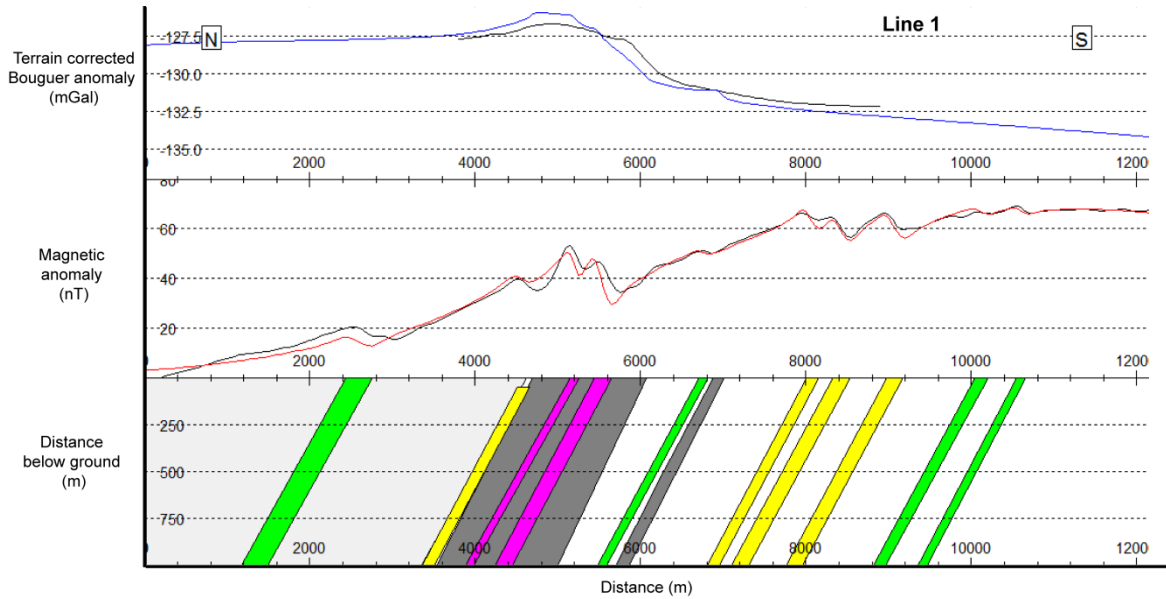
APPENDIX 4 – MODEL RESPONSES

Same scale in all figures. Properties of modeled bodies see table 4 in main text.

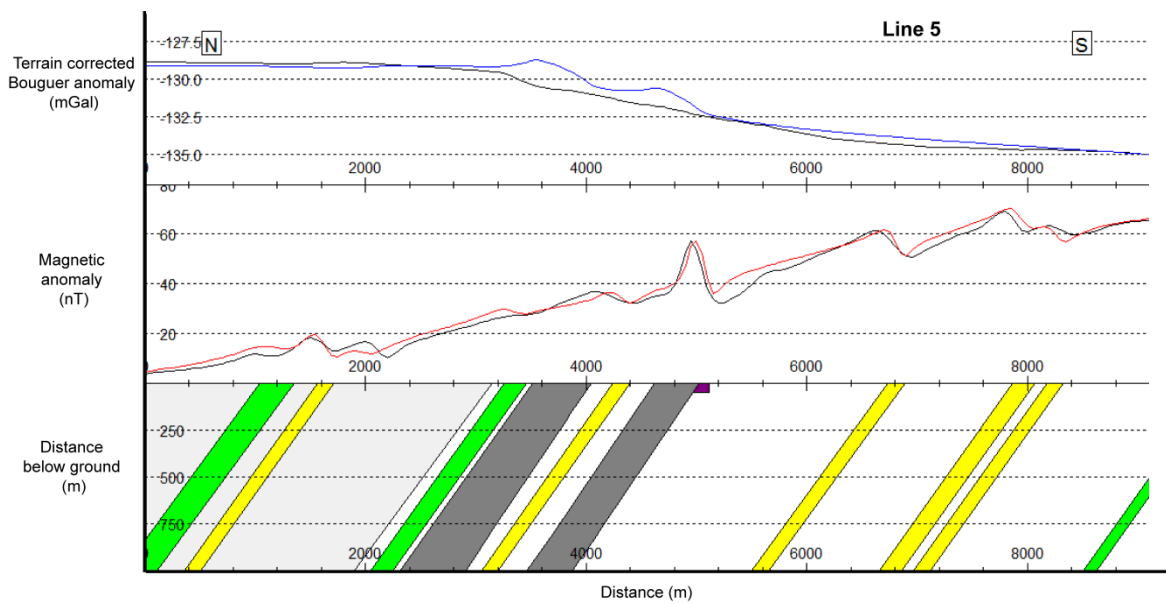
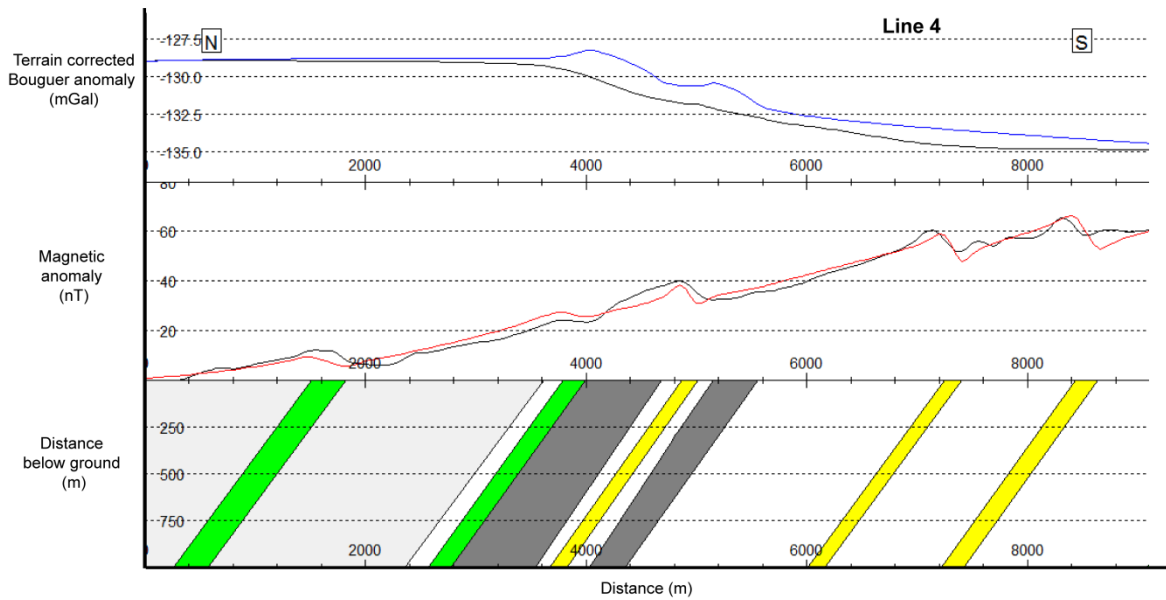
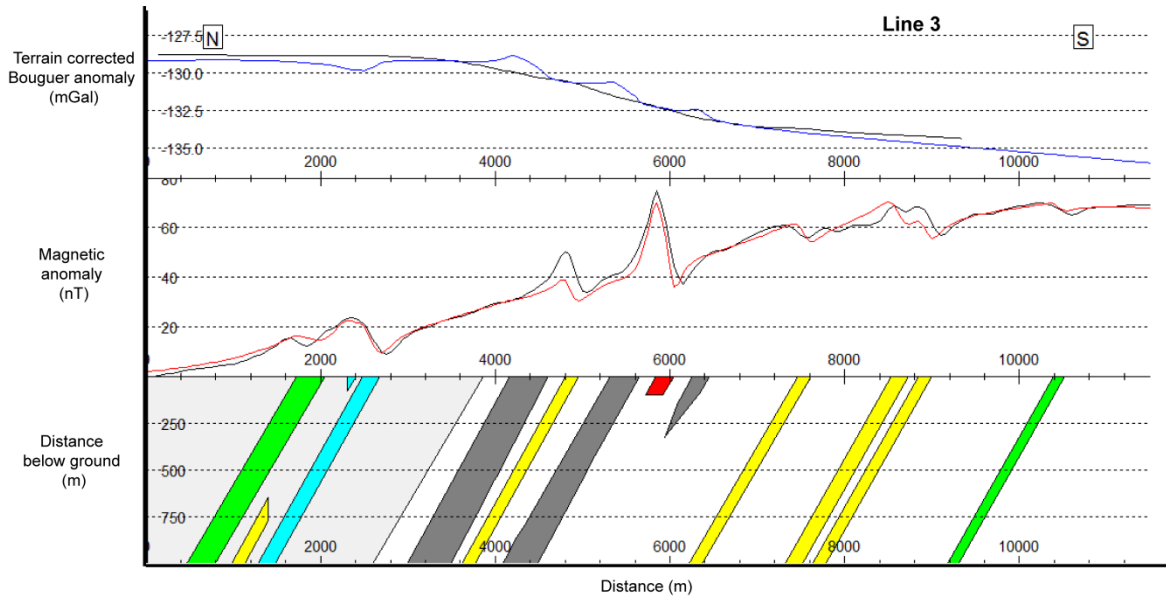
Black line – Measured values

Blue line – Gravity response from model

Red line – Magnetic response from model



Appendix 4 – Model responses



**Tidigare skrifter i serien
”Examensarbeten i Geologi vid Lunds
universitet”:**

327. Ulmius, Jan, 2013: P-T evolution of paragneisses and amphibolites from Romeleåsen, Scania, southernmost Sweden. (45 hp)
328. Hultin Eriksson, Elin, 2013: Resistivitetmätningar för avgränsning av lakvattenplym från Kejsarkullens deponis infiltrationsområde. (15 hp)
329. Mozafari Amiri, Nasim, 2013: Field relations, petrography and $^{40}\text{Ar}/^{39}\text{Ar}$ cooling ages of hornblende in a part of the eclogite-bearing domain, Sveconorwegian Orogen. (45 hp)
330. Saeed, Muhammad, 2013: Sedimentology and palynofacies analysis of Jurassic rocks Eriksdal, Skåne, Sweden. (45 hp)
331. Khan, Mansoor, 2013: Relation between sediment flux variation and land use patterns along the Swedish Baltic Sea coast. (45 hp)
332. Bernhardson, Martin, 2013: Ice advance-retreat sediment successions along the Logata River, Taymyr Peninsula, Arctic Siberia. (45 hp)
333. Shrestha, Rajendra, 2013: Optically Stimulated Luminescence (OSL) dating of aeolian sediments of Skåne, south Sweden. (45 hp)
334. Fullerton, Wayne, 2013: The Kalgoorlie Gold: A review of factors of formation for a giant gold deposit. (15 hp)
335. Hansson, Anton, 2013: A dendroclimatic study at Store Mosse, South Sweden – climatic and hydrologic impacts on recent Scots Pine (*Pinus sylvestris*) growth dynamics. (45 hp)
336. Nilsson, Lawrence, 2013: The alteration mineralogy of Svartliden, Sweden. (30 hp)
337. Bou-Rabee, Donna, 2013: Investigations of a stalactite from Al Hota cave in Oman and its implications for palaeoclimatic reconstructions. (45 hp)
338. Florén, Sara, 2013: Geologisk guide till Söderåsen – 17 geologiskt intressanta platser att besöka. (15 hp)
339. Kullberg, Sara, 2013: Asbestkontamination av dricksvatten och associerade risker. (15 hp)
340. Kihlén, Robin, 2013: Geofysiska resistivitetmätningar i Sjöcrona Park, Helsingborg, undersökning av områdets geologiska egenskaper samt 3D modellering i GeoScene3D. (15 hp)
341. Linders, Victor, 2013: Geofysiska IP-undersökningar och 3D-modellering av geofysiska samt geotekniska resultat i GeoScene3D, Sjöcrona Park, Helsingborg, Sverige. (15 hp)
342. Sidenmark, Jessica, 2013: A reconnaissance study of Rävliiden VHMS-deposit, northern Sweden. (15 hp)
343. Adamsson, Linda, 2013: Peat stratigraphical study of hydrological conditions at Stass Mosse, southern Sweden, and the relation to Holocene bog-pine growth. (45 hp)
344. Gunterberg, Linnéa, 2013: Oil occurrences in crystalline basement rocks, southern Norway – comparison with deeply weathered basement rocks in southern Sweden. (15 hp)
345. Peterffy, Olof, 2013: Evidence of epibenthic microbial mats in Early Jurassic (Sinemurian) tidal deposits, Kulla Gunnarstorp, southern Sweden. (15 hp)
346. Sigeman, Hanna, 2013: Early life and its implications for astrobiology – a case study from Bitter Springs Chert, Australia. (15 hp)
347. Glommé, Alexandra, 2013: Texturella studier och analyser av baddeleyitombvandlingar i zirkon, exempel från sydöstra Ghana. (15 hp)
348. Brådenmark, Niklas, 2013: Alunskiffer på Öland – stratigrafi, utbredning, mäktigheter samt kemiska och fysikaliska egenskaper. (15 hp)
349. Jalnefur Andersson, Evelina, 2013: En MIFO fas 1-inventering av fyra potentiellt förorenade områden i Jönköpings län. (15 hp)
350. Eklöv Pettersson, Anna, 2013: Monazit i Obbhult-komplexet: en pilotstudie. (15 hp)
351. Acevedo Suez, Fernando, 2013: The reliability of the first generation infrared refractometers. (15 hp)
352. Murase, Takemi, 2013: Närkes alunskiffer – utbredning, beskaffenhet och oljeinnehåll. (15 hp)
353. Sjöstedt, Tony, 2013: Geoenergi – utvärdering baserad på ekonomiska och drifttekniska resultat av ett passivt geoenergisystem med värmeuttag ur berg i bostadsrättsföreningen Mandolinen i Lund. (15 hp)

354. Sigfúsdóttir, Thorbjörg, 2013: A sedimentological and stratigraphical study of Veiki moraine in northernmost Sweden. (45 hp)
355. Månsson, Anna, 2013: Hydrogeologisk kartering av Hultån, Sjöbo kommun. (15 hp)
356. Larsson, Emilie, 2013: Identifying the Cretaceous–Paleogene boundary in North Dakota, USA, using portable XRF. (15 hp)
357. Anagnostakis, Stavros, 2013: Upper Cretaceous coprolites from the Münster Basin (northwestern Germany) – a glimpse into the diet of extinct animals. (45 hp)
358. Olsson, Andreas, 2013: Monazite in metasediments from Stensjöstrand: A pilot study. (15 hp)
359. Westman, Malin, 2013: Betydelsen av raka borrhål för större geoenersystem. (15 hp)
360. Åkesson, Christine, 2013: Pollen analytical and landscape reconstruction study at Lake Storsjön, southern Sweden, over the last 2000 years. (45 hp)
361. Andolfsson, Thomas, 2013: Analyses of thermal conductivity from mineral composition and analyses by use of Thermal Conductivity Scanner: A study of thermal properties in Scanian rock types. (45 hp)
362. Engström, Simon, 2013: Vad kan inneslutningar i zirkon berätta om Varbergscharnockiten, SV Sverige. (15 hp)
363. Jönsson, Ellen, 2013: Bevarat maginnehåll hos mosasaurier. (15 hp)
364. Cederberg, Julia, 2013: U-Pb baddeleyite dating of the Pará de Minas dyke swarm in the São Francisco craton (Brazil) – three generations in a single swarm. (45 hp)
365. Björk, Andreas, 2013: Mineralogisk och malm Petrografisk studie av disseminerade sulfider i rika och fattiga prover från Kleva. (15 hp)
366. Karlsson, Michelle, 2013: En MIFO fas 1-inventering av förorenade områden: Kvarnar med kvicksilverbetning Jönköpings län. (15 hp)
367. Michalchuk, Stephen P., 2013: The Sämfold structure: characterization of folding and metamorphism in a part of the eclogite-granulite region, Sveconorwegian orogen. (45 hp)
368. Praszkie, Aron, 2013: First evidence of Late Cretaceous decapod crustaceans from Åsen, southern Sweden. (15 hp)
369. Alexson, Johanna, 2013: Artificial groundwater recharge – is it possible in Mozambique? (15 hp)
370. Ehlorsson, Ludvig, 2013: Hydrogeologisk kartering av grundvattenmagasinet Åsumsfältet, Sjöbo. (15 hp)
371. Santsalo, Liina, 2013: The Jurassic extinction events and its relation to CO₂ levels in the atmosphere: a case study on Early Jurassic fossil leaves. (15 hp)
372. Svantesson, Fredrik, 2013: Alunskiffern i Östergötland – utbredning, mäktigheter, stratigrafi och egenskaper. (15 hp)
373. Iqbal, Faisal Javed, 2013: Paleoecology and sedimentology of the Upper Cretaceous (Campanian), marine strata at Åsen, Kristianstad Basin, Southern Sweden, Scania. (45 hp)
374. Kristinsdóttir, Bárna Dröfn, 2013: U-Pb, O and Lu-Hf isotope ratios of detrital zircon from Ghana, West-African Craton – Formation of juvenile, Palaeoproterozoic crust. (45 hp)
375. Grenholm, Mikael, 2014: The Birimian event in the Baoulé Mossi domain (West African Craton) — regional and global context. (45 hp)
376. Hafnadóttir, Marín Ósk, 2014: Understanding igneous processes through zircon trace element systematics: prospects and pitfalls. (45 hp)
377. Jönsson, Cecilia A. M., 2014: Geophysical ground surveys of the Matchless Amphibolite Belt in Namibia. (45 hp)



LUNDS UNIVERSITET

Geologiska institutionen
Lunds universitet
Sölvegatan 12, 223 62 Lund